REDUCTION-SENSITIVE NANOGELS FOR TUMOR VACCINATION

DANDAN LI

The printing of this thesis was financially supported by:

Utrecht Institute for Pharmaceutical Science (UIPS), Utrecht the Netherlands

© Dandan Li, 2016

ISBN: 978-90-393-6681-3

Cover: Advanced Functional Materials 2015, 25(20): 2993

Printed by GVO drukkers & vormgevers B.V.

Reduction-sensitive nanogels for tumor vaccination

Tumorvaccinatie met reductie-gevoelige nanogelen

(met een samenvatting in het Nederlands)

Proefschrift

ter verkrijging van de graad van doctor aan de Universiteit Utrecht op gezag van de rector magnificus, prof.dr. G.J. van der Zwaan, ingevolge het besluit van het college voor promoties in het openbaar te verdedigen op woensdag 21 december 2016 des middags te 12.45 uur

door

Dandan Li

geboren op 17 April 1986 te Guangxi, China

Promotor: Prof. dr. W.E. Hennink

Copromotoren: Dr. C.F. van Nostrum

Dr. T. Vermonden

This thesis was (partly) accomplished with financial support from China Scholarship Council.

百川东到海，何时复西归。

少壮不努力，老大徒伤悲。

乐府诗集·长歌行

Young idler, an old beggar

Contents

Chapter 1

General introduction

1. Cancer vaccination: promise and challenges

Since developed in the early stage of last century, live attenuated and inactivated vaccines have made an important contribution to preventing infectious diseases, such as poliomyelitis, measles, rubella and mumps.[1] After nearly a century of debate on whether the immune system can also target tumors, now it has become clear that the immune system can indeed be activated against tumors.[2-4] With an increasing number of identified tumor associated antigens, much effort has been directed to the use of tumor antigen based vaccines for active immunization against growing tumors.[2, 4-6] Tumor associated antigens are usually proteins that are overexpressed in tumor cells but minimally expressed in normal tissues.[2] Many approaches involve administration of these tumor associated antigens and targeting them to antigen presenting cells (APCs) for further activation of the immune system to induce antigen specific responses against these tumors.[2, 7]

The aimed mechanism of cancer immunotherapy is to raise a specific cellular or humoral immune response against tumor cells. Cellular and humoral immune responses can be activated via two different pathways. An antigen is often taken and processed by a specialized cell known as the dendritic cell (DC), which are considered to be the most efficient APCs.[8] Subsequently, the processed antigenic peptides can be presented either to $CD8^+$ T cells in major histocompatibility complex (MHC) class I pathway, or to $CD4^+$ T cells in MHC class I pathway. The activated $CD8^+$ T cells can differentiate and proliferate into antigen specific cytotoxic T lymphocytes (CTLs), while $CD4^+$ T cells can produce cytokines that help $CD8^+$ T cells to fully mature and further activate B cells to produce antigen specific antibodies. A cellular immune response, which results in the formation of antigen specific CTLs, is considered to be crucial for the treatment of tumors (Figure 1).[9] For vaccination, in the first step, tumor antigens should be delivered to and taken up by DCs. With suitable activation and/or maturation signals, DCs process tumor antigens and migrate to a local lymph node where they present processed epitopes to activate $CD4^+$ or $CD8^+$ T cells. Subsequently, $CD8^+$ T cells, with assistance of T helper (T_H) cells, differentiate and expand to large numbers of CTLs, which traffic to the circulation, and recognize and eliminate tumor cells.

However, several challenges persist to generate an effective antigen specific T cell response against an established tumor. Firstly, these tumor overexpressed proteins are exogenous antigens with poor immunogenicity, therefore, they are not efficiently recognized and captured by DCs.[10] Additionally, there is a lack of suitable maturation signals to stimulate DCs, which could lead to T cell anergy or production of regulatory T cells that suppress

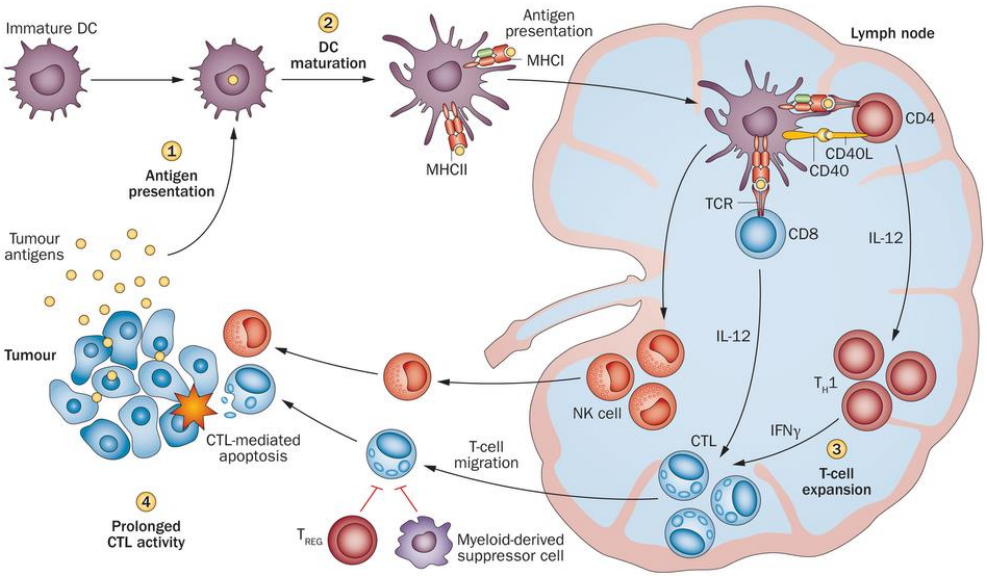

Figure 1. Schematic overview of a cellular immune response against tumor associated antigen. Reproduced from ref.[9]

effector T cells.[11, 12] Further, to induce high numbers of tumor specific CTLs, the antigen needs to be processed and loaded into MHC class I molecule of DCs, which can then be subsequently presented to $CD8^+$ T cells.[13, 14] Usually, antigenic peptides, which are processed in the cytosol of APCs from endogenous antigens, associate with MHC class I molecules. These peptide-MHC class I complexes are subsequently exported to the cell surface to be recognized by $CD8^+$ T cells for presentation (Figure 2).[15] In contrast, exogenous antigens are generally taken up into lysosomes, degraded by lysosomal proteolysis, and subsequently linked to MHC class II molecules followed by $CD4^+$ T cell presentation.[16] Therefore, cancer vaccines based on tumor antigens need to be designed to overcome this conventional pathway and allow DCs to present these exogenous antigens through MHC class I molecules to activate anti-tumor cytotoxic $CD8^+$ T cell responses (referred to as 'cross-presentation'). Moreover, these vaccines preferably also provide the inflammatory signals to fully maturate T cells and avoid immune tolerance.[17-19]

2. Nanogels as vaccine delivery systems

Nanogels are nanometer-sized hydrogels consisting of hydrophilic three dimensional polymer networks that can retain large amounts of water and incorporate diverse classes of bioactive compounds within their networks.[20, 21] Hydrophilic or amphiphilic polymers are

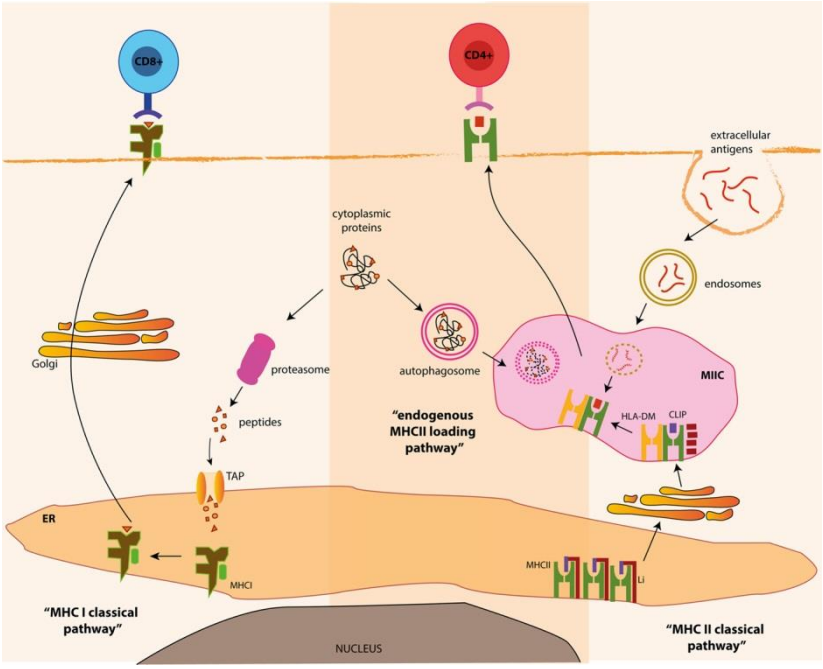

Figure 2. MHC class I and class II antigen processing pathways. Reproduced from ref.[20]

commonly used to form nanogels, which can be classified into two types: natural biopolymers, such as polysaccharides and proteins, and synthetic polymers, like e.g. polyamides and water-soluble polyphosphazenes.[22] Dextran is a neutral hydrophilic polysaccharide, which is composed of glucose units predominantly coupled via α-1,6-glucosidic linkage with some degree of 1,3-branching.[23] Because of its good biocompatibility and derivatization possibilities exploiting its hydroxy groups, dextran has found broad applications, particularly in the tissue engineering and drug delivery fields.[24-26] Many approaches to prepare nanogels have been described, including physical self-assembly of polymers via electrostatic or hydrophobic interactions, polymerization of monomers and macromers by reverse mini emulsion, and crosslinking of functional polymers after their self-assembly into nanocomplexes or micelles.[22]

Nanogels are considered as promising delivery systems for vaccination because they possess several favorable properties including biocompatibility, tunable network structure, flexible nanosize, high loading capability, and ability to protect their content from enzymatic degradation.[20, 21, 27] Moreover, the physicochemical characteristics of nanogels can be tailored by modification with functional groups or surface conjugation of homing devices to achieve responsiveness to environmental factors or targeted delivery to specific cells or subcellular compartments to enhance immunomodulatory properties.[28, 29] With

rational design, these nanogel delivery systems do not only deliver sufficient amounts of tumor antigens to DCs, but also facilitate antigen cross-presentation in the MHC class I pathway.[30-32] Furthermore, some studies showed that certain nanogels as such were able to direct the activation and maturation of DCs.[33, 34] The adjuvant properties of these nanogels stimulating DCs can be an additional advantage for their potential as vaccine delivery systems.

Following the route of nanogels as delivery systems for antigens, the initial step is their cell internalization followed by release and processing of the encapsulated antigens and their subsequent loading into MHC class I and/or MHC class II molecules for further induction of cellular and/or humoral immunity. Endocytosis is the main internalization pathway of nanogels into DCs and the efficiency of uptake can be modulated by the properties of the nanogels, e.g. size, charge, composition, etc.[35] For nano-scaled vaccine systems, the particles with large sizes (>500 nm) stayed at the administration sites, whereas small particles (<10 nm) are rapidly diluted in the interstitium due to their high diffusivity.[36, 37] Particles with sizes below 200 nm, in particular between 40 to 80 nm, have shown to be effectively endocytosed by DCs and have better ability to promote $CD8^+$ T cell immunity, while larger particles (>500 nm) are mainly taken up by local macrophages and tend to present antigens to $CD4^+$ T cells and induce antibody responses.[38-43] It has further been shown that cationic nanogels are more efficiently endocytosed by DCs due to electrostatic interactions between the positively charged nanogels and negatively charged cell membranes as compared to nanogels with a neutral or negative surface charge. However, cationic particles have a tendency to get stuck at the injection site and are therefore not transported to the regional lymph nodes.[44, 45] Importantly, the cationic charge of nanoparticles also plays an important role as the maturation signal to activate DCs.[45-48] Besides exploiting electrostatic attractions between cationic nanogels and cell membranes, endocytosis can be enhanced by surface modification of nanoparticles with ligands that bind to DCs' surface receptors, such as DEC-205, FIRE/CIRE, DC-SIGN, and toll-like receptors.[49, 50]

To increase antigen uptake and facilitate cross-presentation of antigens loaded in nanogels, the antigen needs to be encapsulated or associated with the particles until their internalization by DCs. A burst release or leaking of loaded antigens from nanogels can lead to DC internalization of empty or low antigen loaded nanogels resulting in a weak antigen specific immune response. In recent studies it has indeed been shown that a low-burst release of antigens from carriers is crucial for a strong immune activation.[51, 52] Therefore, responsive systems can be exploited to minimize the leakage of the antigens in the

extracellular environment and to release them once taken up by DCs. In this way, a sufficient dose of the antigen can be internalized into DCs with nanogels and subsequently released intracellularly for further processing and presentation.[30, 31, 53, 54]

1

3. Intracellular delivery strategy utilizing reversible disulfide linkages

The intracellular space is known for its reducing properties because of the presence of low molecular weight redox couples (e.g., glutathione/glutathione disulfide (GSH/GSSG), cysteine/cystine) and macromolecular reductive enzymes (e.g., protein disulfide isomerase (PDI) and gamma interferon-inducible lysosomal thiol reductase (GILT)).[55, 56] It is well known that the reductive microenvironment of the cytosol is caused by a hundred fold higher GSH concentration (approximately 2-10 mM) than that in extracellular fluids (approximately 2-20 μM).[57] It should be noted that the redox potential of endocytic compartments is modulated mainly by a specific reducing enzyme GILT and it has also been reported that the redox potential differs in various cell lines.[55, 58] APCs have the ability to unfold antigenic proteins in both their cytosol and endocytic compartments for subsequent antigen processing and presentation, suggesting that the endocytic compartments have disulfide cleaving activity mainly derived from GILT.[59-62]

Disulfide bonds are readily cleavable in reducing environments and converted to thiols. This rather simple chemistry has inspired researchers to design of novel and versatile responsive delivery systems for intracellular release of antigens. Reduction responsive nanoparticles crosslinked with disulfide linkages and loaded with therapeutic molecules (including antigens) keep, when properly designed, their payloads stably encapsulated in the extracellular space and subsequently release the encapsulated molecules after internalization by DCs.[63-65] Studies have shown that, compared to non-reduction responsive delivery systems, disulfide modified delivery systems can present antigens through both MHC I and MHC II pathways for $CD8^+$ and $CD4^+$ T cell activation in vitro and more importantly enhanced vaccine induced antibody production and $CD8^+$ T cell mediated tumor cell lysis in vivo.[31, 66, 67] Hence, modulating the reductive sensitivity of delivery systems is an effective strategy to develop vaccines requiring $CD8^+$ T cell activation.

4. Aim and outline of the current thesis

An attractive approach to induce a strong immune response against a certain tumor antigen

is targeting it to DCs with a nano-sized carrier that keeps the antigen encapsulated or associated with the particles until the carriers are internalized by DCs. Given the superior properties of nanogels as delivery systems and the responsiveness of disulfide bonds crosslinked systems, reduction sensitive nanogel delivery systems based on dextran and crosslinkers/polymers containing disulfide bonds were developed in this thesis as potential carriers for antigens. The main emphasis was on the preparation of nanogel delivery systems in which a protein antigen is reversibly conjugated to nanogels via disulfide bonds or entrapped in nanogels coated with disulfide crosslinked networks. The antigens should be stably encapsulated in the nanogels in the extracellular space, but should be released in the reducing environment inside DCs. Additionally, this thesis focusses also on obtaining a better insight into the role of the formulation of particulate delivery systems in enhancing antigen specific $CD8^+$ T cell activation *in vitro* and *in vivo* for tumor vaccination.

Chapter 2 provides a literature overview of nanogels for intracellular delivery of biotherapeutics. This review analyzes and discusses the use of biologically responsive (e.g. redox and pH) nanogels for intracellular delivery of biomolecules, such as proteins, antigens and genes.

In **Chapter 3**, the feasibility of cationic dextran nanogels loaded with disulfide conjugated ovalbumin (OVA) as a model vaccine was investigated. The antigen, thiol-modified OVA, was loaded in cationic dextran nanogels via electrostatic interaction and subsequently conjugated to the nanogel networks via disulfide bonds. Reversible immobilization of OVA in the nanogels was investigated by studying the release of the protein in buffer with or without glutathione. Furthermore, the intracellular release of the conjugated antigen from these nanogels in DCs was visualized by confocal microscopy, and the enhancement of MHC class I antigen presentation due to intracellular antigen delivery by reduction sensitive nanogels was studied.

Chapter 4 further investigates the influence of nanogels size and surface charge on their uptake by DCs and capability to maturate DCs. Moreover the intracellular delivery, transportation and processing of conjugated OVA in reduction sensitive nanogels by DCs was studied *in vitro*. The potential use of nanogels with disulfide conjugated antigens as cancer vaccines for prophylactic and therapeutic vaccination *in vivo* was studied in tumor-bearing mice. The production of antigen specific antibodies and the expansion of antigen specific $CD8^+$ T cells *in vivo* were measured after vaccination, and the animals were monitored for tumor growth and survival after tumor inoculation.

To develop a nanogel delivery system in which chemical modification of biotherapeutics is

not necessary, nanogels coated with a reduction sensitive polymer shell were developed for intracellular delivery of antigens in **Chapter 5**. The cationic nanogels loaded with native OVA were coated alternately by electrostatic interactions with polyanions and polycations containing disulfide crosslinkers. After the layer-by-layer coating, the polymer shells were crosslinked by disulfide bonds. These crosslinked shells are impermeable for the encapsulated OVA, whereas importantly release of the antigen only occurs due to the disintegration of the polymer shells under reducing environments. Furthermore, the ability of these core-shell nanogels to deliver antigens intracellularly and to boost the MHC class I antigen presentation were investigated.

Finally, **Chapter 6** gives a summarizing discussion of the achievements described in this thesis, and possible optimization and perspectives.

Reference

1. Rappuoli, R.; Miller, H. I.; Falkow, S. The Intangible value of vaccination. *Science* 2002, 297, 937-939.
2. Butterfield, L. H. Cancer vaccines. *The BMJ* 2015, 350, h988.
3. Blattman, J. N.; Greenberg, P. D. Cancer immunotherapy: a treatment for the masses. *Science* 2004, 305, 200-205.
4. Drake, C. G.; Lipson, E. J.; Brahmer, J. R. Breathing new life into immunotherapy: review of melanoma, lung and kidney cancer. *Nat Rev Clin Oncol* 2014, 11, 24-37.
5. Gilboa, E. The promise of cancer vaccines. *Nat Rev Cancer* 2004, 4, 401-411.
6. Rosenberg, S. A.; Yang, J. C.; Restifo, N. P. Cancer immunotherapy: moving beyond current vaccines. *Nat Med* 2004, 10, 909-915.
7. Schlom, J. Therapeutic cancer vaccines: current status and moving forward. *J Natl Cancer Inst* 2012, 104, 599-613.
8. Palucka, K.; Banchereau, J. Dendritic-cell-based therapeutic cancer vaccines. *Immunity* 2013, 39, 38-48.
9. Melero, I.; Gaudernack, G.; Gerritsen, W.; Huber, C.; Parmiani, G.; Scholl, S.; Thatcher, N.; Wagstaff, J.; Zielinski, C.; Faulkner, I.; Mellstedt, H. Therapeutic vaccines for cancer: an overview of clinical trials. *Nat Rev Clin Oncol* 2014, 11, 509-524.
10. Babiuk, L. A. Broadening the approaches to developing more effective vaccines. *Vaccine* 1999, 17, 1587-1595.
11. Mapara, M. Y.; Sykes, M. Tolerance and cancer: mechanisms of tumor evasion and strategies for breaking tolerance. *J Clin Oncol* 2004, 22, 1136-1151.
12. Xing, Y.; Hogquist, K. A. T-cell tolerance: central and peripheral. *Cold Spring Harb Perspect*

Biol 2012, 4.

13. Joffre, O. P.; Segura, E.; Savina, A.; Amigorena, S. Cross-presentation by dendritic cells. *Nat Rev Immunol* 2012, 12, 557-569.
14. Rodriguez, A.; Regnault, A.; Kleijmeer, M.; Ricciardi-Castagnoli, P.; Amigorena, S. Selective transport of internalized antigens to the cytosol for MHC class I presentation in dendritic cells. *Nat Cell Biol* 1999, 1, 362-368.
15. Crotzer, V. L.; Blum, J. S. Autophagy and adaptive immunity. *Immunology* 2010, 131, 9-17.
16. Vyas, J. M.; Van der Veen, A. G.; Ploegh, H. L. The known unknowns of antigen processing and presentation. *Nat Rev Immunol* 2008, 8, 607-618.
17. Palucka, K.; Banchereau, J. Cancer immunotherapy via dendritic cells. *Nat Rev Cancer* 2012, 12, 265-277.
18. Haring, J. S.; Badovinac, V. P.; Harty, J. T. Inflaming the CD8+ T cell response. *Immunity* 2006, 25, 19-29.
19. Kalinski, P.; Okada, H. Polarized dendritic cells as cancer vaccines: Directing effector-type T cells to tumors. *Semin Immunol* 2010, 22, 173-182.
20. Duraes, F. V.; Niven, J.; Dubrot, J.; Hugues, S.; Gannagé, M. Macroautophagy in endogenous processing of self and pathogen derived antigens for MHC class II presentation. *Front Immunol* 2015, 6.
21. Zhang, H.; Zhai, Y.; Wang, J.; Zhai, G. New progress and prospects: the application of nanogel in drug delivery. *Mat Sci Eng C* 2016, 60, 560-568.
22. Soni, K. S.; Desale, S. S.; Bronich, T. K. Nanogels: an overview of properties, biomedical applications and obstacles to clinical translation. *J Control Release* 2015.
23. Li, Y.; Maciel, D.; Rodrigues, J.; Shi, X.; Tomás, H. Biodegradable polymer nanogels for drug/nucleic acid delivery. *Chem Rev* 2015, 115, 8564-8608.
24. Mehvar, R. Dextrans for targeted and sustained delivery of therapeutic and imaging agents. *J Control Release* 2000, 69, 1-25.
25. Wang, Z.-H.; Zhu, Y.; Chai, M.-Y.; Yang, W.-T.; Xu, F.-J. Biocleavable comb-shaped gene carriers from dextran backbones with bioreducible ATRP initiation sites. *Biomaterials* 2012, 33, 1873-1883.
26. Raemdonck, K.; Naeye, B.; Høgset, A.; Demeester, J.; De Smedt, S. C. Biodegradable dextran nanogels as functional carriers for the intracellular delivery of small interfering RNA. *J Control release* 2010, 148, e95-96.
27. Van Tomme, S. R.; Hennink, W. E. Biodegradable dextran hydrogels for protein delivery applications. *Expert Rev Med Devices* 2007, 4, 147-64.
28. Kabanov, A. V.; Vinogradov, S. V. Nanogels as pharmaceutical carriers: finite networks of infinite capabilities. *Angew Chem Int Ed Engl* 2009, 48, 5418-5429.
29. Tahara, Y.; Akiyoshi, K. Current advances in self-assembled nanogel delivery systems for

immunotherapy. *Adv Drug Deliv Rev* 2015, 95, 65-76.

30. Vartak, A.; Sucheck, S. Recent advances in subunit vaccine carriers. *Vaccines* 2016, 4, 12.
31. Wang, C.; Li, P.; Liu, L.; Pan, H.; Li, H.; Cai, L.; Ma, Y. Self-adjuvanted nanovaccine for cancer immunotherapy: role of lysosomal rupture-induced ROS in MHC class I antigen presentation. *Biomaterials* 2016, 79, 88-100.
32. Li, P.; Luo, Z.; Liu, P.; Gao, N.; Zhang, Y.; Pan, H.; Liu, L.; Wang, C.; Cai, L.; Ma, Y. Bioreducible alginate-poly(ethylenimine) nanogels as an antigen-delivery system robustly enhance vaccine-elicited humoral and cellular immune responses. *J Control Release* 2013, 168, 271-279.
33. Li, D.; Kordalivand, N.; Fransen, M. F.; Ossendorp, F.; Raemdonck, K.; Vermonden, T.; Hennink, W. E.; van Nostrum, C. F. Reduction-sensitive dextran nanogels aimed for intracellular delivery of antigens. *Adv Funct Mater* 2015, 25, 2993-3003.
34. Bivas-Benita, M.; Lin, M. Y.; Bal, S. M.; van Meijgaarden, K. E.; Franken, K. L. M. C.; Friggen, A. H.; Junginger, H. E.; Borchard, G.; Klein, M. R.; Ottenhoff, T. H. M. Pulmonary delivery of DNA encoding mycobacterium tuberculosis latency antigen Rv1733c associated to PLGA–PEI nanoparticles enhances T cell responses in a DNA prime/protein boost vaccination regimen in mice. *Vaccine* 2009, 27, 4010-4017.
35. Standley, S. M.; Mende, I.; Goh, S. L.; Kwon, Y. J.; Beaudette, T. T.; Engleman, E. G.; Fréchet, J. M. J. Incorporation of CpG oligonucleotide ligand into protein-loaded particle vaccines promotes antigen-specific CD8 T-cell immunity. *Bioconjug Chem* 2007, 18, 77-83.
36. Platt, C. D.; Ma, J. K.; Chalouni, C.; Ebersold, M.; Bou-Reslan, H.; Carano, R. A. D.; Mellman, I.; Delamarre, L. Mature dendritic cells use endocytic receptors to capture and present antigens. *P Natl Acad Sci* 2010, 107, 4287-4292.
37. Irvine, D. J.; Swartz, M. A.; Szeto, G. L. Engineering synthetic vaccines using cues from natural immunity. *Nat Mater* 2013, 12, 978-90.
38. Swartz, M. A.; Hirosue, S.; Hubbell, J. A. Engineering approaches to immunotherapy. *Sci Transl Med* 2012, 4, 148rv9-148rv9.
39. Kou, L.; Sun, J.; Zhai, Y.; He, Z. The endocytosis and intracellular fate of nanomedicines: Implication for rational design. *Asian J Pharm Sci* 2013, 8, 1-10.
40. Joshi, V. B.; Geary, S. M.; Salem, A. K. Biodegradable particles as vaccine delivery systems: size matters. *AAPS J* 2013, 15, 85-94.
41. Manolova, V.; Flace, A.; Bauer, M.; Schwarz, K.; Saudan, P.; Bachmann, M. F. Nanoparticles target distinct dendritic cell populations according to their size. *Eur J Immunol* 2008, 38, 1404-1413.
42. Fifis, T.; Gamvrellis, A.; Crimeen-Irwin, B.; Pietersz, G. A.; Li, J.; Mottram, P. L.; McKenzie, I. F.; Plebanski, M. Size-dependent immunogenicity: therapeutic and protective properties of nano-vaccines against tumors. *J Immunol* 2004, 173, 3148-54.

43. Muraoka, D.; Harada, N.; Hayashi, T.; Tahara, Y.; Momose, F.; Sawada, S.-i.; Mukai, S.-a.; Akiyoshi, K.; Shiku, H. Nanogel-based immunologically stealth vaccine targets macrophages in the medulla of lymph node and induces potent antitumor immunity. *ACS Nano* 2014, 8, 9209-9218.
44. Nochi, T.; Yuki, Y.; Takahashi, H.; Sawada, S.-i.; Mejima, M.; Kohda, T.; Harada, N.; Kong, I. G.; Sato, A.; Kataoka, N.; Tokuhara, D.; Kurokawa, S.; Takahashi, Y.; Tsukada, H.; Kozaki, S.; Akiyoshi, K.; Kiyono, H. Nanogel antigenic protein-delivery system for adjuvant-free intranasal vaccines. *Nat Mater* 2010, 9, 572-578.
45. Thomann-Harwood, L. J.; Kaeuper, P.; Rossi, N.; Milona, P.; Herrmann, B.; McCullough, K. C. Nanogel vaccines targeting dendritic cells: contributions of the surface decoration and vaccine cargo on cell targeting and activation. *J Control Release* 2013, 166, 95-105.
46. Ma, Y.; Zhuang, Y.; Xie, X.; Wang, C.; Wang, F.; Zhou, D.; Zeng, J.; Cai, L. The role of surface charge density in cationic liposome-promoted dendritic cell maturation and vaccine-induced immune responses. *Nanoscale* 2011, 3, 2307-2314.
47. Foged, C.; Brodin, B.; Frokjaer, S.; Sundblad, A. Particle size and surface charge affect particle uptake by human dendritic cells in an in vitro model. *Int J Pharm* 2005, 298, 315-322.
48. Soema, P. C.; Willems, G.-J.; Jiskoot, W.; Amorij, J.-P.; Kersten, G. F. Predicting the influence of liposomal lipid composition on liposome size, zeta potential and liposome-induced dendritic cell maturation using a design of experiments approach. *Eur J Pharm Biopharm* 2015, 94, 427-435.
49. Luo, Z.; Li, P.; Deng, J.; Gao, N.; Zhang, Y.; Pan, H.; Liu, L.; Wang, C.; Cai, L.; Ma, Y. Cationic polypeptide micelle-based antigen delivery system: a simple and robust adjuvant to improve vaccine efficacy. *J Control Release* 2013, 170, 259-267.
50. Apostolopoulos, V.; Thalhammer, T.; Tzakos, A. G.; Stojanovska, L. Targeting antigens to dendritic cell receptors for vaccine development. *J Drug Deliv* 2013, 2013, 22.
51. Apostolopoulos, V.; Pietersz, G. A.; Tsibanis, A.; Tsikkinis, A.; Stojanovska, L.; McKenzie, I. F. C.; Vassilaros, S. Dendritic cell immunotherapy: clinical outcomes. *Clin Trans Immunol* 2014, 3, e21.
52. Silva, A. L.; Rosalia, R. A.; Sazak, A.; Carstens, M. G.; Ossendorp, F.; Oostendorp, J.; Jiskoot, W. Optimization of encapsulation of a synthetic long peptide in PLGA nanoparticles: Low-burst release is crucial for efficient CD8+ T cell activation. *Eur J Pharm Biopharm* 2013, 83, 338-345.
53. Tan, J. P. K.; Wang, Q.; Tam, K. C. Control of burst release from nanogels via layer by layer assembly. *J Control Release* 2008, 128, 248-254.
54. Cohen, J. A.; Beaudette, T. T.; Tseng, W. W.; Bachelder, E. M.; Mende, I.; Engleman, E. G.; Fréchet, J. M. J. T-Cell activation by antigen-loaded pH-sensitive hydrogel particles in vivo: the effect of particle size. *Bioconjug Chem* 2009, 20, 111-119.

55. Hu, Y.; Litwin, T.; Nagaraja, A. R.; Kwong, B.; Katz, J.; Watson, N.; Irvine, D. J. Cytosolic delivery of membrane-impermeable molecules in dendritic cells using pH-responsive core−shell nanoparticles. *Nano Letters* 2007, 7, 3056-3064.
56. Brülisauer, L.; Gauthier, M. A.; Leroux, J.-C. Disulfide-containing parenteral delivery systems and their redox-biological fate. *J Control Release* 2014, 195, 147-154.
57. Saito, G.; Swanson, J. A.; Lee, K.-D. Drug delivery strategy utilizing conjugation via reversible disulfide linkages: role and site of cellular reducing activities. *Adv Drug Deliv Rev* 2003, 55, 199-215.
58. Schafer, F. Q.; Buettner, G. R. Redox environment of the cell as viewed through the redox state of the glutathione disulfide/glutathione couple. *Free Radic Biol Med* 2001, 30, 1191-1212.
59. Phan, U. T.; Arunachalam, B.; Cresswell, P. Gamma-Interferon-inducibleLysosomal Thiol Reductase (GILT): maturation, activity, and mechanism of action. *J Biol Chem* 2000, 275, 25907-25914.
60. Balce, D. R.; Allan, E. R. O.; McKenna, N.; Yates, R. M. γ-Interferon-inducible lysosomal thiol reductase (GILT) maintains phagosomal proteolysis in alternatively activated macrophages. *J Biol Chem* 2014, 289, 31891-31904.
61. Collins, D. S.; Unanue, E. R.; Harding, C. V. Reduction of disulfide bonds within lysosomes is a key step in antigen processing. *J Immunol* 1991, 147, 4054-9.
62. West, L. C.; Cresswell, P. Expanding roles for GILT in immunity. *Curr Opin Immunol* 2013, 25, 103-108.
63. Jensen, P. E. Antigen unfolding and disulfide reduction in antigen presenting cells. *Semin Immunol* 1995, 7, 347-353.
64. Cheng, R.; Feng, F.; Meng, F.; Deng, C.; Feijen, J.; Zhong, Z. Glutathione-responsive nano-vehicles as a promising platform for targeted intracellular drug and gene delivery. *J Control Release* 2011, 152, 2-12.
65. Mura, S.; Nicolas, J.; Couvreur, P. Stimuli-responsive nanocarriers for drug delivery. *Nat Mater* 2013, 12, 991-1003.
66. Colson, Y. L.; Grinstaff, M. W. Biologically responsive polymeric nanoparticles for drug delivery. *Adv Mat* 2012, 24, 3878-3886.
67. Hirosue, S.; Kourtis, I. C.; van der Vlies, A. J.; Hubbell, J. A.; Swartz, M. A. Antigen delivery to dendritic cells by poly(propylene sulfide) nanoparticles with disulfide conjugated peptides: cross-presentation and T cell activation. *Vaccine* 2010, 28, 7897-7906.
68. Heffernan, M. J.; Murthy, N. Disulfide-crosslinked polyion micelles for delivery of protein therapeutics. *Ann Biomed Eng* 2009, 37, 1993-2002.

Chapter 2

Nanogels for intracellular delivery of biotherapeutics

Dandan Li, Cornelus F. van Nostrum, Enrico Mastrobattista,

Tina Vermonden and Wim E. Hennink

Department of Pharmaceutics, Utrecht Institute for Pharmaceutical Sciences, Utrecht University

Submitted for publication

Abstract. Many biomolecules, such as proteins, antigens and genes, are presently used as therapeutics. However, their delivery to target sites inside cells is challenging because of their large molecular size, difficulties to pass cellular membranes and their susceptibility for enzymatic and chemical degradation. Nanogels, three-dimensional networks of hydrophilic polymers, are attractive carrier systems for these biotherapeutics because they protect the biologicals against degradation and, importantly, facilitate cell internalization. Furthermore, the development of responsive nanogel delivery systems has resulted in particles that release their payloads due to a certain physiological trigger inside cells. This paper reviews and discusses the use of nanogels, with special emphasis on biologically responsive systems, for intracellular delivery of biotherapeutics.

1. Introduction

Many biotherapeutics (e.g. proteins, antigens, and nucleic acids) have their targets inside the cells[1-4]. However, delivery of biotherapeutics to these intracellular targets is challenging due to their unfavorable biopharmaceutical properties (hydrophilic molecules with a high molecular weight), which make them prone to both enzymatic and chemical degradation and prevent them to cross cellular membranes by Fickian diffusion[5-7]. Nanoparticle delivery systems have been shown to be effective in protecting drugs from degradation, overcoming biological barriers, and controlling the rate and duration of drug release[7-13]. Moreover, nano-sized particles can after e.g. intravenous administration accumulate in sites of high vascular permeability (sites of inflammation in e.g. tumors) via the enhanced permeability and retention (EPR) effect[13-15], and nanoparticles can also be rendered cell-specific by coupling of targeting ligands to their surface[16, 17]. So far, various types of nanoparticle systems have been developed and applied for (targeted) drug delivery, among which polymer based nanoparticles, micelles, liposomes, as well as inorganic particles[18-24].

Hydrogels are crosslinked networks of hydrophilic polymers that retain a large content of water and can be used for loading and release of biotherapeutics because of this feature[25-27]. Since their discovery and application in the biomedical field, macroscopic systems of hydrogels have been developed and investigated for the design of tissue engineering scaffolds and for local delivery of biotherapeutics[28-31] Nanogels are nano-sized hydrogel particles, which in contrast to macroscopic hydrogel particles, can be injected in the circulation to reach target tissues and deliver their payloads locally and also intracellularly[32-37]. The hydrophilicity of nanogels contributes to some of their desirable features including biocompatibility and high loading capacity for hydrophilic biotherapeutics, and their network protects the encapsulated molecules against degradation because enzymes cannot penetrate into the particles[34-38]. Importantly, the characteristics of nanogels can be tailored by altering their size, crosslink density, and surface properties (PEGylation and surface decoration with targeting ligands)[36, 37, 39]. However, it is difficult to load and retain molecules with a size that is smaller than the pore meshes in nanogels because the loaded molecules will be released from the particles during their preparation. This can be solved by increasing the crosslink density of nanogels to stably entrap their payloads during gel formation. However, once the bioactives are loaded in hydrogel particles during preparation, this might result in chemical modification of the loaded molecules[40-43]. In some methods, strongly charged biotherapeutics, such as nucleic acids, can be stably immobilized in oppositely charged nanogels under physiological conditions[44-48]. For both approaches, the entrapped biotherapeutics can subsequently be

released by hydrolytic degradation of the gel network[46-50]. However, this sustained release in turn will result in low concentrations of the released biotherapeutics for prolonged times in the extracellular as well as intracellular environment, which is particularly not wanted for drugs that have their sites of action inside cells. Fast intracellular release of therapeutics can be established by the design of nanogels that are taken up by cells and subsequently degrade rapidly in a triggered manner because of physiological differences between the intracellular environment and the extracellular space. Particularly the low pH of the endo/lysosomes as well the low reduction potential in cells have been exploited to develop nanogels that release their payload in a triggered manner, as discussed in the next sections of this review.

2. The needs and challenges for intracellular delivery of biotherapeutics

Over the last decades, biotherapeutics have evolved as attractive agents for the treatment of various diseases[1, 3, 51, 52]. Pharmaceutical peptides and proteins as well as nucleic acid based drugs are developed to interfere with key pathways of the target cells to treat both chronic and acute pathologies[1, 3, 53]. Besides, vaccination with specific antigens provides immunological protection and treatment against different types of cancer and infectious diseases[54, 55]. Many peptides and proteins, including antibodies, exert their effect by interactions with cell surface receptors[1, 56]. However, a significant number of peptides and proteins have their therapeutic actions inside cells, e.g. in the cytoplasm and specific cellular compartments[2, 53, 57]. Various forms of RNA based drug (siRNA, mRNA, and miRNA) need to be delivered into the cytoplasm where the cellular translation machinery is located, while pDNA must also cross the nuclear membrane to enable expression of the target genes[3]. In the case of vaccine delivery to induce antigen specific humoral or cellular immune responses, the antigen needs to be translocated in lysosomes or the cytosol of antigen presenting cells (APCs), where it is processed and presented to T cells[58-60].

Biotherapeutics in their free form have some unfavorable pharmaceutical properties. Firstly, these complex molecules are often rapidly eliminated from the circulation by renal filtration (for biotherapeutics ~< 60 kD) or by scavenger cells in the liver (for larger biotherapeutics) and/or inactivated by enzymatic degradation. Secondly, they do not spontaneously pass biological barriers such as lipid membranes of cells. For these reasons, appropriate delivery systems of biotherapeutics are essential to prevent their fast degradation and renal clearance, and to render their intracellular delivery possible. Therefore, in recent years various nano-sized delivery carriers have been developed for encapsulation of biotherapeutics to

increase their stability, improve their efficacy by assisting their intracellular delivery to reach to intracellular target sites[5, 35, 61]. Besides that biotherapeutics need to be retained by the carriers until they reach their target sites, intracellular delivery of these biomolecules with nano-carriers is another key step. These nano-carriers can enter cells from the extracellular space by cell uptake processes including endocytosis and phagocytosis to result in their localization of these particles in endo/lysosomes[62, 63]. To reach the aimed intracellular target sites in the cytoplasm or nucleus, the particles and/or the released payload have to undergo endo/lysosomal escape[64-66].

3. Biologically responsive nanogels as delivery systems

As pointed out in the previous sections, biotherapeutics can be stably encapsulated either in highly crosslinked nanogels or by strong electric interactions with nanogels to minimize their premature leakage. Such nanogels mostly slowly release the encapsulated biomolecules due to hydrolytic degradation of (crosslinks in) the polymer network. However, this sustained release may also lead to too low concentrations of the biotherapeutics at their site of action. Therefore, in recent years, nanogels have been designed with crosslinks that can be broken by extrinsic stimuli such as temperature, light, and ultrasound, or by biological triggers, such as differences in pH and/or reduction potential that might result in rapid swelling and/or degradation which in turn is associated with release of the payload [35, 36, 67, 68]. For nanogels that respond to extrinsic stimuli, highly functionalized equipment is required to provide the external trigger after the nanogels reach their targets, which is not always feasible. Therefore, in the following subsections, the focus is on the triggered release of biotherapeutics from responsive nanogels by biological stimuli.

3.1 Reduction responsive nanogels

The intracellular environment is characterized by a reducing environment which is due to the fact that the glutathione (GSH) levels in the cytosol and nucleus (approximately 2-10 mM) are hundred-fold higher than that in the extracellular fluids (approximately 2-20 μM)[69]. This substantial difference in GSH concentration can be exploited as a potential stimulus for cytosolic release of biotherapeutics from internalized carrier systems. Particularly disulfide linkages are readily cleavable in reducing environments and converted to thiols[70], which can be exploited for the design of intracellular degradable nanogels. However, as mentioned in section 2, nanogels and nanoparticles in general enter cells mostly via

endocytic pathways[39, 71-73]. Therefore, these reduction responsive nanogels are likely to be entrapped in endo/lysosomes in which the GSH concentration is much lower than in the cytosol[74, 75]. This means that the nanoparticles need to escape from the endo/lysosomes to access GSH[64-66]. It should be noted that endocytic compartments also provide reducing environments for disulfide reduction by other means[76]. To mention, it has been reported that redox enzymes expressed on cell surfaces or secreted by cells, such as protein disulfide isomerase (PDI), are transported into endosomes during the invagination process[77]. However, PDIs loses their catalytic activity at low pH of the late endo/lysosomes[76]. Thus, the activity of PDI is likely restricted to the early endosomes. The redox potential in endocytic compartmentsis mainly modulated by a specific reducing enzyme called gamma interferon-inducible lysosomal thiol reductase (GILT), which has its optimal enzymatic activity at a low pH (4.5–5.5)[78]. Furthermore, the reductive activity of GILT has been reported to be maintained by cysteine and GSH[79-81]. Taken together, disulfide crosslinks may also be reduced in the endocytic compartments.

Biotherapeutics can be reversibly immobilized in nanogels via reduction sensitive disulfide bonds exploiting mainly two approaches. Firstly, therapeutics can be covalently conjugated via disulfide linkages to nanogel networks and in this way burst release of the conjugated molecules is avoided[82-84]. The release requires a reductive trigger in the cells to cleave the link between the carrier and therapeutic molecules. For example, DeSimone et al.[82] synthesized siRNA coupled via a degradable disulfide linkage to a polymerizable acrylate (Figure 1A). Subsequently, the derivatized siRNA was copolymerized with PEG dimethacrylate, PEG acrylate and 2-aminoethyl methacrylate to prepare cationic nanogels in which siRNA was covalently incorporated via a disulfide linkage. Triggered release of siRNA was indeed observed in a reducing environment while the therapeutic retained in the nanogel particles under physiological conditions. Furthermore, dose-dependent silencing of luciferase expression was elicited for the Hela cells incubated with disulfide-conjugated siRNA nanogels, while the control nanogels loaded with free/non-degradable-conjugated siRNA did not show significant gene silencing effects (Figure 1B). It should be mentioned that for this strategy, the biotherapeutics lacking free thiol groups need to be chemically modified with functional groups, which is not always feasible because the conjugation reaction might lead to lower biological activity or loss of function [70, 85].

In another approach, biotherapeutics are physically entrapped in disulfide-crosslinked nanogel networks. The release of the encapsulated molecules occurs due to the reductive response to break the structure of the nanogels and allowing subsequent release of the payload[47, 48, 86-89]. Physical entrapment of the biotherapeutics adds versatility to a reduction

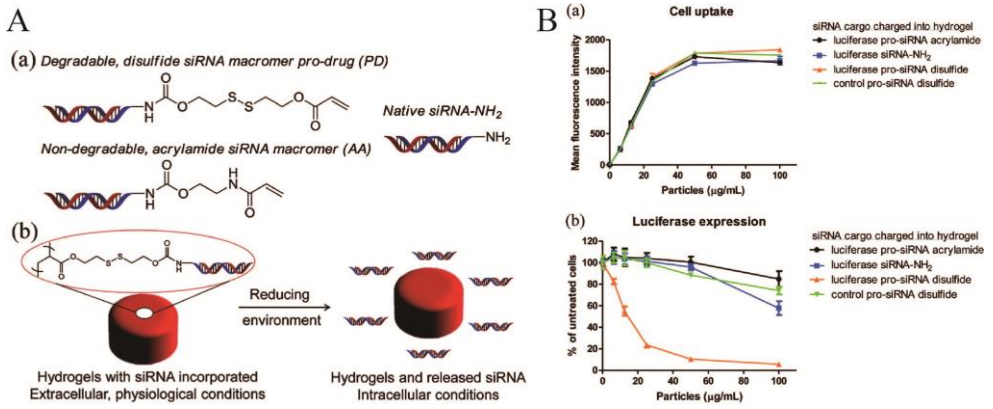

Figure 1. (A) Structures of degradable and nondegradable siRNA macromers as well as native siRNA (a) and illustration of nanogels with disulfide-conjugated siRNA behavior under physiological and intracellular conditions (b). (B) Cellular uptake (a) and luciferase expression (b) in HeLa/luc cells after incubation with nanogels loaded with various modified siRNA. Reproduced with permission from ref [82].

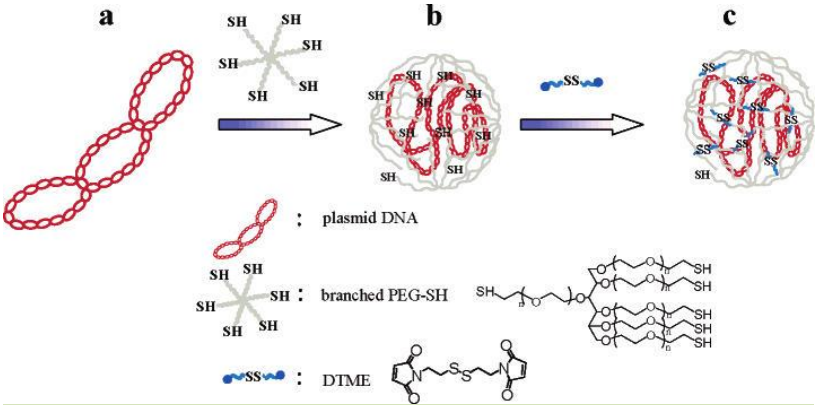

Figure 2. Preparation of disulfide-crosslinked DNA/PEG nanogels. Reproduced with permission from ref [90].

responsive nanogel system because a variety of different molecules can be entrapped into the same nanogel particles. Reduction responsive nanogels containing disulfide linkages in their crosslinks keep their payloads stably encapsulated in the extracellular space provided that the hydrodynamic size of the entrapped compounds is greater than the mesh sizes of

the hydrogel network. The release of the encapsulated molecules can subsequently occur after internalization of the nanogels and reduction of the disulfide crosslinks which results in an increased hydrogel mesh size or complete disintegration of the nanogel structure allowing diffusion of the payloads into the intracellular space. Park et al.[90] reported that DNA/thiol-functionalized six-arm branched PEG complexes were crosslinked through the formation of disulfide linkages between the thiol groups, resulting in stable DNA/PEG nanogels (Figure 2). Because the hydrodynamic size of DNA was greater than the meshes of the crosslinked PEG nanogels, DNA release only occurred in presence of GSH due to the cleavage of disulfide crosslinks. Moreover, the transfected cells exhibited appreciable green fluorescent protein (GFP) protein expression once incubated with the DNA-loaded reducible PEG nanogels, but the level of GFP transfection efficiency was lower than that of commercially available transfection agents (Lipofectamine or polyethylenimine (PEI)-based formulations). This might be due to entrapment of the DNA/PEG nanogels in the endocytic compartments preventing DNA translocation into the nucleus. Beside physical entrapment of biotherapeutics in strongly disulfide-crosslinked nanogels, another approach to stably immobilize actives, particularly long chain nucleic acids with highly negative charges, in cationic disulfide-crosslinked nanogels is by strong electrostatic interaction. Under reductive conditions, cleavage of disulfide linkages resulted in breakdown of the nanogels and release of the payloads.[47, 48, 91] Hollinger et al. [92] prepared cationic nanogels with disulfide crosslinks for the delivery of two types of siRNA (against GAPDH or GFP) for gene silencing. Nanogels were prepared by copolymerizing dimethyl aminoethylmethacrylate, oligo(ethylene oxide) methacrylate, and a water soluble disulfide methacrylate crosslinker using a poly(ethylene glycol 2-bromoisobutyrate) initiator via electron transfer atom transfer radical polymerization. SiRNA was encapsulated in these cationic nanogels by electronic interaction with a high efficiency. The expressing of GAPDH was inhibited by reduction responsive nanogels-mediated GAPDH siRNA delivery to MC3T3 cells. Further, it was demonstrated that these GFP siRNA loaded nanogels facilitated the knockdown of GFP in a GFP expression mouse model after intramuscular administration. Our group reported on decationized disulfide-crosslinked nanogels for intracellular gene delivery[93-95]. Cationic polyplexes were prepared by the transient presence cationic groups coupled to the polymer backbone to allow electrostatic driven condensation with pDNA. After condensation, cationic nanogels were formed by disulfide crosslinking of polymer chains in which pDNA was thus entrapped. Finally, the labile cationic groups were removed by hydrolysis at pH 9, yielding neutral nanogels with a core of disulfide crosslinked poly(hydroxypropyl methacrylamide) and a shell of poly(ethylene glycol). pDNA was stably entrapped in the disulfide crosslinked core of

decationized nanogels under physiological conditions, and released from the nanogels triggered by intracellular reducing environment due to cleavage of the disulfide crosslinks. Furthermore, forced introduction of the nanogels into the cytosol of HeLa cells by electroporation resulted in a high level of gene expression similar as naked pDNA, demonstrating intracellular disassemble of the nanogel and release of entrapped pDNA. These decationized nanogels exhibited excellent cytocompatibility, an increased circulation time and higher tumor accumulation when compared to their cationic precursors. Furthermore, histological analysis of tumors sections showed that decationized nanogels were able to induced transgene expression *in vivo*.

Most of reported reduction responsive nanogels increased the efficacy of the loaded biotherapeutics likely due to the relative higher amount of biomolecules that are delivered and released into cells compared to those from their non-reducible counterparts. Although the observed effects with the reduction sensitive formulations are conclusive, at present no convincing paper has been published in which the intracellular trafficking and fate of disulfide containing carriers and/or their payloads were visualized, probably because of limitations of confocal imaging technologies. Nam et al. [83] developed an approach in which thiol-terminated siRNA was grafted onto thiol-functionalized linear PEI (LPEI) via disulfide bonds to form stable siRNA/PEI nanogels (referred to as MCN, Figure 3A). As control, unmodified siRNA loaded LPEI nanogels (referred to as CN) only with the crosslinking between LPEI chains were used, and uncrosslinked siRNA/LPEI polyplex (referred to as UC) using naked siRNA and unmodified LPEI were also prepared. Confocal images of Cy5-labeled LPEI carriers incubated with MDA-MB-435-GFP cells showed that MCN was internalized to a greater extent than the other two controls (CN and UC, Figure 3B). Furthermore, the red fluorescent dots observed in the cytoplasm suggested that a considerable number of the internalized particles were entrapped in the lyso/endosomes. Nevertheless, MCN showed excellent gene silencing activity as compared to CN and UC. In another approach, Dai et al.[91] coupled two amine groups of L-cystine with acetaldehyde to form disulfide bond-linked double Schiff-bases, aldehyde-L-cystine, which possesses autofluorescence based on the $n \rightarrow \pi^*$ electron transition (-N=C-). Subsequently, the two carboxyl groups of aldehyde-L-cystine can be further used to crosslinked branched PEIs via amine coupling reaction to generate cationic nanogels with disulfide crosslinks. These cationic nanogels showed high pDNA loading due to strong electrostatic interactions. The release of pDNA occurred upon degradation of the nanogels via cleavage of the disulfide bonds in the reductive intracellular environment. Meanwhile, cleavage of disulfide bonds also led to loss of autofluorescence of aldehyde-L-cysteines, which enabled tracking the

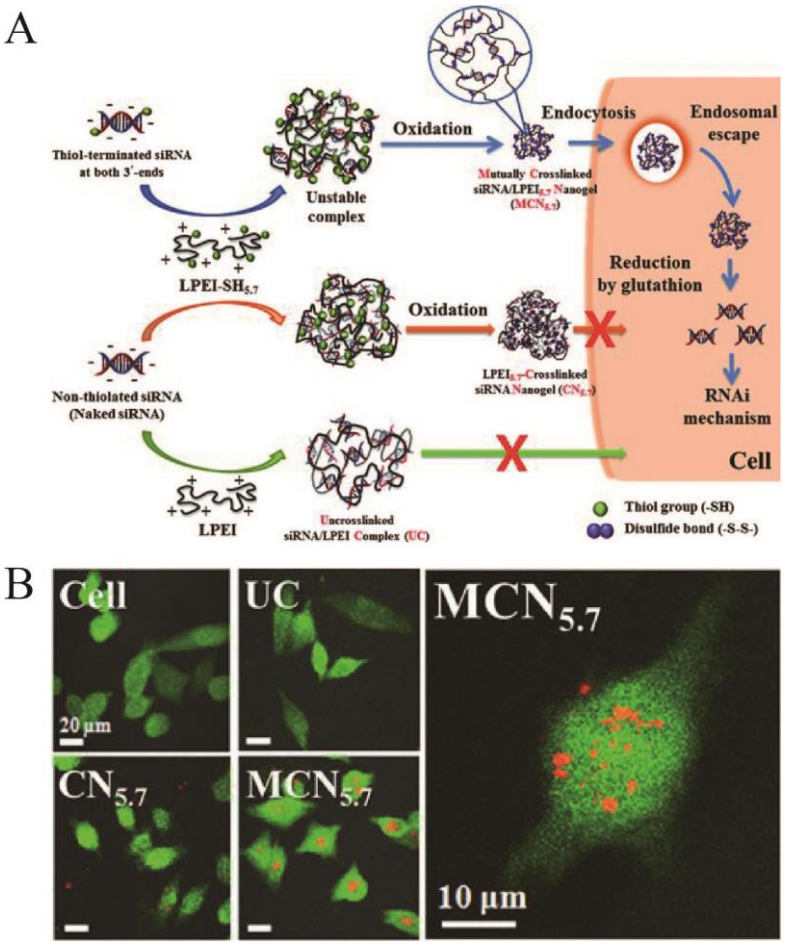

Figure 3. (A) Schematic illustration of the preparation and intracellular processing of siRNA/LPEI nanogels (MCN), naked siRNA loaded LPEI nanogels (CN) and uncrosslinked siRNA/LPEI complexes (UC), respectively. (B) Confocal microscopy images of MDA-MB-435-GFP cells after the cellular uptake of Cy5-labeled carriers. High magnification confocal image of the cell treated with MCN. Reproduced with permission from ref [83].

intracellular degradation of the nanogels. Confocal images of HeLa cells exposed to these pDNA loaded nanogels during the first 6 h of incubation showed that fluorescent signals increased within endo/lysosomal membrane, indicating cellular uptake and internalization of the nanogels by endocytosis. The decrease of fluorescence was observed after 6 h likely because disulfide bonds were cleaved and subsequently aldehyde-L-cysteines lost their

autofluorescence, indicating degradation of the nanogels. However, due to the loss of fluorescence after degradation, no direct evidence of cytosolic release can be obtained. To prove that reductive degradation of nanogels contributed to pDNA transfection in CHO cells, a GSH inhibitor (duroquinone) was used to deplete GSH during the cell transfection process and it was observed that transfection efficiency decreases by ~50% in the presence of this GSH inhibitor. This observation suggests that the reduction responsiveness of these nanogels indeed plays an important role in the transfection process.

The release of loaded biotherapeutics from reduction sensitive nanogels and their biological effects do not only depend on the design of the carriers, but is also dependent on the reducing potential of the intracellular environment, which differs for various cell types. Park et al.[96] synthesized thiolated heparin-pluronic firstly by coupling carboxylated pluronic (F127) to the hydroxyl groups of heparin. Subsequently, amino groups of cystamine were conjugated to carboxyl groups in heparin and the disulfide bonds of cystamine were cleaved to form thiol groups. RNase A is an enzyme that can hydrolyze single stranded RNA without sequence specificity in the cytosol and the nucleus and thereby inducing cytotoxic effect. However, this enzyme is not able to pass cellular membranes by diffusion. RNase A has a high pI and therefore binds at neutral pH to thiolated heparin-pluronic via electrostatic interaction to yield nanogels. Subsequently, stable nanogels were obtained by oxidation of the thiol groups of thiolated heparin-pluronic to form disulfide crosslinks. The release of RNase A from these disulfide crosslinked nanogels was much slower than that from non-crosslinked nanogels. A sustained release of ~40% RNase A from disulfide-crosslinked nanogels was observed during 20 h in a non-reducing environment, while ~80% was released under reductive conditions in the presence of 10 mM GSH during same time period. However, the cytotoxicity results showed no improved effect of RNase A loaded disulfide-crosslinked heparin-pluronic nanogels after incubation with NIH3T3 cells compared to drug-free nanogels. Nevertheless, in another paper [97], the same authors reported that the cytotoxicity of RNase A loaded non-crosslinked heparin-pluronic nanogels was significantly increased as compared to free RNase A. It should be noted that the cytotoxicity study of RNase A loaded disulfide-crosslinked heparin-pluronic nanogels was performed on NIH3T3 cells. The NIH3T3 cell line is a fibroblast cell line that is known for its non-reductive endo/lysosomal compartments with relatively low levels of intracellular GSH[81, 98, 99], which might explain the low effects observed in this study. Some tumor cell lines have been shown upregulated expression of GILT, which increases the reducing potential of lysosomes[100, 101]. Zhong et al.[102] developed reduction sensitive degradable nanogels based on poly(ethylene

glycol)-b-poly(2-(hydroxyethyl) methacrylate-co-acryloyl carbonate) block copolymers and tested them on HeLa cells. These copolymers formed disulfide-crosslinked nanogels in the presence of cystamines via ring-opening reaction with pendant cyclic carbonate groups (Figure 4). Cytochrome C is a membrane-impermeable protein, which initiates the caspase mediated apoptosis cascade in the cytoplasm that results in programmed cell death[103]. Cytochrome C was encapsulated in the disulfide crosslinked network during formation of nanogels with high loading efficiency. It was shown that ~30% of the loaded cytochrome C was released in 22 h in non-reducing environment, while ~ 95% was released in same time period under reductive conditions in the presence of 10 mM DTT. Cytochrome C encapsulated in these reduction sensitive nanogels were more cytotoxic than cytochrome C loaded in reduction-insensitive control nanogels as well as free cytochrome C after incubation with HeLa cells.

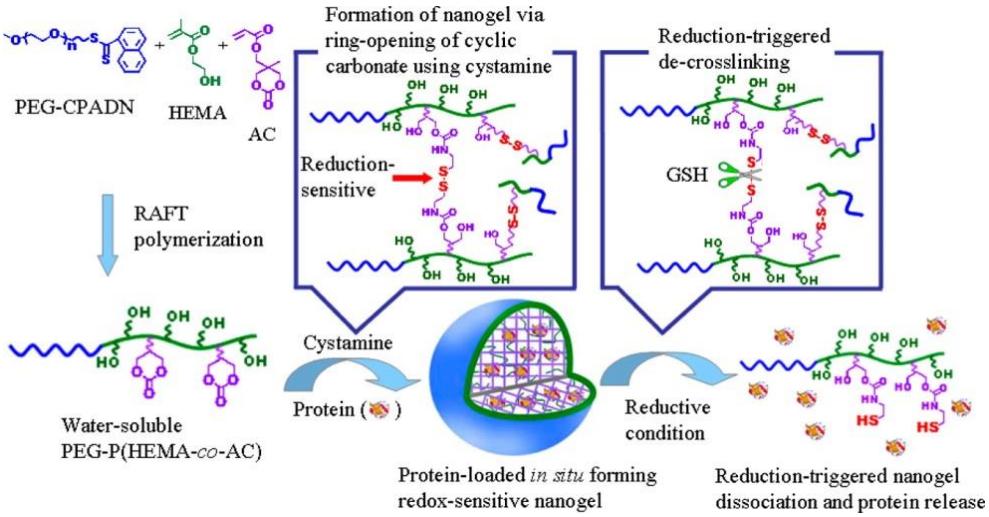

Figure 4. Illustration of in situ forming reduction-sensitive nanogels for loading and triggered release of proteins. Reproduced with permission from ref [102].

In addition to the delivery of nucleic acid based drugs and therapeutic proteins as discussed so far, nanogels have also been used for the delivery of protein and peptide antigens in antigen presenting cells (APCs) for vaccination purposes. GILT is constitutively expressed in APCs and plays an important role in exogenous antigen processing and presentation via

the endocytic pathway by cleavage of the disulfide bonds for protein unfolding[104-106]. In addition, GILT is considered to facilitate transfer of disulfide containing antigens into the cytosol, thereby enhancing their cross-presentation in the MHC (major histocompatibility complex) class I pathway for cellular immune response[107, 108]. Ma et al.[109] developed bioreducible cationic nanogels by the electrostatic interaction of negatively charged alginate with branched PEI, followed by crosslinking with a disulfide linker, 3,3'-dithiobis(sulfosuccinimidyl propionate). A model protein antigen, ovalbumin (OVA), was loaded in these nanogels by electrostatic interactions. The stability of OVA encapsulation in these nanogels in reducing and non-reducing conditions was not studied. However, confocal images showed that more OVA as reduction sensitive nanogel formulation was processed by dendritic cells (DCs) as compared to their non-reducible counterparts. Furthermore, the percentage of DCs that have detectable antigen fragments in the cytosol was ~2 fold higher than those incubated with of non-reducible nanogels. Moreover, compared with non-reducible nanogels, the bioreducible nanogels enhanced both MHC class I and II antigen presentation *in vitro* and *in vivo*. Our group developed cationic dextran based nanogels containing thiol-reactive groups[84]. Thiolated OVA was absorbed in these particles exploiting electrostatic interactions between the negatively charged protein and the positively charged network and subsequently covalently linked via disulfide bonds. The release of OVA only occurred in reducing environments in the presence of 2.5 mM GSH. Furthermore, MHC class I antigen presentation was substantially enhanced by intracellular delivery of disulfide conjugated OVA as compared nanogels that were only physically loaded with the same protein.

3.2 pH responsive nanogels

After endocytosis of carriers by cells, an acidification process causes a decrease in pH values to as low as 5.5 or even 4.5 in endosomal and/or lysosomal compartments, respectively[110, 111]. This relatively low pH in endo/lysosomes can be exploited to design nanogels for intracellular delivery of biotherapeutics. One strategy for development of pH responsive nanogels is to use materials having acid-labile functional groups within the polymer backbone or crosslinks[111-113]. The triggered degradation of these nanogels is based on cleavage of acid-labile bonds within the nanogel networks upon lowering the pH. The release of encapsulated biomolecules in turn results from the rapid degradation of nanogels at low pH. Therefore, pH sensitive nanogels can retain the loaded biotherapeutics in physiological conditions, and release their payloads in acidic cellular compartments after their internalization[114-120]. Thayumanavan et al.[118] prepared pH degradable nanogels by copolymerizing tetraethylene glycol methacrylate with a crosslinker containing

β-thiopropionate, which is cleavable at low pH. Acid α-glucosidase, an enzyme which is essential for the conversion of glycogen to glucose in lysosomes and which has its highest activity at low pH, was loaded in the nanogels during gel formation. It is hypothesized by the authors that the enzyme would be less available to the substrate when encapsulated, and therefore would have a lower activity. No enzymatic activity was detected when exposing the non-pH-degradable control nanogels to pH 5 buffer. However, enzymatic activity was observed after incubation of the degradable nanogels for 30 mins with the same buffer, indicating release of the enzyme due to nanogel degradation. Lu et al.[116] reported a pH triggerable delivery system based on single protein nanogels. Polymerizable vinyl groups (5 to 20 per protein) were covalently coupled to Caspase-3, an essential protein involved in apoptosis by cleaving cellular proteins involved in DNA repair and cell structure. Subsequently, the derivatized protein was loaded in a pH degradable crosslinked polymer shell by copolymerizing it with acrylamide, 2-dimethylaminoethyl methacrylate and an acid cleavable glycerol dimethacrylate crosslinker. These Caspase-3-nanogels were broken down and the Caspase-3 was released after cellular internalization in HeLa cells. Moreover, the labelled nanogels showed colocalization with early endosomes and lysosome after 30 min, with gradual release to the cytosol, which suggested endo/lysosomal escape. These Caspase-3-nanogels showed significantly higher cytotoxicity than their non-degradable counterparts after incubation with HeLa cells, confirming that the protein was indeed released in the cells.

Another frequently applied strategy for the design of pH responsive nanogels concerns the use polymer with functional groups that ionize at low pH, such as amines.[111, 121, 122] Given the pH difference that exists between the extracellular environment/cytosol on the one hand and endo/lysosomal vesicles on the other hand, polymers with a pK_a between 5.0 and 8.0 show changes in their physicochemical properties. Protonation of these groups in the intracellular acidic compartments can cause swelling or disassembly of the nanogels, which leads to triggered release of the encapsulated biomolecules[111, 112]. Most importantly, protonation of the polymers/nanogels not only provides a trigger for the release of their payloads at low pH, but can also facilitate escape from the endo/lysosomal compartments by the so-called proton sponge effect[64]. The proton sponge mechanism relies on the buffering effect of polymers undergoing protonation that consumes protons, which in turn induces an influx of protons and counter- ions into the endo/lysosomal compartments to maintain their desired pH. Subsequently, the high ion concentration in the endo/lysosomes causes water inflow from the cytosol, which eventually leads to osmotic swelling and rupture of the endo/lysosomal membrane and thereby releasing the entrapped

components into the cytoplasm[66]. PEI is frequently used for gene delivery because of its proton sponge effect upon protonation of the amine groups present in its structure[123-125]. Park et al.[126] synthesized catechol grafted branched PEI for siRNA delivery. These polymers self-assembled in acidic and neutral aqueous solutions, and subsequent self-crosslinking under basic conditions by Michael addition between quinones of the oxidized catechol group and amines of PEI occurred to yield cationic PEI nanogels. SiRNA silencing GFP expression was loaded in the nanogels and stable siRNA/nanogel complexes were formed by electrostatic interactions. The hydrodynamic diameter of the nanogels gradually increased with decreasing pH, suggesting that the amine groups were protonated causing absorption of significant amount of water in the gel structure at reduced pH values. Although endosomal escape was not clearly seen by confocal imaging, the siRNA/nanogel complexes exhibited enhanced cellular uptake and promoted gene silencing efficiency when incubated with GFP over-expressing MDAMB-435 cells. Besides PEI, other polyamines have shown to be susceptible for the proton sponge effect as well. Tasciotti et al.[127] described a one-pot synthesis method to produce nanogels based on free radical co-polymerization of the cationic monomer 2-(diethylamino)ethyl methacrylate and the monomeric silica coupling agent vinyltrimethoxysilane in the presence of polyethylene glycol methacrylate and triethylene glycol dimethacrylate linkers (Figure 5A). Nanogels with a crosslinked 2-(diethylamino)ethyl methacrylate hydrogel shell around silica nanoparticle cores were obtained, and siRNA was loaded in the cationic hydrogel shell via electrostatic interactions. When the pH changed from 7 to 5, the tertiary amine groups of the poly (2-dimethylamino) ethyl methacrylate shell were protonated, which resulted in swelling and in a ~16-fold increase in hydrodynamic volume (diameter increased from 100 to 250 nm). Further, the ability of these nanogels to escape endo/lysosomal compartments was evaluated using a human breast cancer cell line (MDA-MB-231) by transmission electron microscopy (TEM). TEM images (Figure 5B) showed that untreated and non-responsive nanogels treated cells maintained distinguishable vesicles with compact borders, while cells incubated with the pH responsive nanogels showed subcellular structures with an irregular shape and a non-continuous borders. Moreover, the pH responsive nanogels were scattered throughout the cytoplasm, indicating that these nanogels indeed escaped from endo/lysosomal vesicles. Furthermore, CXCR4 siRNA delivered by these pH sensitive nanogels in MDA-MB-231 cells showed reduced protein expression of CXCR4 with an efficacy comparable to that of a commercial HiPerFect transfection reagent. Moreover, mice that received intravenously injected siRNA-loaded pH sensitive nanogels showed a reduction of CXCR4 expression at the tumor site as compared to mice treated with free siRNA and non-responsive nanogels.

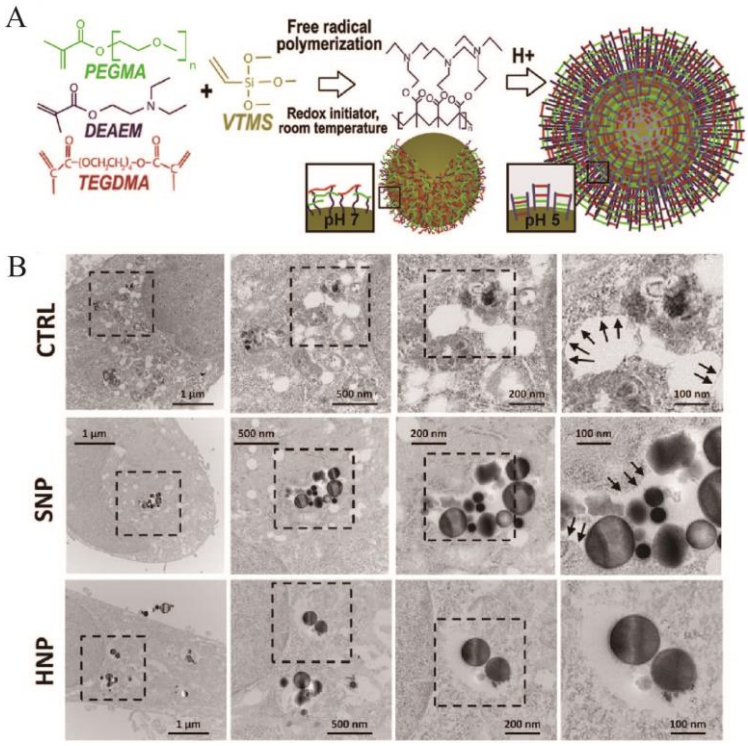

Figure 5. (A) Schematic representation of the preparation of pH responsive nanogels based on free radical polymerization of the cationic monomer 2-(diethylamino)ethyl methacrylate (DEAEM) and the monomeric silica precursor vinyltrimethoxysilane (VTMS) in the presence of polyethylene glycol methacrylate (PEGMA) and triethylene glycol dimethacrylate (TEGDMA) linkers. (B) TEM images of MDA-MB-231 cells 3 h after treatment with pH responsive nanogels (HNP), non-responsive nanogels (SNP) and untreated (CTRL). The black arrows show the border of endo/lysosomes. Reproduced with permission from ref [127].

In other studies, pH-dependent charge-reversal nanogels were designed to maintain a negative surface charge to increase their stability under physiological conditions (pH 7.4), and subsequently reverse their surface charge to enhance cell uptake at the tumor site due to decrease of pH value[128, 129]. For example, Liu et al.[129] synthesized pH responsive charge conversional chitosan-agmatine conjugates (Figure 6A). Chitosan was reacted with dimethylmaleic anhydride to convert its primary amines into amides with a carboxylic functional group. This amide could be hydrolyzed quickly at a slightly acidic pH value (<pH 6.8) to result in the re-formation of the primary amines and thus charge reversal. The

modified chitosan was subsequently coupled to agmatine. Vascular endothelial growth factor (VEGF) is a protein that is essential for tumor growth, progression, and metastasis[130]. The chitosan-agmatine conjugates condensed VEGF suppressing siRNA into the cationic agmatine core to form stable nanogels with an acid responsive charge-reversal anionic shell. Chitosan/VEGF siRNA complexes were prepared as a control and had the same particle size as VEGF siRNA nanogels (around 150 nm). These nanogels were stable in the presence of serum at physiological pH (7.4) owing to their negatively charged surface, whereas chitosan/VEGF siRNA nanogels rapidly aggregated in the presence of serum proteins. The zeta potential of the nanogels reversed rapidly within 30 min from -12 to +9 mV when the pH was decreased from 7.4 to 6.5. VEGF suppressing siRNA loaded charge conversional nanogels were administered to Hela tumor-bearing nude mice by intravenous administration to investigate their therapeutic effects (Figure 6B). It was shown that these siRNA loaded charge-conversional nanogels effectively suppressed VEGF expression and

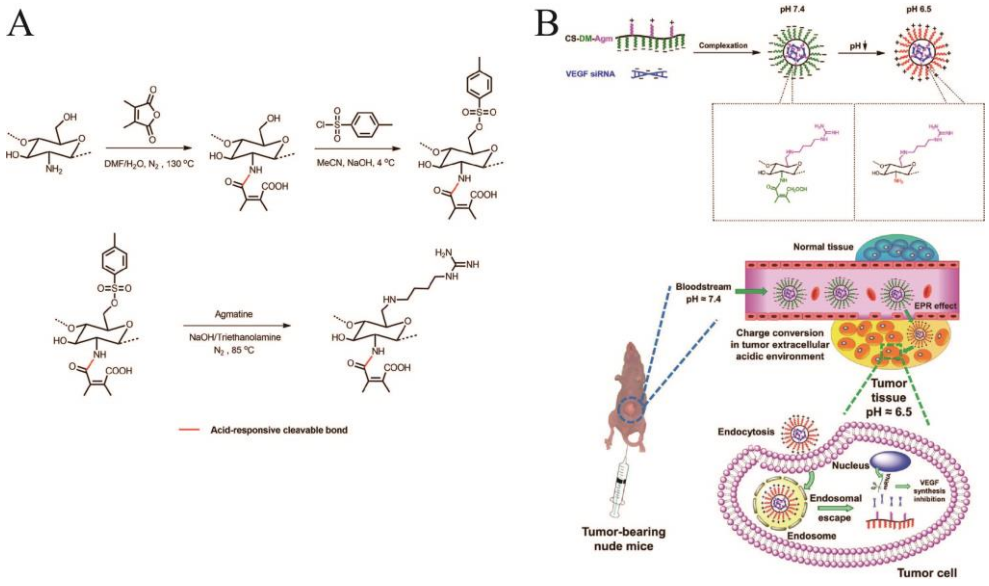

Figure 4. (A) Synthetic procedure of chitosan-agmatine conjugates. (B) Schematic illustration of the formation of VEGF siRNA complexes by the pH responsive charge conversional chitosan-agmatine conjugates (CS-DM-Agm), the change of surface charge property in response to the tumor acidity, and the hypothesized mechanism for tumor suppression of the siRNA complexes. Reproduced with permission from ref [129].

microvessel growth, and also inhibited tumor cell proliferation as compared to chitosan/VEGF siRNA complexes. This better efficacy is likely because the initial negative surface charge prolonged the blood circulation kinetics and as consequence a higher number of particles deposited in the tumor due to the EPR effect. Moreover, the exposed cationic amine groups after charge reversal at the tumor provided the nanogels a higher affinity for the negatively charged cell membrane and facilitated cellular uptake and endo/lysosomal escape via the proton sponge effect.

Besides nucleic acid based therapies, there is also a growing interest in development of pH sensitive nanocarriers that can enhance cytoplasmic entry of antigenic peptides and proteins in APCs. To improve the efficacy of vaccines against tumors, the antigen specific cellular immune response is considered to be crucial[131-133]. The delivery of antigens to the cytosol of APCs is essential, in order to facilitate antigen processing and loading into MHC class I molecules to generate a $CD8^+$ T cell response[134, 135]. Irvine et al.[136] developed pH responsive nanogels for endosomal escape and cytosolic delivery of an antigen (OVA). The nanogels were synthesized by a two-stage polymerization reaction to yield particles with a pH sensitive crosslinked core containing poly(2-dimethylamino)ethyl methacrylate) and a pH insensitive hydrophilic shell layer of poly(2-aminoethyl methacrylate) (Figure 7A). OVA was electrostatic adsorbed to the cationic surfaces of the core-shell particles. These nanogels swelled abruptly due to protonation of tertiary amines in the core between pH 7.0 and 6.8, corresponding to a ~22-fold volume change. Calcein, a membrane-impermeable fluorophore, was used to monitor the integrity of endosomes/phagosomes following particle uptake. DC2.4 cells were co-incubated with labeled pH sensitive nanogels, calcein and lysotracker Red DND-99 for 1 h to label endo/lysosomal compartments. The confocal images (Figure 7B) revealed that a significant fraction of the internalized pH sensitive nanogels did not colocalize with endo/lysosomal vesicles while calcein fluorescence was observed throughout the cytosol and nucleus. However, cells treated with non-responsive nanogels exhibited a punctuate distribution of the nanogels and calcein fluorescence, which both colocalized with lysotracker. These observations suggest that the pH sensitive nanogels indeed facilitate endo/lysosomes escape. To obtain more direct evidence of endo/lysosomal escape, TEM images of cells treated with nanogels were taken (Figure 7B). These images showed that pH-insensitive nanogels were localized within membrane-bound compartments, while pH sensitive nanogels were observed both within membrane-bound vesicles as well as within the cytosol. Ma et al.[137] reported that galactosyl dextran-retinal (GDR) pH sensitive nanogels enhanced MHC class I antigen cross presentation of OVA and anticancer immunity. Amphiphilic pH sensitive GDR was synthesized by conjugating

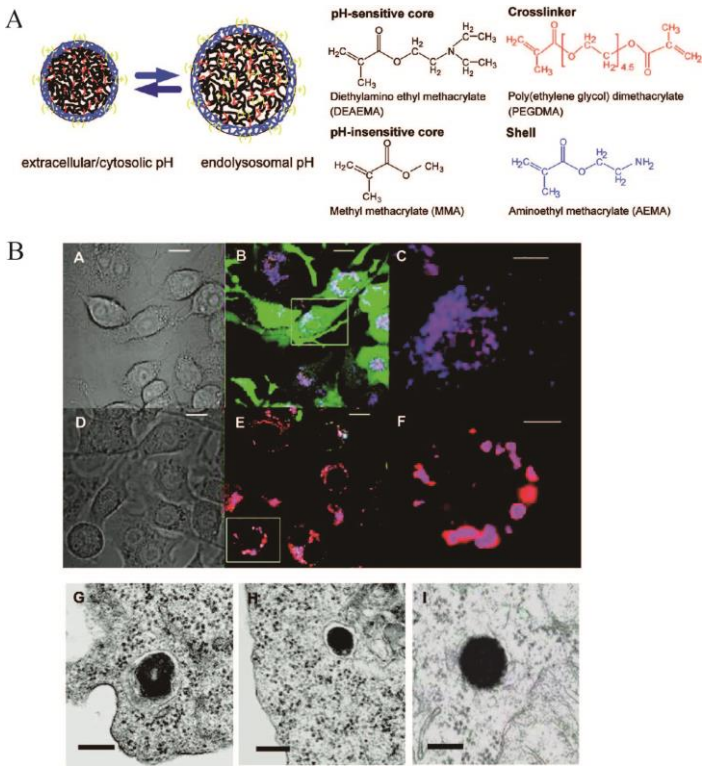

Figure 7. (A) Schematic structure and chemical composition of pH responsive and non-responsive nanogels based on two-stage polymerization reaction to yield particles with either a pH sensitive core of poly(2-dimethylamino)ethyl methacrylate) or a pH insensitive core of poly(methyl methacrylate) with a pH insensitive shell layer of poly(2-aminoethyl methacrylate). (B) Endosomal escape of pH responsive nanogels. DC2.4 cells were co-incubated with LysoTracker Red DND-99 (red), calcein (green), and either pH responsive (A-C) or non-responsive (D−F) nanogels (blue). TEM images of cell sections with non-responsive nanogel in membrane-bound compartments (G) and pH responsive nanogels either in membrane-bound compartments (H) or in the cell cytosol without a clear binding membrane structure (I). Reproduced with permission from ref [136].

all-trans retinal (a metabolite of vitamin A) to dextran through a pH sensitive hydrazone bond, followed by galactosylation of dextran. Upon dissolving in water in the presence of OVA as a model antigen, GDR self-assembled into pH sensitive nanogels loaded with OVA. The cleavage of the hydrazone bond at pH 5 led to release of retinal from the GDR nanogels, which in turn caused disassembly of the nanogels and release of OVA. GDR

nanogels were shown to promote antigen uptake after incubation with DCs for 2 h as compared to free antigen, and the labeled antigen did not colocalize with lysotracker. The authors hypothesized that the cleavage of hydrazone bonds in the endo/lysozymes consumed a considerable amount of protons leading to lysosomal escape; however, no evidence is presented. Antigen loaded pH sensitive GDR nanogels enhanced both MHC I and II antigen presentation *in vitro* and evoked stronger anticancer immune responses *in vivo* than the free antigen.

3.3 Enzyme responsive nanogels

An increased expression of a number of certain enzymes (e.g., proteolytic enzymes, hyaluronidase, lipase, matrix metalloproteinases and plasmin) is often observed under pathological conditions, such as cancer and sites of inflammation[138-142]. Enzyme responsive nanogels can take advantage of the altered expression of local enzymes to develop enzyme-triggerable drug delivery systems. Most reported enzyme-mediated nanogel delivery systems respond to enzymes in the extracellular environment, such as matrix metalloproteinases and plasmin[143-146]. Besides, it is also possible to deliver bioactive molecules into cells using enzymes present in intracellular compartments, such as lysosomal enzymes[147, 148]. Tang et al.[149] described protein-containing nanogels that are degradable upon the digestion by furin, an endoprotease present in various intracellular locations. To prepare the protein-containing nanogels, monomers acrylamide and positively charged N-(3-aminopropyl) methacrylamide and a peptide crosslinker were first physically adsorbed onto the surface of the target anionic protein, which included enhanced green fluorescence protein, caspase-3, bovine serum albumin, or the transcription factor Klf4, in this study. This was followed by in situ free radical interfacial polymerization to form the polymeric shell and to assemble nanogels on the protein, and the size increased from ~5 nm to ~10 nm after these proteins were loaded in such nanogels. The peptide crosslinker can be specifically recognized and cleaved by furin, which leads to degradation of nanogels and subsequent release of the entrapped protein. These nanogels showed increased uptake and intracellular release as compared to the free proteins and non-degradable nanogels in different cell lines, including CHO, HeLa and MEF cells. Furthermore, cell death was observed in HeLa cells incubated with furin-degradable caspase-3 nanogels, while cells exposed to free caspase-3 and non-degradable nanogels exhibited minimal apoptotic death, confirming the increased uptake and intracellular release of the protein by furin-degradable nanogels.

4. Conclusion

Current knowledge provides us the insight that biotherapeutic molecules require not only delivery to the site of diseases but often also inside target cells, or even into specific subcellular compartments. There is no doubt that nanogels are suitable carriers for biomolecules that can protect their payloads from premature degradation and facilitate cellular internalization. Furthermore, it is clear from the papers summarized and discussed in this review that many biologically responsive nanogels significantly enhance the therapeutic effect of biomolecules by their delivery and release in relatively high doses intracellularly. For reduction sensitive nanogel systems, many studies have provided indirect evidence that disulfide bonds are cleaved and encapsulated therapeutic molecules are released intracellularly, as evidenced by significantly enhanced therapeutic efficacy, e.g., cytotoxicity, transfection efficiency, and antigen presentation, etc., in comparison to their non-reducible counterparts. Nevertheless, it should be noted that little is known about the exact intracellular fate of these reduction responsive nanogels, especially within endo/lysosomal compartments, due to the lack of direct evidence of breaking of disulfide bonds. The use of pH responsive nanogels allows endo/lysosomal release of biotherapeutics at low pH and facilitates endo/lysosomal escape for their cytosolic release. Although the effect and mechanism of endo/lysosomal escape is often explained by the proton sponge effect of the pH sensitive materials, detailed understanding is still lacking. Therefore, the further development of responsive delivery systems requires better comprehension of their intracellular trafficking and fate. Moreover, the need for targeting biotherapeutics to specific sites *in vivo* is expected to lead to new design requirements for nanogel delivery systems. With rational design, responsive nanogels are expected to advance biotherapeutics based therapies.

References

1. Leader, B.; Baca, Q. J.; Golan, D. E. Protein therapeutics: a summary and pharmacological classification. *Nat Rev Drug Discov* 2008, 7, 21-39.
2. Torchilin, V. Intracellular delivery of protein and peptide therapeutics. *Drug Discov Today* 2008, 5, e95-e103.
3. Naldini, L. Gene therapy returns to centre stage. *Nature* 2015, 526, 351-360.
4. Amigorena, S.; Savina, A. Intracellular mechanisms of antigen cross presentation in dendritic cells. *Curr Opin Immunol* 2010, 22, 109-117.
5. Sarisozen, C.; Torchilin, V. P. Intracellular delivery of proteins and peptides. *Drug Delivery*, 2016, 576-622.

6. Lächelt, U.; Wagner, E. Nucleic acid therapeutics using polyplexes: A journey of 50 years (and beyond). *Chem Rev* 2015, 115, 11043-11078.
7. Benne, N.; van Duijn, J.; Kuiper, J.; Jiskoot, W.; Slütter, B. Orchestrating immune responses: How size, shape and rigidity affect the immunogenicity of particulate vaccines. *J Control Release* 2016, 234, 124-134.
8. Couvreur, P. Nanoparticles in drug delivery: Past, present and future. *Adv Drug Deliv Rev* 2013, 65, 21-23.
9. Blanco, E.; Shen, H.; Ferrari, M. Principles of nanoparticle design for overcoming biological barriers to drug delivery. *Nat Biotech* 2015, 33, 941-951.
10. Manzoor, A. A.; Lindner, L. H.; Landon, C. D.; Park, J.-Y.; Simnick, A. J.; Dreher, M. R.; Das, S.; Hanna, G.; Park, W.; Chilkoti, A.; Koning, G. A.; ten Hagen, T. L. M.; Needham, D.; Dewhirst, M. W. Overcoming limitations in nanoparticle drug delivery: Triggered, intravascular release to improve drug penetration into tumors. *Cancer Res* 2012, 72, 5566-5575.
11. Saraiva, C.; Praça, C.; Ferreira, R.; Santos, T.; Ferreira, L.; Bernardino, L. Nanoparticle-mediated brain drug delivery: Overcoming blood–brain barrier to treat neurodegenerative diseases. *J Control Release* 2016, 235, 34-47.
12. Kanapathipillai, M.; Brock, A.; Ingber, D. E. Nanoparticle targeting of anti-cancer drugs that alter intracellular signaling or influence the tumor microenvironment. *Adv Drug Deliv Rev* 2014, 79–80, 107-118.
13. Suk, J. S.; Xu, Q.; Kim, N.; Hanes, J.; Ensign, L. M. PEGylation as a strategy for improving nanoparticle-based drug and gene delivery. *Adv Drug Deliv Rev* 2016, 99, Part A, 28-51.
14. Fang, J.; Nakamura, H.; Maeda, H. The EPR effect: Unique features of tumor blood vessels for drug delivery, factors involved, and limitations and augmentation of the effect. *Adv Drug Deliv Rev* 2011, 63, 136-151.
15. Azzopardi, E. A.; Ferguson, E. L.; Thomas, D. W. The enhanced permeability retention effect: a new paradigm for drug targeting in infection. *J Antimicrob Chemother* 2012, 68, 257-274.
16. Xu, S.; Olenyuk, B. Z.; Okamoto, C. T.; Hamm-Alvarez, S. F. Targeting receptor-mediated endocytotic pathways with nanoparticles: Rationale and advances. *Adv Drug Deliv Rev* 2013, 65, 121-138.
17. van der Meel, R.; Vehmeijer, L. J. C.; Kok, R. J.; Storm, G.; van Gaal, E. V. B. Ligand-targeted particulate nanomedicines undergoing clinical evaluation: Current status. *Adv Drug Deliv Rev* 2013, 65, 1284-1298.
18. Danhier, F.; Ansorena, E.; Silva, J. M.; Coco, R.; Le Breton, A.; Préat, V. PLGA-based nanoparticles: An overview of biomedical applications. *J Control Release* 2012, 161, 505-522.
19. Allen, T. M.; Cullis, P. R. Liposomal drug delivery systems: From concept to clinical applications. *Adv Drug Deliv Rev* 2013, 65, 36-48.
20. Liong, M.; Lu, J.; Kovochich, M.; Xia, T.; Ruehm, S. G.; Nel, A. E.; Tamanoi, F.; Zink, J. I.

Multifunctional inorganic nanoparticles for imaging, targeting, and drug delivery. *ACS Nano* 2008, 2, 889-896.

21. Gong, J.; Chen, M.; Zheng, Y.; Wang, S.; Wang, Y. Polymeric micelles drug delivery system in oncology. *J Control Release* 2012, 159, 312-323.
22. Chacko, R. T.; Ventura, J.; Zhuang, J.; Thayumanavan, S. Polymer nanogels: A versatile nanoscopic drug delivery platform. *Adv Drug Delive Rev* 2012, 64, 836-851.
23. Eetezadi, S.; Ekdawi, S. N.; Allen, C. The challenges facing block copolymer micelles for cancer therapy: In vivo barriers and clinical translation. *Adv Drug Deliv Rev* 2015, 91, 7-22.
24. Nochi, T.; Yuki, Y.; Takahashi, H.; Sawada, S.-i.; Mejima, M.; Kohda, T.; Harada, N.; Kong, I. G.; Sato, A.; Kataoka, N.; Tokuhara, D.; Kurokawa, S.; Takahashi, Y.; Tsukada, H.; Kozaki, S.; Akiyoshi, K.; Kiyono, H. Nanogel antigenic protein-delivery system for adjuvant-free intranasal vaccines. *Nat Mater* 2010, 9, 572-578.
25. Peppas, N. A.; Hilt, J. Z.; Khademhosseini, A.; Langer, R. Hydrogels in biology and medicine: from molecular principles to bionanotechnology. *Adv Mater* 2006, 18, 1345-1360.
26. Buwalda, S. J.; Boere, K. W. M.; Dijkstra, P. J.; Feijen, J.; Vermonden, T.; Hennink, W. E. Hydrogels in a historical perspective: From simple networks to smart materials. *J Control Release* 2014, 190, 254-273.
27. Jiang, Y.; Chen, J.; Deng, C.; Suuronen, E. J.; Zhong, Z. Click hydrogels, microgels and nanogels: Emerging platforms for drug delivery and tissue engineering. *Biomaterials* 2014, 35, 4969-4985.
28. Vermonden, T.; Censi, R.; Hennink, W. E. Hydrogels for protein delivery. *Chem Rev* 2012, 112, 2853-2888.
29. Censi, R.; Di Martino, P.; Vermonden, T.; Hennink, W. E. Hydrogels for protein delivery in tissue engineering. *J Control Release* 2012, 161, 680-692.
30. Annabi, N.; Tamayol, A.; Uquillas, J. A.; Akbari, M.; Bertassoni, L. E.; Cha, C.; Camci-Unal, G.; Dokmeci, M. R.; Peppas, N. A.; Khademhosseini, A. 25th Anniversary article: Rational design and applications of hydrogels in regenerative medicine. *Adv Mater* 2014, 26, 85-124.
31. Lee, K. Y.; Mooney, D. J. Hydrogels for tissue engineering. *Chem Rev* 2001, 101, 1869-1880.
32. Sasaki, Y.; Akiyoshi, K. Nanogel engineering for new nanobiomaterials: from chaperoning engineering to biomedical applications. *Chem Rec* 2010, 10, 366-376.
33. Thomann-Harwood, L. J.; Kaeuper, P.; Rossi, N.; Milona, P.; Herrmann, B.; McCullough, K. C. Nanogel vaccines targeting dendritic cells: Contributions of the surface decoration and vaccine cargo on cell targeting and activation. *J Control Release* 2013, 166, 95-105.
34. Zhang, H.; Zhai, Y.; Wang, J.; Zhai, G. New progress and prospects: The application of nanogel in drug delivery. *Mater Sci Eng C* 2016, 60, 560-568.
35. Li, Y.; Maciel, D.; Rodrigues, J.; Shi, X.; Tomás, H. Biodegradable polymer nanogels for drug/nucleic acid delivery. *Chem Rev* 2015, 115, 8564-8608.

36. Wu, H.-Q.; Wang, C. Biodegradable smart nanogels: A new platform for targeting drug delivery and biomedical diagnostics. *Langmuir* 2016, 32, 6211-6225.
37. Soni, K. S.; Desale, S. S.; Bronich, T. K. Nanogels: An overview of properties, biomedical applications and obstacles to clinical translation. *J Control Release*, in press.
38. Zhang, X.; Malhotra, S.; Molina, M.; Haag, R. Micro- and nanogels with labile crosslinks - from synthesis to biomedical applications. *Chem Socy Rev* 2015, 44, 1948-1973.
39. Yang, H.; Wang, Q.; Huang, S.; Xiao, A.; Li, F.; Gan, L.; Yang, X. Smart pH/redox dual-responsive nanogels for on-demand intracellular anticancer drug release. *ACS Appl Mater Interfaces* 2016, 8, 7729-7738.
40. Shirangi, M.; Sastre Toraño, J.; Sellergren, B.; Hennink, W. E.; Somsen, G. W.; van Nostrum, C. F. Methyleneation of peptides by N,N,N,N-tetramethylethylenediamine (TEMED) under conditions used for free radical polymerization: A mechanistic study. *Bioconjug Chem* 2015, 26, 90-100.
41. Cadée, J. A.; van Steenbergen, M. J.; Versluis, C.; Heck, A. J. R.; Underberg, W. J. M.; den Otter, W.; Jiskoot, W.; Hennink, W. E. Oxidation of recombinant human interleukin-2 by potassium peroxodisulfate. *Pharm Res* 2001, 18, 1461-1467.
42. Gregoritza, M.; Goepferich, A. M.; Brandl, F. P. Polyanions effectively prevent protein conjugation and activity loss during hydrogel cross-linking. *J Control Release* 2016, 238, 92-102.
43. Hammer, N.; Brandl, F. P.; Kirchhof, S.; Messmann, V.; Goepferich, A. M. Protein compatibility of selected cross-linking reactions for hydrogels. *Macromol Biosci* 2015, 15, 405-413.
44. Raemdonck, K.; Naeye, B.; Hogset, A.; Demeester, J.; De Smedt, S. C. Biodegradable dextran nanogels as functional carriers for the intracellular delivery of small interfering RNA. *J Control Release* 2010, 148, e95-6.
45. Toita, S.; Sawada, S.-i.; Akiyoshi, K. Polysaccharide nanogel gene delivery system with endosome-escaping function: Co-delivery of plasmid DNA and phospholipase A2. *J Control Release* 2011, 155, 54-59.
46. Raemdonck, K.; Van Thienen, T. G.; Vandenbroucke, R. E.; Sanders, N. N.; Demeester, J.; De Smedt, S. C. Dextran microgels for time-controlled delivery of siRNA. *Adv Func Mater* 2008, 18, 993-1001.
47. Nuhn, L.; Kaps, L.; Diken, M.; Schuppan, D.; Zentel, R. Reductive decationizable block copolymers for stimuli-responsive mRNA delivery. *Macromol Rapid Commun* 2016, 37, 924-933.
48. Nuhn, L.; Braun, L.; Overhoff, I.; Kelsch, A.; Schaeffel, D.; Koynov, K.; Zentel, R. Degradable cationic nanohydrogel particles for stimuli-responsive release of siRNA. *Macromol Rapid Commun* 2014, 35, 2057-2064.
49. Raemdonck, K.; Naeye, B.; Buyens, K.; Vandenbroucke, R. E.; Høgset, A.; Demeester, J.; De

Smedt, S. C. Biodegradable dextran nanogels for RNA interference: Focusing on endosomal escape and intracellular siRNA delivery. *Adv Func Mater* 2009, 19, 1406-1415.

50. Nagahama, K.; Ouchi, T.; Ohya, Y. Biodegradable nanogels prepared by self-assembly of poly(l-lactide)-grafted dextran: Entrapment and release of proteins. *Macromol Biosci* 2008, 8, 1044-1052.
51. Rader, R. A. (Re)defining biopharmaceutical. *Nat Biotech* 2008, 26, 743-751.
52. Kinch, M. S. An overview of FDA-approved biologics medicines. *Drug Discov Today* 2015, 20, 393-398.
53. Fosgerau, K.; Hoffmann, T. Peptide therapeutics: current status and future directions. *Drug Discov Today* 2015, 20, 122-128.
54. Couzin-Frankel, J. Cancer immunotherapy. *Science* 2013, 342, 1432-1433.
55. Manohar, A.; Ahuja, J.; Crane, J. K. Immunotherapy for infectious diseases: Past, present, and future. *Immunol Invest* 2015, 44, 731-737.
56. Chan, A. C.; Carter, P. J. Therapeutic antibodies for autoimmunity and inflammation. *Nat Rev Immunol* 2010, 10, 301-316.
57. Nathan, D. G.; Orkin, S. H. Musings on genome medicine: enzyme-replacement therapy of the lysosomal storage diseases. *Genome Med* 2009, 1, 1-3.
58. Guermonprez, P.; Valladeau, J.; Zitvogel, L.; Thery, C.; Amigorena, S. Antigen presentation and T cell stimulation by dendritic cells. *Annu Rev Immunol* 2002, 20, 621-67.
59. Joffre, O. P.; Segura, E.; Savina, A.; Amigorena, S. Cross-presentation by dendritic cells. *Nat Rev Immunol* 2012, 12, 557-569.
60. Roche, P. A.; Furuta, K. The ins and outs of MHC class II-mediated antigen processing and presentation. *Nat Rev Immunol* 2015, 15, 203-216.
61. Tahara, Y.; Akiyoshi, K. Current advances in self-assembled nanogel delivery systems for immunotherapy. *Adv Drug Deliv Rev* 2015, 95, 65-76.
62. Sahay, G.; Alakhova, D. Y.; Kabanov, A. V. Endocytosis of nanomedicines. *J Control Release* 2010, 145, 182-195.
63. Kou, L.; Sun, J.; Zhai, Y.; He, Z. The endocytosis and intracellular fate of nanomedicines: Implication for rational design. *Asian J Pharm Sci* 2013, 8, 1-10.
64. Shete, H. K.; Prabhu, R. H.; Patravale, V. B. Endosomal Escape: A Bottleneck in Intracellular Delivery. *J Nanosci Nanotechnol* 2014, 14, 460-474.
65. Martens, T. F.; Remaut, K.; Demeester, J.; De Smedt, S. C.; Braeckmans, K. Intracellular delivery of nanomaterials: How to catch endosomal escape in the act. *Nano Today* 2014, 9, 344-364.
66. Varkouhi, A. K.; Scholte, M.; Storm, G.; Haisma, H. J. Endosomal escape pathways for delivery of biologicals. *J Control Release* 2011, 151, 220-228.
67. Ye, Y.; Yu, J.; Gu, Z. Versatile protein nanogels prepared by in situ polymerization. *Macromol*

Chem Physics 2016, 217, 333-343.

68. Soni, G.; Yadav, K. S. Nanogels as potential nanomedicine carrier for treatment of cancer: A mini review of the state of the art. *Saudi Pharm J* 2016, 24, 133-139.
69. Schafer, F. Q.; Buettner, G. R. Redox environment of the cell as viewed through the redox state of the glutathione disulfide/glutathione couple. *Free Radic Biol Med* 2001, 30, 1191-1212.
70. Roberts, M. J.; Bentley, M. D.; Harris, J. M. Chemistry for peptide and protein PEGylation. *Adv Drug Deliv Rev* 2012, 64, Supplement, 116-127.
71. Zhang, S.; Gao, H.; Bao, G. Physical principles of nanoparticle cellular endocytosis. *ACS Nano* 2015, 9, 8655-8671.
72. Yameen, B.; Choi, W. I.; Vilos, C.; Swami, A.; Shi, J.; Farokhzad, O. C. Insight into nanoparticle cellular uptake and intracellular targeting. *J Control Release* 2014, 190, 485-499.
73. Tammam, S. N.; Azzazy, H. M. E.; Lamprecht, A. How successful is nuclear targeting by nanocarriers? *J Control Release* 2016, 229, 140-153.
74. Hwang, C.; Sinskey, A.; Lodish, H. Oxidized redox state of glutathione in the endoplasmic reticulum. *Science* 1992, 257, 1496-1502.
75. Appenzeller-Herzog, C. Glutathione- and non-glutathione-based oxidant control in the endoplasmic reticulum. *J Cell Sci* 2011, 124, 847-855.
76. Brülisauer, L.; Gauthier, M. A.; Leroux, J.-C. Disulfide-containing parenteral delivery systems and their redox-biological fate. *J Control Release* 2014, 195, 147-154.
77. Saito, G.; Swanson, J. A.; Lee, K.-D. Drug delivery strategy utilizing conjugation via reversible disulfide linkages: role and site of cellular reducing activities. *Adv Drug Deliv Rev* 2003, 55, 199-215.
78. Arunachalam, B.; Phan, U. T.; Geuze, H. J.; Cresswell, P. Enzymatic reduction of disulfide bonds in lysosomes: Characterization of a Gamma-interferon-inducible lysosomal thiol reductase (GILT). *Proc Natl Acad Sci* 2000, 97, 745-750.
79. Phan, U. T.; Arunachalam, B.; Cresswell, P. Gamma-interferon-induciblelysosomal thiol reductase (GILT): maturation, activity, and mechanism of action. *J Biol Chem* 2000, 275, 25907-25914.
80. Gainey, D.; Short, S.; McCoy, K. L. Intracellular location of cysteine transport activity correlates with productive processing of antigen disulfide. *J Cell Physiol* 1996, 168, 248-254.
81. Short, S.; Merkel, B. J.; Caffrey, R.; McCoy, K. L. Defective antigen processing correlates with a low level of intracellular glutathione. *Eur J Immunol* 1996, 26, 3015-3020.
82. Dunn, S. S.; Tian, S.; Blake, S.; Wang, J.; Galloway, A. L.; Murphy, A.; Pohlhaus, P. D.; Rolland, J. P.; Napier, M. E.; DeSimone, J. M. Reductively responsive sirna-conjugated hydrogel nanoparticles for gene silencing. *J Am Chem Soc* 2012, 134, 7423-7430.
83. Hong, C. A.; Kim, J. S.; Lee, S. H.; Kong, W. H.; Park, T. G.; Mok, H.; Nam, Y. S. Reductively dissociable sirna-polymer hybrid nanogels for efficient targeted gene silencing. *Adv Func Mater*

2013, 23, 316-322.

84. Li, D.; Kordalivand, N.; Fransen, M. F.; Ossendorp, F.; Raemdonck, K.; Vermonden, T.; Hennink, W. E.; van Nostrum, C. F. Reduction-sensitive dextran nanogels aimed for intracellular delivery of antigens. *Adv Func Mater* 2015, 25, 2993-3003.
85. Watts, J. K.; Deleavey, G. F.; Damha, M. J. Chemically modified siRNA: tools and applications. *Drug Discov Today* 2008, 13, 842-855.
86. Li, R.-Q.; Wu, W.; Song, H.-Q.; Ren, Y.; Yang, M.; Li, J.; Xu, F.-J. Well-defined reducible cationic nanogels based on functionalized low-molecular-weight PGMA for effective pDNA and siRNA delivery. *Acta Biomater* 2016, 41, 282-292.
87. Zhao, M.; Biswas, A.; Hu, B.; Joo, K.-I.; Wang, P.; Gu, Z.; Tang, Y. Redox-responsive nanocapsules for intracellular protein delivery. *Biomaterials* 2011, 32, 5223-5230.
88. Mishina, M.; Minamihata, K.; Moriyama, K.; Nagamune, T. Peptide tag-induced horseradish peroxidase-mediated preparation of a streptavidin-immobilized redox-sensitive hydrogel. *Biomacromolecules* 2016, 17, 1978-1984.
89. Lee, H.; Mok, H.; Lee, S.; Oh, Y. K.; Park, T. G. Target-specific intracellular delivery of siRNA using degradable hyaluronic acid nanogels. *J Control Release* 2007, 119, 245-252.
90. Mok, H.; Park, T. G. PEG-assisted DNA solubilization in organic solvents for preparing cytosol specifically degradable PEG/DNA nanogels. *Bioconjug Chem* 2006, 17, 1369-1372.
91. Shi, B.; Zhang, H.; Qiao, S. Z.; Bi, J.; Dai, S. Intracellular microenvironment-responsive label-free autofluorescent nanogels for traceable gene delivery. *Adv Healthc Mater* 2014, 3, 1839-1848.
92. Shrivats, A. R.; Mishina, Y.; Averick, S.; Matyjaszewski, K.; Hollinger, J. O. In vivo GFP knockdown by cationic nanogel-siRNA polyplexes. *Bioengineering* 2015, 2, 160-175.
93. Novo, L.; van Gaal, E. V. B.; Mastrobattista, E.; van Nostrum, C. F.; Hennink, W. E. Decationized crosslinked polyplexes for redox-triggered gene delivery. *J Control Release* 2013, 169, 246-256.
94. Novo, L.; Rizzo, L. Y.; Golombek, S. K.; Dakwar, G. R.; Lou, B.; Remaut, K.; Mastrobattista, E.; van Nostrum, C. F.; Jahnen-Dechent, W.; Kiessling, F.; Braeckmans, K.; Lammers, T.; Hennink, W. E. Decationized polyplexes as stable and safe carrier systems for improved biodistribution in systemic gene therapy. *J Control Release* 2014, 195, 162-175.
95. Novo, L.; Mastrobattista, E.; van Nostrum, C. F.; Hennink, W. E. Targeted decationized polyplexes for cell specific gene delivery. *Bioconjug Chem* 2014, 25, 802-812.
96. Nguyen, D. H.; Hoon Choi, J.; Ki Joung, Y.; Dong Park, K. Disulfide-crosslinked heparin-pluronic nanogels as a redox-sensitive nanocarrier for intracellular protein delivery. *J Bioact Compat Polym* 2011, 26, 287-300.
97. Choi, J. H.; Jang, J. Y.; Joung, Y. K.; Kwon, M. H.; Park, K. D. Intracellular delivery and anti-cancer effect of self-assembled heparin-Pluronic nanogels with RNase A. *J Control Release*

2010, 147, 420-427.

98. Merkel, B. J.; Mandel, R.; Ryser, H. J.; McCoy, K. L. Characterization of fibroblasts with a unique defect in processing antigens with disulfide bonds. *J Immunol* 1995, 154, 128-36.
99. Pisoni, R. L.; Acker, T. L.; Lisowski, K. M.; Lemons, R. M.; Thoene, J. G. A cysteine-specific lysosomal transport system provides a major route for the delivery of thiol to human fibroblast lysosomes: possible role in supporting lysosomal proteolysis. *J Cell Biol* 1990, 110, 327-335.
100. Nguyen, J.; Bernert, R.; In, K.; Kang, P.; Sebastiao, N.; Hu, C.; Hastings, K. T. Gamma-interferon-inducible lysosomal thiol reductase is upregulated in human melanoma. *Melanoma Res* 2016, 26, 125-137.
101. Xiang, Y.-J.; Guo, M.-M.; Zhou, C.-J.; Liu, L.; Han, B.; Kong, L.-Y.; Gao, Z.-C.; Ma, Z.-B.; Wang, L.; Feng, M.; Chen, H.-Y.; Jia, G.-T.; Gao, D.-Z.; Zhang, Q.; Li, L.; Li, Y.-Y.; Yu, Z.-G. Absence of gamma-interferon-inducible lysosomal thiol reductase (GILT) is associated with poor disease-free survival in breast cancer patients. *PLoS ONE* 2014, 9, e109449.
102. Chen, W.; Zheng, M.; Meng, F.; Cheng, R.; Deng, C.; Feijen, J.; Zhong, Z. In Situ Forming Reduction-sensitive degradable nanogels for facile loading and triggered intracellular release of proteins. *Biomacromolecules* 2013, 14, 1214-1222.
103. Jiang, X.; Wang, X. Cytochrome C-mediated apoptosis. *Annu Rev Biochem* 2004, 73, 87-106.
104. Balce, D. R.; Allan, E. R. O.; McKenna, N.; Yates, R. M. γ-Interferon-inducible lysosomal thiol reductase (GILT) maintains phagosomal proteolysis in alternatively activated macrophages. *J Biol Chem* 2014, 289, 31891-31904.
105. Collins, D. S.; Unanue, E. R.; Harding, C. V. Reduction of disulfide bonds within lysosomes is a key step in antigen processing. *J Immunol* 1991, 147, 4054-9.
106. Jensen, P. E. Antigen unfolding and disulfide reduction in antigen presenting cells. *Semin Immunol* 1995, 7, 347-353.
107. Hastings, K. T.; Cresswell, P. Disulfide reduction in the endocytic pathway: Immunological functions of gamma-interferon-inducible lysosomal thiol reductase. *Antioxid Redox Signal* 2011, 15, 657-668.
108. West, L. C.; Cresswell, P. Expanding roles for GILT in immunity. *Curr Opin Immunol* 2013, 25, 103-108.
109. Li, P.; Luo, Z.; Liu, P.; Gao, N.; Zhang, Y.; Pan, H.; Liu, L.; Wang, C.; Cai, L.; Ma, Y. Bioreducible alginate-poly(ethylenimine) nanogels as an antigen-delivery system robustly enhance vaccine-elicited humoral and cellular immune responses. *J Control Release* 2013, 168, 271-279.
110. Karimi, M.; Eslami, M.; Sahandi-Zangabad, P.; Mirab, F.; Farajisafiloo, N.; Shafaei, Z.; Ghosh, D.; Bozorgomid, M.; Dashkhaneh, F.; Hamblin, M. R. pH-Sensitive stimulus-responsive nanocarriers for targeted delivery of therapeutic agents. *Wiley Interdiscip Rev Nanomed Nanobiotechnol* 2016, 8, 696-716.

111. Kanamala, M.; Wilson, W. R.; Yang, M.; Palmer, B. D.; Wu, Z. Mechanisms and biomaterials in pH-responsive tumour targeted drug delivery: A review. *Biomaterials* 2016, 85, 152-167.
112. Colson, Y. L.; Grinstaff, M. W. Biologically responsive polymeric nanoparticles for drug delivery. *Adv Mater* 2012, 24, 3878-3886.
113. Molina, M.; Asadian-Birjand, M.; Balach, J.; Bergueiro, J.; Miceli, E.; Calderon, M. Stimuli-responsive nanogel composites and their application in nanomedicine. *Chem Soc Rev* 2015, 44, 6161-6186.
114. Zeng, Z.; She, Y.; Peng, Z.; Wei, J.; He, X. Enzyme-mediated in situ formation of pH-sensitive nanogels for proteins delivery. *RSC Adv* 2016, 6, 8032-8042.
115. Morimoto, N.; Hirano, S.; Takahashi, H.; Loethen, S.; Thompson, D. H.; Akiyoshi, K. Self-assembled pH-sensitive cholesteryl pullulan nanogel as a protein delivery vehicle. *Biomacromolecules* 2013, 14, 56-63.
116. Yan, M.; Du, J.; Gu, Z.; Liang, M.; Hu, Y.; Zhang, W.; Priceman, S.; Wu, L.; Zhou, Z. H.; Liu, Z.; Segura, T.; Tang, Y.; Lu, Y. A novel intracellular protein delivery platform based on single-protein nanocapsules. *Nat Nano* 2010, 5, 48-53.
117. Shi, L.; Khondee, S.; Linz, T. H.; Berkland, C. Poly(N-vinylformamide) nanogels capable of pH-sensitive protein release. *Macromolecules* 2008, 41, 6546-6554.
118. Molla, M. R.; Marcinko, T.; Prasad, P.; Deming, D.; Garman, S. C.; Thayumanavan, S. Unlocking a caged lysosomal protein from a polymeric nanogel with a pH trigger. *Biomacromolecules* 2014, 15, 4046-4053.
119. Ahmed, M.; Narain, R. Intracellular delivery of DNA and enzyme in active form using degradable carbohydrate-based nanogels. *Mol Pharm* 2012, 9, 3160-3170.
120. Oishi, M.; Hayashi, H.; Itaka, K.; Kataoka, K.; Nagasaki, Y. pH-Responsive PEGylated nanogels as targetable and low invasive endosomolytic agents to induce the enhanced transfection efficiency of nonviral gene vectors. *Colloid Polym Sci* 2007, 285, 1055-1060.
121. Fleige, E.; Quadir, M. A.; Haag, R. Stimuli-responsive polymeric nanocarriers for the controlled transport of active compounds: Concepts and applications. *Adv Drug Deliv Rev* 2012, 64, 866-884.
122. Mura, S.; Nicolas, J.; Couvreur, P. Stimuli-responsive nanocarriers for drug delivery. *Nat Mater* 2013, 12, 991-1003.
123. Lungwitz, U.; Breunig, M.; Blunk, T.; Göpferich, A. Polyethylenimine-based non-viral gene delivery systems. *Eur J Pharm Biopharm* 2005, 60, 247-266.
124. Boussif, O.; Lezoualc'h, F.; Zanta, M. A.; Mergny, M. D.; Scherman, D.; Demeneix, B.; Behr, J. P. A versatile vector for gene and oligonucleotide transfer into cells in culture and in vivo: polyethylenimine. *Proc Natl Acad Sci USA* 1995, 92, 7297-301.
125. Godbey, W. T.; Wu, K. K.; Mikos, A. G. Poly(ethylenimine) and its role in gene delivery. *J Control Release* 1999, 60, 149-160.

126. Kim, C.; Lee, Y.; Lee, S. H.; Kim, J. S.; Jeong, J. H.; Park, T. G. Self-crosslinked polyethylenimine nanogels for enhanced intracellular delivery of siRNA. *Macromol Res* 2011, 19, 166-171.
127. Khaled, S. Z.; Cevenini, A.; Yazdi, I. K.; Parodi, A.; Evangelopoulos, M.; Corbo, C.; Scaria, S.; Hu, Y.; Haddix, S. G.; Corradetti, B.; Salvatore, F.; Tasciotti, E. One-pot synthesis of pH-responsive hybrid nanogel particles for the intracellular delivery of small interfering RNA. *Biomaterials* 2016, 87, 57-68.
128. Zhang, X.; Zhang, K.; Haag, R. Multi-stage, charge conversional, stimuli-responsive nanogels for therapeutic protein delivery. *Biomater Science* 2015, 3, 1487-1496.
129. Li, Y.; Yang, J.; Xu, B.; Gao, F.; Wang, W.; Liu, W. Enhanced therapeutic sirna to tumor cells by a pH-sensitive agmatine–chitosan bioconjugate. *ACS Appl Mater Interfaces* 2015, 7, 8114-8124.
130. Ferrara, N.; Gerber, H.-P.; LeCouter, J. The biology of VEGF and its receptors. *Nat Med* 2003, 9, 669-676.
131. Drake, C. G.; Lipson, E. J.; Brahmer, J. R. Breathing new life into immunotherapy: review of melanoma, lung and kidney cancer. *Nat Rev Clin Oncol* 2014, 11, 24-37.
132. Blattman, J. N.; Greenberg, P. D. Cancer immunotherapy: A treatment for the masses. *Science* 2004, 305, 200-205.
133. Butterfield, L. H. Cancer vaccines. *The BMJ* 2015, 350, h988.
134. Burgdorf, S.; Kautz, A.; Böhnert, V.; Knolle, P. A.; Kurts, C. Distinct pathways of antigen uptake and intracellular routing in CD4 and CD8 T cell activation. *Science* 2007, 316, 612-616.
135. Vyas, J. M.; Van der Veen, A. G.; Ploegh, H. L. The known unknowns of antigen processing and presentation. *Nat Rev Immunol* 2008, 8, 607-618.
136. Hu, Y.; Litwin, T.; Nagaraja, A. R.; Kwong, B.; Katz, J.; Watson, N.; Irvine, D. J. Cytosolic delivery of membrane-impermeable molecules in dendritic cells using ph-responsive core−shell nanoparticles. *Nano Letters* 2007, 7, 3056-3064.
137. Wang, C.; Li, P.; Liu, L.; Pan, H.; Li, H.; Cai, L.; Ma, Y. Self-adjuvanted nanovaccine for cancer immunotherapy: Role of lysosomal rupture-induced ROS in MHC class I antigen presentation. *Biomaterials* 2016, 79, 88-100.
138. Gialeli, C.; Theocharis, A. D.; Karamanos, N. K. Roles of matrix metalloproteinases in cancer progression and their pharmacological targeting. *FEBS J* 2011, 278, 16-27.
139. Jacob, M. P. Extracellular matrix remodeling and matrix metalloproteinases in the vascular wall during aging and in pathological conditions. *Biomed Pharm* 2003, 57, 195-202.
140. Gurtner, G. C.; Werner, S.; Barrandon, Y.; Longaker, M. T. Wound repair and regeneration. *Nature* 2008, 453, 314-321.
141. Das, S. K.; Hoefler, G. The role of triglyceride lipases in cancer associated cachexia. *Trends Mol Med* 2013, 19, 292-301.
142. McAtee, C. O.; Barycki, J. J.; Simpson, M. A. Chapter One - Emerging roles for hyaluronidase

in cancer metastasis and therapy. *Adv Cancer Res* 2014, 123, 1-34.

143. Shiomi, T.; Lemaître, V.; D'Armiento, J.; Okada, Y. Matrix metalloproteinases, a disintegrin and metalloproteinases, and a disintegrin and metalloproteinases with thrombospondin motifs in non-neoplastic diseases. *Pathol Int* 2010, 60, 477-496.
144. Roth, D.; Piekarek, M.; Paulsson, M.; Christ, H.; Bloch, W.; Krieg, T.; Davidson, J. M.; Eming, S. A. Plasmin Modulates Vascular Endothelial Growth Factor-A-Mediated Angiogenesis during Wound Repair. *Am J Pathol* 2006, 168, 670-684.
145. Wen, J.; Anderson, S. M.; Du, J.; Yan, M.; Wang, J.; Shen, M.; Lu, Y.; Segura, T. Controlled protein delivery based on enzyme-responsive nanocapsules. *Adv Mater* 2011, 23, 4549-4553.
146. Zhu, S.; Nih, L.; Carmichael, S. T.; Lu, Y.; Segura, T. Enzyme-responsive delivery of multiple proteins with spatiotemporal control. *Adv Mater* 2015, 27, 3620-3625.
147. Bernardos, A.; Mondragón, L.; Aznar, E.; Marcos, M. D.; Martínez-Máñez, R.; Sancenón, F.; Soto, J.; Barat, J. M.; Pérez-Payá, E.; Guillem, C.; Amorós, P. Enzyme-responsive intracellular controlled release using nanometric silica mesoporous supports capped with "saccharides". *ACS Nano* 2010, 4, 6353-6368.
148. Lee, J. S.; Groothuis, T.; Cusan, C.; Mink, D.; Feijen, J. Lysosomally cleavable peptide-containing polymersomes modified with anti-EGFR antibody for systemic cancer chemotherapy. *Biomaterials* 2011, 32, 9144-9153.
149. Biswas, A.; Joo, K.-I.; Liu, J.; Zhao, M.; Fan, G.; Wang, P.; Gu, Z.; Tang, Y. Endoprotease-mediated intracellular protein delivery using nanocapsules. *ACS Nano* 2011, 5, 1385-1394.

Chapter 3

Reduction-Sensitive Dextran Nanogels Aimed for Intracellular Delivery of Antigens

Dandan Li [a], Neda Kordalivand [a], Marieke F. Fransen [b], Ferry Ossendorp [b], Koen Raemdonck [c], Tina Vermonden [a], Wim E. Hennink [a] and Cornelus F. van Nostrum [a]

[a]Department of Pharmaceutics, Utrecht Institute for Pharmaceutical Sciences, Utrecht University.
[b]Department of Immunohematology and Blood Transfusion, Leiden University Medical Center.
[c]Laboratory of General Biochemistry and Physical Pharmacy, Ghent University

Advanced Functional Materials, 2015, 25(20): 2993-3003

Abstract: Targeting of antigens to dendritic cells (DCs) to induce strong cellular immune response can be established by loading in a nano-sized carrier and keeping the antigen associated with the particles until they are internalized by DCs. In the present study, a model antigen (ovalbumin, OVA) is immobilized in cationic dextran nanogels via disulfide bonds. These bonds are stable in the extracellular environment but are reduced in the cytosol of DCs due to the presence of glutathione. Reversible immobilization of OVA in the nanogels was demonstrated by the fact that hardly any release of the protein occurred at pH 7 in the absence of glutathione, whereas rapid release of OVA occurred once the nanogels were incubated in buffer with glutathione. Furthermore, these OVA conjugated nanogels showed intracellular release of the antigen in DCs and boost the MHC class I antigen presentation, demonstrating the feasibility of this concept for the aimed intracellular antigen delivery.

1. Introduction

Many peptides and proteins have been used as antigens for the generation of antigen-specific immune responses. Protein antigens are in their soluble form usually safe and well tolerated, however, they induce low levels of immune responses because of their poor uptake by antigen presenting cells.[1-4] A promising strategy to enhance protein and peptide vaccine potency is to incorporate them into particulate carriers.[4-10] Nanoparticulate delivery systems (e.g. liposomes, polymeric carriers) have been used for vaccination, as they offer advantages in many aspects. They protect the antigen against degradation, and encapsulation of antigen in particles results in an increased uptake by dendritic cells (DCs) and delivery of relative large quantities of antigens into DCs.[11, 12] Moreover, particles enable co-delivery of the antigen and an adjuvant.[11, 13] Overall, these features result in an increased immunogenicity of the antigen. A vaccine delivery vehicle needs to be designed to target the immune system, particularly DCs. It has been shown that the size of vaccine delivery systems is a critical parameter affecting immunogenicity. Small nanoparticles (< 200 nm) can after e.g. subcutaneous administration traffic to the draining lymph nodes where they are then internalized by antigen presenting cells (APCs), while large particles (500–2000 nm) are taken up by local APCs at the injection site. However, large particles are predominantly internalized and digested by local macrophages.[14-17] Smaller sized particles (< 500 nm), in particular <50 nm, are taken up more efficiently than large particles by DCs and have better ability to promote $CD8^+$ T-cell immunity, which is crucial for immunotherapy against cancer and viral infectious diseases. In contrast, larger particles (> 500 nm) tend to present antigens to $CD4^+$ T-cells and induce antibody responses for bacterial infectious diseases.[17, 18] Another important factor to enhance the immune response is keeping the antigen encapsulated or associated with the particles until their internalization by DCs and it has been shown that low-burst release is crucial for a strong immune activation.[19]

One of the most attractive nanosized delivery systems for proteins are nanogels because of their 1) tunable chemically or physically crosslinked structures, 2) high water content (resulting in good protein/antigen compatibility) and 3) high loading capacity for water-soluble proteins/peptides.[20, 21] Physically crosslinked gels are mechanically weak and prone to rapid dissociation in the body.[22] Therefore chemically crosslinked nanogels are preferred for drug delivery applications. However, a disadvantage of chemically crosslinked nanogels is the instability of proteins due to exposure to crosslinking agents. This exposure may cause unwanted chemical modification of the protein, or the protein may be grafted to the network, which could lead to incomplete release.[21, 23, 24] To avoid this,

post-loading after nanogel fabrication is a good alternative, however, such approach may suffer from burst or preliminary release before the particles are internalized by cells due to the gel's high water content and often large pore sizes.[25]

Depending on the pH of the medium, above or below the iso-electric point (pI), a protein is electrostatically charged, so it can be post-loaded into oppositely charged nanogels exploiting electrostatic interactions between protein and particle as the driving force, and thereby avoiding protein damage during hydrogel formation.[23, 26, 27] In this work, in order to control the protein release after their uptake by cells, we have designed dextran nanogels in which proteins are reversibly immobilized via disulfide bonds after electrostatically driven post-loading. A designed disulfide-containing linker is used to couple the protein derivatized with succinimidyl S-acetylthioacetate (SATA) groups to the nanogels. This method was recently used by Verheyen et al. with bulk hydrogels and by Matsumoto et al. with nanogels.[28-30] The disulfide bonds between proteins and nanogels are stable in the extracellular environment but are degraded in the cytosol of cells, because of relatively high intracellular levels of glutathione as compared to the extracellular space,[31-35] so that triggered released of the loaded antigen can be achieved after their internalization by DCs (scheme 1). This study focuses on developing antigen-nanogel conjugates, using ovalbumin (OVA) as the model protein antigen, that show triggered release of their payload in a reductive environment.

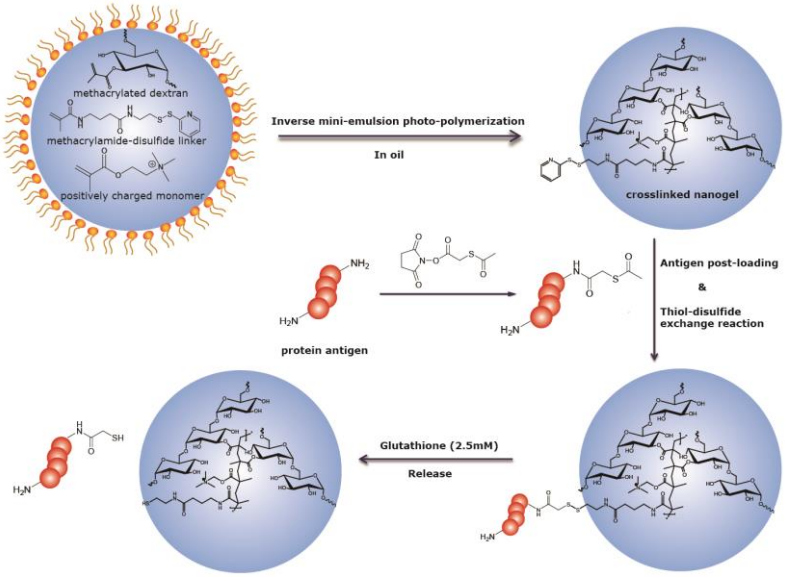

Scheme 1. Schematic representation of the preparation of dextran nanogels and loading/triggered release of protein.

2. Results and Discussion

OVA (43 kDa), due to its pI of 4.9,[36] is negatively charged at pH 7. Therefore cationic dextran nanogels were prepared by inverse mini-emulsion photo-polymerization of methacrylated dextran (dex-MA),[37-39] trimethyl aminoethyl methacrylate (TMAEMA) and a pyridyldisulfide containing methacrylamide monomer (see Scheme 1). Free radical polymerization of the methacrylate groups of dex-MA in aqueous solution provides a stable hydrogel. Dextran gels have been used as protein delivery systems and its biocompatibility has been shown previously.[40] The network density of the formed gel can be tuned by the degree of methacrylate substitution (DS, the number of methacrylate groups per 100 saccharide moieties) of dex-MA and/or by its concentration.[41, 42] Introducing TMAEMA, a cationic methacrylate monomer, provides the nanogels with positive charges while the zeta potential of the nanogel particles depends on the amount of charged monomers per surface area.[43] The charge density of the networks (reflected by the zeta-potential) in turn, influences the absorption behavior of the loaded protein including loading amount and distribution.[26] A specially designed linker containing a methacrylamide unit and a pyridinedisulfide unit was synthesized (scheme 2). This linker was copolymerized with dex-MA and TMAEMA in the nanogel networks to allow subsequent conjugation with thiolated OVA through a thiol-disulfide exchange reaction, so that the modified antigen is chemically linked to the nanogels via disulfide bonds.[29]

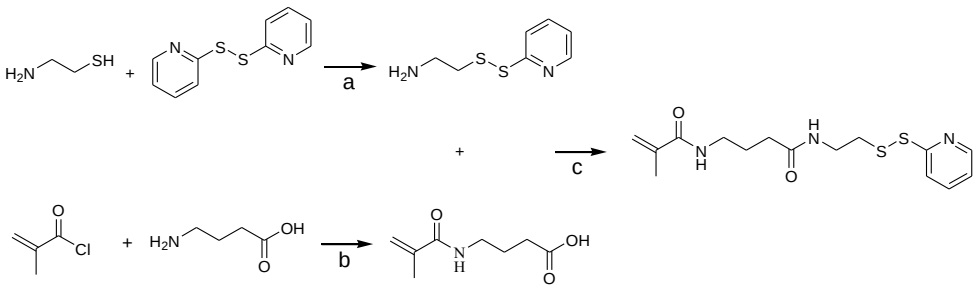

Scheme 2. Synthesis of N-(4-(2-(pyridine-2-yldisulfanyl)ethyl)-amidobutyl) methacrylamide. a) acetic acid, CH_3OH, b) $NaOH/H_2O$, HCl, c) EDC, HOBt, TEA, CH_3Cl.

2.1. Influence of Network density and Surface Charge on OVA Loading

We prepared 8 dextran nanogel formulations with variable network density and zeta potential to investigate the effect of dextran DS, dextran concentration and zeta potential on the OVA loading in nanogels (Table 1). All nanoparticles had a mean particle size around

Table 1. Characterization of nanogels used in this study. Z-average hydrodynamic diameter (Z_{ave}) and zeta potential (before and after OVA loading) of nanogels with variable degree of methacrylate substitution of dextran (DS), content of dex-MA and molar ratio of TMAEMA to MA in dex-MA, and the maximum loading capacity (LC) of OVA for the nanogel formulations. The nanogels were dispersed in HEPES buffer (20 mM, pH 7.4). Mean values with corresponding standard deviations are shown (n=3).

DS	Content[a] (w/w)	TMAEMA : MA	Z_{ave} (nm)	ζ-potential before loading (mV)	Max LC[b] (wt %)	ζ-potential after Max loading (mV)
4	20%	25	203±5	23.0±0.9	74.5±5.5	-3.3±0.7
8	20%	13	186±2	22.4±0.6	75.3±1.9	0.9±0.8
10	20%	10	185±3	22.3±0.3	75.0±3.1	-5.1±0.4
8	25%	13	198±6	22.6±0.4	76.1±1.7	2.2±0.3
8	20%	0	213±8	-0.2±0.1	ND[c]	-0.6±0.1
8	20%	2	193±9	11.6±0.2	39.3±9.5	-3.3±0.2
8	20%	4	180±2	16.3±0.3	60.1±6.2	-5.1±0.4
8	20%	21	207±7	26.2±1.2	80.7±1.6	5.5±0.5

[a] dex-MA/water weight ratio; [b] maximum loading capacity (loaded OVA/dry nanogels plus loaded OVA weight×100%) by measuring the OVA remaining in the supernatant of nanogels suspension when incubated the nanogels with a sufficient amount of OVA; [c] Not detectable, no OVA (within the experimental error) was loaded in the neutral nanogels.

200 nm with a polydispersity index of ~0.15 (dynamic light scattering analysis). The zeta potential of the nanogels increased with increasing feed of TMAEMA and neutral nanogels were prepared without charged monomers. The nanogels were incubated with an OVA solution in HEPES buffer of low ionic strength, and the loading capacity was determined by UPLC analysis of the remaining protein concentration of the supernatant. OVA was not absorbed by the nanogels without TMAEMA because of the lack of electrostatic attraction between the protein and neutral nanogels. In contrast, all cationic nanogels showed rapid absorption and high loading of OVA. It is remarked that loading efficiency reached up to 97% and was similar for different incubation times (1, 24 and 48 hour), demonstrating that OVA could be quantitatively absorbed into the gel network within 1 hour. Table 1 also shows that the zeta potentials of the OVA loaded nanogels were close to zero (from -5 to +5 mV) demonstrating that the protein neutralized the charge of the nanogels. The

maximum loading capacity for each nanogel formulation depended on the charge density of the empty nanogels and accordingly nanogels with higher zeta potential had higher maximum loading capacity (Table 1). The properties of the different nanogel formulations only differed in maximum loading capacity, which illustrates that the mesh size of the gel network is big enough to allow OVA molecules penetration regardless of DS and content of dex-MA. The high maximum loading capacity of these nanogels is likely because of their porous structure, which is also observed for the loading capacity of porous silicon dioxide and porous calcium silicate materials.[44-46] In further experiments, we focused on dextran nanogels prepared using DS 8, 20% w/w dex-MA and 13 molar ratio of TMAEMA to MA in dex-MA.

Table 2. Number of free NH_2 groups and ATA groups after modification of OVA with 0-6 equivalents of SATA (OS_x) determined by the TNBS assay (n=3).

Sample	SATA equivalents/OVA	Free NH_2 groups	ATA groups per OVA
Native	0	11.7 ±0.2	0
OS_2	2	9.7 ±0.7	1.9 ±0.7
OS_4	4	8.9 ±0.4	2.7 ±0.4
OS_6	6	8.4 ±0.0	3.2 ±0.2

2.2. Modification of OVA with SATA

For covalent immobilization of OVA in the gel networks, the antigen was modified with protected thiol functions using SATA[29] for subsequent coupling with the linker present in the particles. OVA has 20 amine groups in the form of lysine units.[47] Varying numbers of thiol groups were introduced by incubating OVA with SATA at different molar ratios (Table 2). It is shown that 12 amine groups were available for modification (TNBS assay), likely because the other 8 lysine residues are deeply buried in the protein.[47] The number of introduced SATA groups was ~3 for both OS_4 and OS_6 (OS_x, where x stands for the equivalents of SATA used), in accordance with the fact that three of the lysine residues are localized on the surface of the protein and are therefore most reactive, while the other amine groups are less accessible and thus less susceptible for derivatization.[47] The structure of the modified protein was investigated by spectral analysis (Figure 1). The UV, circular dichroism and fluorescence spectra of native and modified protein showed no significant differences, which illustrates that neither aggregation nor significant changes in the

secondary and tertiary structure occurred. OS_4 with an average of 2.7 SATA modifications was used for further study.

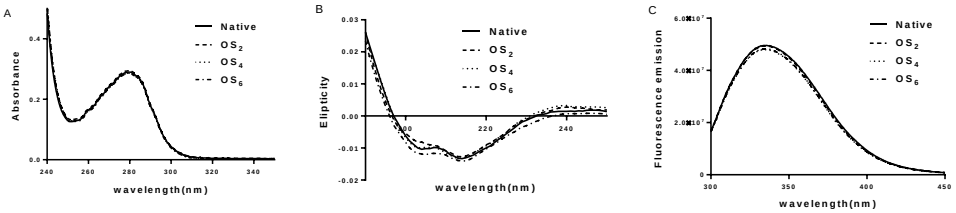

Figure 1. UV-Vis spectra (A), Far-UV CD spectra (B) and fluorescence emission spectra (C) of SATA-modified ova samples (ratio SATA/OVA = 2, 4 and 6). Spectra (average of 3) were taken of OVA samples at a concentration of 0.5 (UV), 0.25 (CD), and 0.1 (FS) mg mL^{-1} in PBS (pH 7.4).

2.3. Preparation of OVA Nanogel Conjugates

Dex-MA nanogels with TMAEMA and different linker contents (linker-containing nanogels, LNG_x, where x stands for the equivalents of linker present in nanogels, i.e. 1-3 linker to OVA equivalents were investigated) were prepared to investigate the efficiency of chemical immobilization of the modified protein. OVA (15 mg dissolved in 7.5 mL HEPES buffer) was mixed with the different nanogels (85 mg freeze dried particles suspended in 42.5 mL HEPES buffer 20 mM, pH 7.4) for loading. Subsequently, a deacetylation solution (hydroxylamine and EDTA in HEPES buffer) was added. As a result, SATA modified proteins were deprotected[48] to allow conjugation of the generated free thiol groups to the linkers in the nanogel networks via a thiol-disulfide exchange reaction. No significant changes in size and zeta potential of nanogels were observed after OVA loading (Table 3), which indicates that no particle aggregation occurred and that the protein was absorbed into the nanoparticles rather than adsorbed on the surface. In this respect it should be noted that substantial lower OVA loadings were applied (~10-14%, see Table 3), which explains the minimal change in zeta potential, in contrast to the previous experiments (Table 1) where loading capacities of ~40-80% were obtained and neutral particles were formed after maximum protein loading. Native OVA that could not be covalently linked to the nanogels because of the absence of free thiol groups, was used in control formulations. Loading efficiencies of 98% native OVA in nanogels with and without linkers were obtained after washing with HEPES buffer (Table 3). This table also shows that when these nanogels were washed with buffer of higher ionic strength (PBS), almost quantitative desorption of the

loaded native protein occurred. Also quantitative loading of the modified OVA in the nanogels occurred. Importantly, after deprotection of the SATA groups (addition of hydroxylamine and EDTA in HEPES buffer) to allow reaction of the formed thiolated protein with the linker, only 28% of the loaded protein was desorbed after washing with PBS. This strongly demonstrates that the protein was indeed covalently linked to the hydrogel network. No significant differences between the loading efficiencies of the three nanogels with different linker contents were observed. For LNG_1, an approximately equivalent number of protein molecules and linker units in the nanogels was present, while for LNG_2 and LNG_3, a two and three-fold excess of linker units was used, respectively. Since OS_4 has around three SATA groups per molecule (Table 2), the SATA/linker molar ratios for these formulations were 3/1, 3/2 and 1/1. By measuring the 2-mercaptopyridine released due to the thiol-disulfide exchange reaction, the percentage of reacted linkers was determined. The linker units present in LNG1 reacted quantitatively with the modified protein, while 87% and 78% were converted for LNG_2 and LNG_3， respectively.

Table 3. Characterization of OVA loaded nanogels. Z-average hydrodynamic diameter (Z_{ave}), zeta potential, loading capacity (LC) and loading efficiency (LE) of OVA-loaded nanogels. The nanogels were dispersed in HEPES buffer (20 mM, pH 7.4). Mean values with corresponding standard deviations are shown (n=3).

Nanogels - OVA	Z_{ave}[a] before loading (nm)	ζ-potential before loading (mV)	LC[b] Washing with HEPES (wt %)	LC[b] Washing with PBS (wt %)	LE[c] (%)	Z_{ave}[a] after loading (nm)	ζ-potential after loading (mV)
LNG_0 - Native	192 ±8	23.7 ±0.6	14.6 ±0.1	1.2 ±0.1	97.4 ±0.6	189 ±9	22.1 ±0.6
LNG_3 - Native	194 ±7	23.4 ±0.4	14.7 ±0.0	1.3 ±0.1	98.1 ±0.1	208 ±6	21.6 ±0.1
LNG_1 - OS_4	186 ±2	23.7 ±0.3	14.6 ±0.1	10.6 ±0.2	70.9 ±1.1	193 ±3	23.2 ±0.7
LNG_2 - OS_4	198 ±5	22.4 ±1.2	14.5 ±0.0	10.7 ±0.1	71.7 ±0.7	202 ±2	22.3 ±0.2
LNG_3 - OS_4	194 ±7	23.4 ±0.4	14.7 ±0.0	10.8 ±0.1	72.1 ±0.5	199 ±1	23.2 ±0.5

[a] Polydispersity index (PDI) was <0.15 for all formulations; [b] Loading capacity (loaded OVA/dry nanogels plus loaded OVA weight ×100%); [c] Loading efficiency (loaded OVA in nanogels/feed OVA weight ×100%). Loading efficiency for the native OVA are the numbers after washing with HEPES buffer, and for the modified OVA are the numbers after washing with PBS.

2.4. In Vitro OVA Release from OVA Loaded Dextran Nanogels

Figure 2 shows that more than 90% of the native OVA desorbed when the gels were dispersed in a buffer of physiological ionic strength (PBS, pH 7.4, 37 ℃). The ionic strength of PBS (167.2 mM) is much higher than that of HEPES buffer (20 mM, which was used for gel preparation and OVA loading), so the release of native OVA was mediated only by increase of the ionic strength of the medium. The nanogels in which modified OVA was immobilized showed a release of very limited amount of protein during 8 h in PBS (<1% of the loading for LNG_2 and LNG_3, <5% for LNG_1) demonstrating that modified OVA was indeed stably covalently linked to the particles. Importantly, after addition of glutathione to a final concentration that corresponds with intracellular levels (2.5 mM),[31] more than 80% of the covalently bound OVA was released within 1 hour as a consequence of the reduction of the disulfide bridges. After 24 h, glutathione was added to a final concentration of 10 mM, causing further release of the remaining 5 to 10% of protein that was still in the gels (Figure 2).

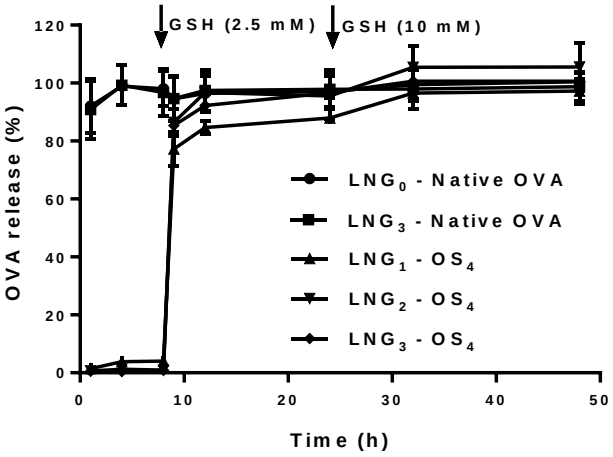

Figure 2. OVA release from dextran nanogels in PBS pH 7.4 at 37 ℃; Glutathione was added to 2.5 mM final concentration at 8h and to 10 mM at 24h. OVA release was measured by UPLC as described in the supporting information.

2.5. Confocal Images of Distribution, Penetration and Release of OVA Dextran Microgels

To visualize the distribution of OVA in dextran gels and release behavior of OVA by fluorescence microscopy, experiments were carried out using FITC-labeled OVA. Because

nanogels are too small for microscopy, neutral and cationic microgels instead of nanogels, with similar network and charge densities, were prepared using a dextran/PEG water-in-water emulsion polymerization method (Table 4).[49, 50] The microparticles had mean sizes of around 4 μm, and the maximum loading capacities were similar to those of the corresponding nanogels. The microgels were incubated with FITC-labeled OVA for 2 h, to obtain OVA loaded microgels with loading capacities of 15 wt%. The samples were analyzed by confocal laser scanning microscopy (CLSM). CLSM images demonstrated that no fluorescence could be detected in the neutral particles that were immersed in an FITC-OVA solution (Figure 3A). In contrast, FITC-OVA was evenly distributed in the different cationic microgels (Figure 3C and D), suggesting that the pore sizes in the different gels are big enough to allow absorption of the protein into the particles.[42]

Table 4. Size, zeta potential and the maximum OVA loading capacity of microgels (n=3).

DS	Content (w/w)	TMAEMA : MA	d[a] (μm)	ζ-potential before loading (mV)	Max LC[b] (wt %)	ζ-potential after Max loading (mV)
4	20%	25	2.89 ±1.58	21.8 ±0.3	78.4 ±8.6	2.5 ±0.4
8	20%	13	3.21 ±1.76	21.2 ±0.6	74.0 ±2.1	-0.6 ±0.5
10	20%	10	2.64 ±1.12	21.3 ±0.7	77.2 ±5.4	2.8 ±0.2
8	25%	13	4.38 ±3.26	22.3 ±0.2	75.0 ±0.1	-0.7 ±0.8
8	20%	0	4.38 ±2.98	-1.1 ±0.2	ND[c]	-3.6 ±0.8
8	20%	2	2.45 ±1.35	11.1 ±0.7	33.8 ±3.8	-1.4 ±0.7
8	20%	4	4.07 ±2.68	16.1 ±0.4	55.7 ±9.3	-3.8 ±0.2
8	20%	21	3.25 ±1.83	25.4 ±0.3	80.0 ±4.4	1.2 ±0.7

[a] Number mean diameter; [b] Maximum loading capacity (loaded OVA/dry microgels plus loaded OVA weight ×100%); [c] Not detectable, no OVA was detected in the neutral microgels.

CLSM images were recorded in time (1 frame/30 s) to visualize the process of OVA penetration into dextran microgels in HEPES buffer (Figure 4A). After addition of FITC-OVA solution to a microgel suspension, fluorescence was already detected in the particles after 30 seconds. The fluorescence increased in time (not shown) and reached a maximum at 5 minutes indicating that the protein was quantitatively absorbed by the

particles. It is further noted that fluorescence was homogenously distributed in the particles demonstrating that the pores in hydrogel network are bigger than the hydrodynamic diameter of the protein. Since in this case FITC-OVA was not covalently linked to the network of particles, addition of PBS buffer led to release of OVA within minutes (Figure 4B).

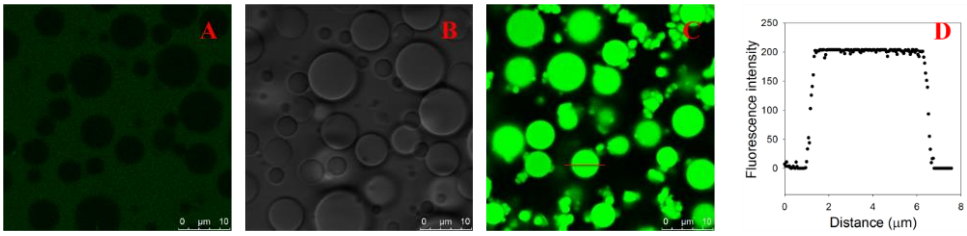

Figure 3. A) CLSM image and B) differential interference contrast image of neutral dextran microgels in FITC-OVA solution. C) CLSM image of OVA loaded cationic dextran microgels (DS 8, 20% w/w, 13 molar ratio TMAEMA, and 15 wt% loading of OVA). D) Corresponding fluorescence intensity profile, plotted along a microgel cross-section indicated by the line in image C.

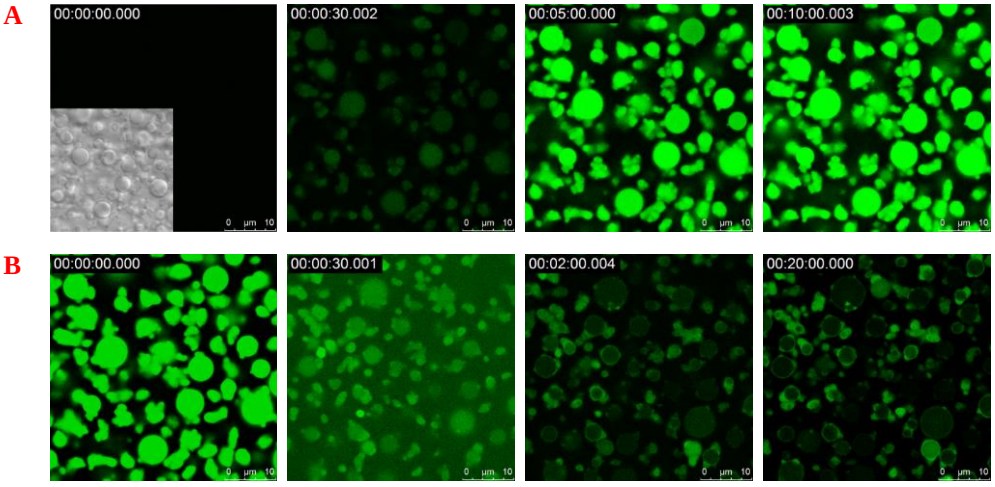

Figure 4. (A) Confocal snapshots of cationic dex-MA microgels (DS 8, 20% w/w, 13 molar ratio TMAEMA) dispersed in a FITC-OVA solution in 20 mM HEPES pH 7.4 at ambient temperature. The images shown (upper panels from left to right) were taken at 0, 30, 300, and 600 s while FITC-OVA was added at 10s. (B) Confocal snapshots of FITC-OVA loaded dex-MA microgels (DS 8.0, 20% w/w, 13 molar ratio TMAEMA) upon addition of PBS at ambient temperature. The images shown (lower panels from left to right) were taken at 0, 30, 120, and 1200 s while PBS was added at 10s.

FITC-OVA was also modified with SATA and conjugated to microgel particles containing the pyridyldisulfide linker. The release behavior was again visualized by CLSM (Figure 5). After addition of PBS to the microgel suspension, no significant decrease in fluorescence intensity was observed demonstrating that the protein remained immobilized in the hydrogel network. However, after addition of glutathione, the fluorescence in the particles substantially dropped within 1 min indicating extremely fast release due to cleavage of the disulfide bonds.

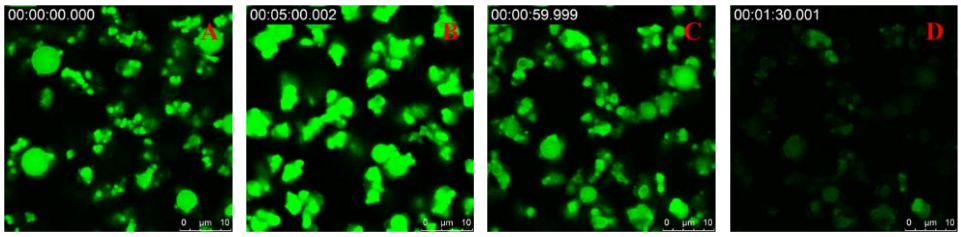

Figure 5. A and B) Confocal snapshots of FITC-OVA microgels conjugate at ambient temperature. The images shown were taken at 0 and 600 s while PBS was added at 10s. After 5 min incubation in PBS, the imaging was stopped. C and D) New snapshots of FITC-OVA microgels conjugate dispersed in PBS was started and the images shown were taken at 60 and 90 s while glutathione (2.5 mM) was added at 40s.

2.6. Intracellular release of OVA from Nanogels in D1 Cells (DCs)

To show the intracellular release of the conjugated OVA, OVA loaded nanogels were double labeled. The nanogels were labeled with Alexa Fluor 488 (AF488), while OVA was labeled with Alexa Fluor 647 (AF647). Confocal images were taken after incubation of the OVA nanogels with D1 cells for 24 h. Cells incubated with OVA conjugate nanogels showed colocalization of the labels on the surface of the cells (yellow, overlap of green and red, in Figure 6A). On the other hand, within the cells only empty nanogels (green) were observed, which indicates that the conjugated OVA was released from the nanogels upon their internalization. It should be noted that no signal was observed for released AF674-OVA likely because the released OVA is diluted in the cells below detection level. However, in some cases, the released OVA had a sufficient high concentration in the cytosol, and the released OVA could be visualized (see supporting information, Figure S1). In contrast, Figure 6B shows only green spots, indicating that the non-conjugated OVA nanogels released the protein before they were taken up by cells. After 24h incubation, neither free OVA nor neutral nanogels were internalized by D1 cells (Figure 6C and D).

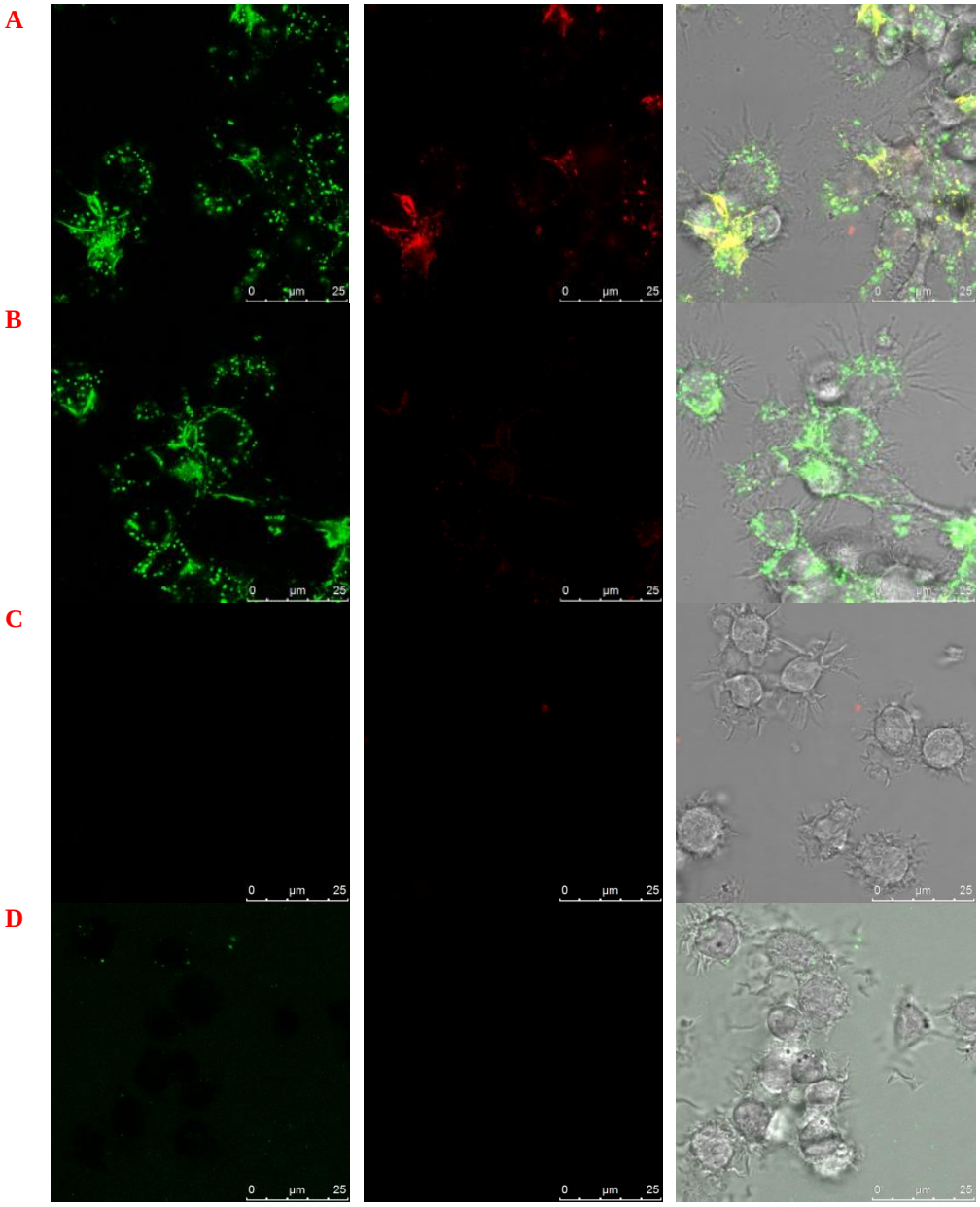

Figure 6. Intracellular release of OVA nanogels was studied by confocal microscopy. The nanogels were labelled with AF488 (green), and AF647 (red) labelled OVA was loaded. D1 dendritic cells were incubated with nanogels for 24h at 37 ℃ and the images were taken (left: AF 488-nanogels, middle: AF647-OVA, right: merged image of AF488, AF647 and differential interference contrast image). A) Conjugated OVA nanogels, B) non-conjugated OVA nanogels, C) free OVA and D) neutral nanogels.

2.7. MHC Class I Antigen Presentation

The ability of OVA conjugated particles for antigen presentation by DCs and subsequent activation of $CD8^+$ T cells was tested in vitro. An MHC class I antigen presentation assay[51] was performed with DC incubated with both OVA nanogels and microgels (Table 5) and compared with soluble OVA and H-2Kb-restricted OVA class I epitope SIINFEKL (the OVA fragment which is presented by the class I MHC molecule[52]). D1 cells were incubated for 24 h with titrated amounts of OVA and particles before $CD8^+$ T cell hybridoma B3Z cells were added, followed by 24 h incubation at 37 ℃. The hybridoma B3Z cells produce β-galactosidase after activation by DCs that present SIINFEKL, thus allowing measurement of MHC class I antigen presentation by a colorimetric assay using chlorophenol red-β-D-galactopyranoside (CPRG). As shown in Figure 7, D1 cells incubated with soluble OVA or a mixture of OVA and empty neutral nanogels were not able to activate T cells, which indicates that free OVA is inefficiently taken up by DCs and/or processed in the MHC class I pathway. In contrast, the OVA nanogel/microgel conjugates showed significantly (a factor of 2.5) higher extent of T cell activation compared to their non-conjugated counterparts, and we showed that OVA nanogels were more efficient in stimulating B3Z $CD8^+$ T cells than microgels. This is presumably because of the smaller size and better uptake of the OVA nanogels by D1 cell[14, 16, 18]. It should be noted that for positively charged nanogels and microgels, the highest concentration of OVA led to lower T cell activation than lower concentrations likely due to cytotoxicity (Figure 8). Therefore, we also included in this study a nanogel preparation with a lower excess of cationic charge (ζ-potential of 12 mV). The extent of T cell activation stimulated by these lowly charged

Table 5. Z-average hydrodynamic diameter (Z_{ave}), polydispersity index (PDI), zeta potential, and loading capacity (LC) of OVA loaded particles used in antigen presentation studies.

OVA loaded particles	Z_{ave}	PDI	ζ-potential (mV)	LC (wt %)
Non-conjugated OVA nanogels	198 ±6 nm	0.13 ±0.02	20.6 ±0.3	11.1 ±0.1
Conjugated OVA nanogels	207 ±3 nm	0.07 ±0.01	20.6 ±0.7	11.7 ±0.1
Conjugated OVA nanogels-Lowly charged	225 ±7 nm	0.12 ±0.04	12.2 ±0.6	10.5 ±0.3
Non-conjugated OVA microgels	2.75 ±1.72 μm		20.8 ±0.7	14.0 ±0.1
Conjugated OVA microgels	2.54 ±2.19 μm		22.3 ±0.2	14.3 ±0.2
Conjugated OVA microgels-Bigger size	8.55 ±8.33 μm		22.4 ±0.1	14.2 ±0.1

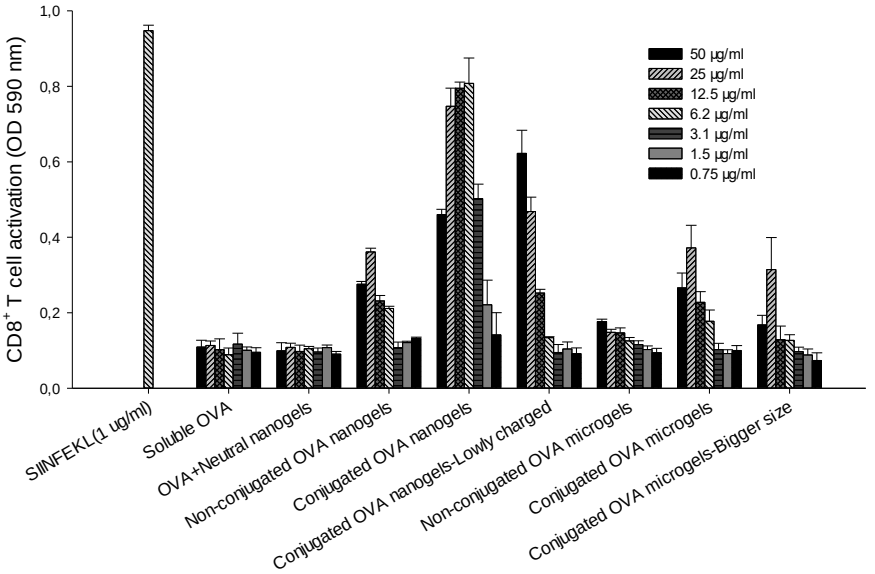

Figure 7. $CD8^+$ T cell activation of SIINFEKL-specific $CD8^+$ T cells (B3Z) after co-culturing with DCs. DCs were incubated with SIINFEKL (1 µg mL^{-1}, positive control), soluble OVA, soluble OVA mixed with empty neutral nanogels and various OVA loaded particles (Table 5) for 24h with titrated amounts of OVA. Data are shown as means of triplicate measurement ± SD. Representative results from one out of three experiments are shown.

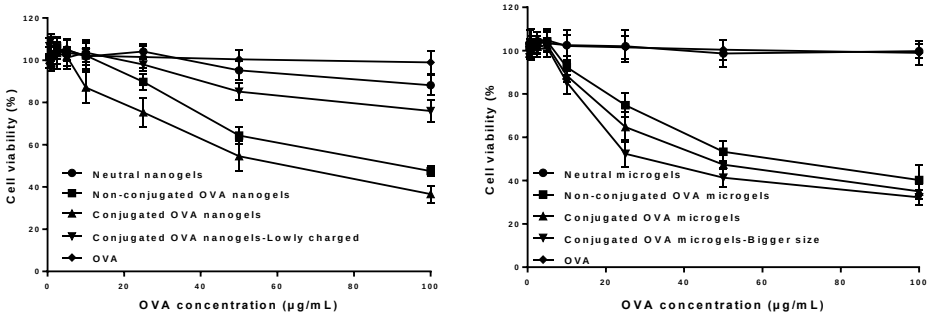

Figure 8. Viability of D1 cells, incubated for 24 h with soluble OVA, neutral particles and OVA loaded particles. The colorimetric reading at 490 nm of non-treated cells was set at 100% and all data are shown as mean ± SD (n=4). Representative results from one out of three experiments are shown. The neutral nano/microgels do not contain OVA. The concentrations of particles were equal to those of the OVA-loaded nano/microgels.

OVA conjugated nanogels did show dose dependency meaning that in the dose range investigated the lowly charged nanogels have a good cytocompatibility and are therefore the preferred formulations. The improved MHC class I antigen presentation by OVA conjugated nanogels demonstrates that a high amount of OVA was delivered and released into the D1 cells and the nanogels facilitated processing and presentation of extracellular antigens in MHC class I molecules to $CD8^+$ T cells (cross-presentation).

3. Conclusion

In conclusion, we have developed dextran nanogels in which a model antigen (OVA) was covalently linked via disulfide bonds. An important advantage of this system is that the protein remained stably entrapped in a non-reducing environment, however triggered and rapid release in the presence of glutathione occurred. Furthermore, high loading capacities were obtained, which enables delivery of large quantities of antigen into DCs to maximize exposure of antigen to the immune system. Finally, these particles show intracellular delivery and release of antigens in DCs and efficiently facilitates the MHC class I antigen cross-presentation. This technology can be broadly applied for encapsulating a wide variety of therapeutics that can be modified with a thiol group, thus making it a promising system for intracellular antigen delivery.

4. Experimental

Synthesis of N-(4-(2-(pyridine-2-yldisulfanyl)ethyl)-amidobutyl) methacrylamide: a) Synthesis of pyridine dithioethylamine hydrochloride: Methanol (25 mL) was used to dissolve 2,2'-dithiodipyridine (11.0 g, 50 mmol, Sigma) and mixed glacial acetic acid (2 mL, 35.0 mmol) under nitrogen. Cysteamine hydrochloride (2.86 g, 25.0 mmol, Sigma) dissolved in 20 mL methanol was added slowly to the mixture. The reaction mixture was stirred for 48 h at room temperature. The product was precipitated by dropping the reaction mixture into cold ether (200 mL), and purified by redissolving in methanol (15 mL) and precipitating in cold ether (200 mL) until a white powder (4.54g, 82% yield) was obtained. b) Synthesis of *N*-methacryloyl aminobutanoic acid: Aminobutyric acid (8.2 g, 80 mmol, Sigma) and NaOH (6.4 g, 160 mmol) were dissolved in water (15 mL) at 0 ^oC. A spatula tip of hydroquinone monomethylether was added to the mixture to prevent polymerization. Next, methacryloyl chloride (8.4 g, 80 mmol, Sigma) was slowly added to the mixture which was subsequently stirred overnight. HCl was added after the reaction to adjust to pH

3. The reaction mixture was extracted three times with chloroform. The combined organic layers were washed with water, dried with $MgSO_4$ and filtered. The filtrate was concentrated by rotary evaporation to obtain the product (11.1 g, 81% yield) as a colourless oil. c) *N*-(4-(2-(pyridine-2-yldisulfanyl)ethyl)-amidobutyl) methacrylamide: Pyridine dithioethylamine hydrochloride (4.0 g, 18 mmol), *N*-methacryloyl aminobutanoic acid (5.8 g, 36 mmol), HoBt (5.8 g, 43 mmol) and TEA (3.5 mL, 26 mmol) were dissolved in dry DCM (70 mL) under nitrogen. The reaction mixture was cooled on ice and EDC (8.1 g, 43 mmol) was subsequently added to the mixture. The reaction mixture was allowed to warm to room temperature and stirred for 24 h. The reaction mixture was washed with 5% $NaHCO_3$ and brine. Most of the solvent was evaporated and the remaining was purified on a silica gel column (ethyl acetate / acetone, 3:2 (v/v), R_f: 0.37). The product (3.4 g, 55% yield) was obtained as a white powder (purity: 99.5%, which is determined by HPLC).

Modification of OVA with succinimidyl S-acetylthioacetate: SATA (10 mg mL^{-1}, dissolved in dry DMSO, Sigma) was added to OVA solutions (2.5 mg mL^{-1}, dissolved in PBS, Serva Electrophoresis GmbH) with molar ratios of 2:1, 4:1 and 6:1. The mixtures were incubated for 30 minutes at room temperature. The modified OVA was dialyzed against distilled water for 24 h at 4℃. The number of modified lysine residues was determined by using the TNBS assay.

Spectral analysis of SATA modified OVA: a) UV-vis absorption spectra of 0.5 mg mL^{-1} native and modified OVA in PBS buffer were measured in the range of 250-350 nm by a Shimadzu UV-2450 UV/Vis spectrophotometer (Shimadzu Corporation, Kyoto, Japan). b) Far UV-CD spectra of 0.25 mg mL^{-1} native and modified OVA in PBS buffer were recorded from 250 to 195 nm by a dual beam DSM 1000 CD spectropolarimeter (On-Line Instruments Systems, Bogart, GA) using cuvettes with a path length of 0.20 mm. c) Fluorescence measurements were carried out with Horiba Fluorolog fluorometer FL3-21 (Horiba Jobin Yvon, Longjumeau Cedex, France). The excitation wavelength was set at 280 nm and the emission spectra were recorded in the range of 300-350 nm. Native and modified OVA were measured at a concentration of 0.1 mg mL^{-1} in PBS at pH 7.4.

Preparation and characterization of empty dextran nanogels: Dex-MA (120 mg) was dissolved in distilled water without or with a known amount of the cationic methacrylate monomer TMAEMA (e.g., 160 µL TMAEMA solution for 13 molar ratio of TMAEMA to dextran formulation, Sigma) and without or with linker solution (e.g., for LNG_3 formulation: 40 µL linker solution of 120 mg mL^{-1} in 50:50 v/v DMSO/H_2O) to a final volume of 360 µL. Subsequently, photoinitiator solution (irgacure 2959, 10mg mL^{-1} in water, 120 µL, Ciba)

was added. This dextran solution was emulsified in the external phase (light mineral oil (Sigma), containing 10% v/v ABIL EM 90 surfactant (Goldschmidt)) by vortexing and ultrasonication for 2 mins (cycle-1, amplitude 60%, Labsonic Tip Sonifier, Braun, Melsungen, Germany). The emulsified nanodroplets were polymerized by UV irradiation (15 minutes, Bluepoint UV source, Hönle UV technology, Germany). The crosslinked nanoparticles were purified by 5 times washing with acetone/hexane (50:50 v/v), then rehydrated and lyophilized (Yield: ~90%). The average size and zeta-potential of the nanogels was measured using DLS (Malvern ALV/CGS-3 Goniometer, Malvern Instruments, Malvern, UK) and Zetasizer (Zetasizer Nano, Malvern instrument, USA). The linker content of nanogels was determined by incubating the nanogels (10 mg) with DTT (5 mM in PBS, 1 mL), and then measuring 2-mercaptopyridine in the supernatant which was cleaved and released from the linker present in nanogels. 2-Mercaptopyridine was determined by HPLC (Waters, USA) equipped with a Sunfire C18 column 5 μm (4.6×150 mm) (Waters) and tunable ultraviolet/visible light detector (Waters) set at 280 nm. A gradient elution was applied with mobile phase A being a 10% ACN aqueous solution and mobile phase B being 100% ACN. The gradient was from 100% to 60% mobile phase A over a period of 6 min with a flow rate of 1 mL min^{-1}. The 2-mercaptopyridine calibration curve was linear between 1 and 50 μg mL^{-1}.

Preparation and characterization of empty dextran microgels: PEG (2.77 g), dex-MA (81.6 mg), known amounts of TMAEMA and linker solutions (500 mg mL^{-1} in DMSO) were added in HEPES buffer (100 mM pH 7.4) to final 20 g in a 50 mL tube. The mixture was flushed with nitrogen and vortexed for 2 minute at maximum intensity. A water-in-water emulsion was formed and then allowed to stabilize for 10 min. Next, a sodium bisulfite solution (720 μL, 20 mg mL^{-1}) and a KPS solution (720 μL, 50 mg mL^{-1}) were added to the mixture. The formed droplets were allowed to crosslink overnight at room temperature. The polymerized particles were purified by 3 times washing with water and then lyophilized (Yield: ~80%). The particle size distribution and zeta-potential of the microgels were measured using AccuSizer (PSS-Nicomp, Sta Barbara, CA, USA) and Zetasizer (see above), respectively. The linker content was determined by HPLC as described in the previous paragraph.

Determination of loading capacity and loading efficiency of the gels: The concentration of OVA solution was fixed at 2 mg mL^{-1} in 20 mM HEPES buffer pH 7.4. Different nanogels/microgels suspensions (0.5 mg mL^{-1} in 20 mM HEPES buffer, pH 7.4) were mixed with this OVA solution at a volume ratio of 1:1. Samples were taken at different time points (1h, 24h and 48h) and the particles were centrifuged at 15,000 rmp for 60 min

(nanogels) or 30 min (microgels). The concentration of OVA in the supernatant was measured by BCA protein assay (25-2000 μg mL^{-1}). Loading capacity (LC) and loading efficiency (LE) were calculated as follows: LC= loaded OVA / dry nanogels plus loaded OVA weight *100% and LE= loaded OVA in particles / feed OVA weight *100%.

Preparation and characterization of 15 wt% OVA loaded nanogels/microgels: OVA solution (native or SATA modified, FITC-labeled or non-labeled, 2 mg mL^{-1}, 7.5 mL) was mixed with particles suspension (without or with varying amount of linker, 2 mg mL^{-1}, 42.5 mL) in HEPES buffer (20 mM, pH 7.4). The mixture was incubated at room temperature for 1 hour to allow OVA loading into the particles. Subsequently, a deacetylation solution (1.72 g hydroxylamine 50% water solution, 0.365 g EDTA in 50 mL HEPES buffer, 5 mL) was added and the mixture was incubated for 2 h. The OVA loaded particles were collected and purified by multiple washing and centrifugation steps (thrice with PBS for modified OVA or with HEPES buffer for native OVA, 60 min, 15,000 rpm), and then lyophilized (Yield: ~70% for nanogels and ~80% for microgels). The size and zeta-potential of the nanogels/microgels before and after OVA loading were measured by DLS/AccuSizer and Zetasizer as described above. The loading capacity and loading efficiency were determined by measuring the OVA concentration in the washing fluids with a UPLC system (Waters, USA) equipped with an Acquity BEH C4 column 1.7 μm (2.1×50 mm) (Waters) and a fluorescence detector (FLR, Waters). The mobile phase consisted of 0.1% TFA in 10% ACN aqueous (mobile phase A) and 0.1% TFA in 100% ACN (mobile phase B). The gradient elution was from 100% to 70% mobile phase A in 5 min. The flow rate was 0.25 mL min^{-1} and the analyses were performed at 50 ± 1 ℃. The OVA calibration curve was linear between 10 and 1000 μg mL^{-1}.

In vitro OVA release from OVA loaded dextran nanogels: OVA loaded nanogels were dispersed in PBS (150 mM, pH 7.4) to 4 mg mL^{-1}. Glutathione was added at 8 h at a concentration of 2.5 mM and again at 24 h to a final concentration of 10 mM for triggered release of conjugated OVA. The release of OVA was monitored at 37℃ by taking samples at different time points, spinning down the particles (60 min, 15,000 rpm) and analyzing the supernatant for OVA concentration (see previous paragraph).

Confocal images of distribution, penetration and release of OVA dextran microgels: a) Microgels were incubated with FITC-labeled OVA (Invirogen) for 24h and confocal images were taken by confocal laser scanning microscopy (CLSM, Confocal Leica SPE-II, Leica Microsystems, Wetzlar, Germany). b) FITC-labeled OVA (0.25 mg mL^{-1}, 15 μL) was added to empty dextran microgel suspensions (0.25 mg mL^{-1}, 85 μL) in 20 mM HEPES buffer

(pH 7.4) and immediately visualized with CLSM (1 frame/30 s) to record OVA penetration into the dextran microgels. c) Release of FITC-OVA (non-conjugated and conjugated to the microgels) was monitored via CLSM. First, the loaded particles were dispersed in 20 mM HEPES buffer (0.25 mg mL^{-1}, 100 μL), then PBS (100 μL) and glutathione (up to a concentration of 2.5 mM) were added subsequently. Confocal micrographs were taken every 30 s.

Cell lines and Culture Conditions: D1 cells, a long-term growth factor-dependent immature myeloid dendritic cell line of splenic origin derived from a female C57BL/6 mouse, was cultured. Culture medium was IMDM (Lonza) containing 10% heat-inactivated FBS (Sigma), 2 mM GlutaMax (GIBCO), 50 μM β-mecaptoethanol (in IMDM) and fibroblast supernatant (SN) from NIH/3T3 cells which was collected from confluent cultures and filtered. B3Z cells, a T cell hybridoma expressing a T-cell receptor that specifically recognizes H-2Kb-restricted OVA MHC class I epitope SIINFEKL which carries a lacZ construct, was cultured. Culture medium was IMDM containing 10% heat-inactivated FBS, 2 mM GlutaMax, 50 μM β-mecaptoethanol (in IMDM).

Cytosolic release of OVA from nanogels: OVA loaded nanogels were double labeled. The dextran nanogels were labeled with Alexa Fluor 488 dye (Invitrogen), while Alexa Fluor 647 labeled OVA (commercially available from Invitrogen) was modified with SATA and loaded in the nanogels. D1 cells were incubated with OVA loaded nanogels at final OVA concentration of 5 μg mL^{-1} for 24 h at 37 ℃. Subsequently, confocal images were taken by CLSM.

MHC class I antigen presentation assay: D1 cells (50,000 cells/well) in a 96-well plate were incubated with H-2Kb-restricted OVA class I epitope SIINFEKL, soluble OVA, soluble OVA with empty neutral nanogels and various OVA loaded nanogel/microgel formulations at titrated amounts of OVA for 24 h at 37 ℃. Subsequently, B3Z cells (50,000 cells/well) were added to D1 cells and co-incubated with D1 cells for 24 h at 37 ℃. The hybridoma B3Z cells produces β-galactosidase after being activated by DCs that present SIINFEKL, thus allowing measurement of MHC class I antigen presentation by a colorimetric assay using CPRG. β-Galactosidase activity of B3Z cells was measured by incubating the cells with 100 μL of CPRG buffer for 1 h. The β-galactosidase converted the yellow-orange substrate CPRG into the red chromophore chlorophenol red absorbing at 590 nm, and the absorbance was read by SPECTROstar (BMG Labtech, Germany).

Cytotoxicity of nanogels/microgels towards D1 cells: D1 cells (50,000 cells/well) in a 96-well plate were incubated with soluble OVA, empty neutral nanogels/microgels and

various OVA loaded nanogel/microgel formulations at titrated amounts of OVA for 24 h at 37 ℃. The relative cell viability was quantified by CellTiter 96 AQueous One Solution Cell Proliferation Assay (Promega).

References

1. Kang, T. H.; Monie, A.; Wu, L. S. F.; Pang, X.; Hung, C.-F.; Wu, T. C. Enhancement of protein vaccine potency by in vivo electroporation mediated intramuscular injection. *Vaccine* 2011, 29, 1082-1089.
2. Perrie, Y.; Mohammed, A. R.; Kirby, D. J.; McNeil, S. E.; Bramwell, V. W. Vaccine adjuvant systems: enhancing the efficacy of sub-unit protein antigens. *Int J Pharm* 2008, 364, 272-80.
3. Houghton, A. N.; Gold, J. S.; Blachere, N. E. Immunity against cancer: lessons learned from melanoma. *Curr Opin Immunol* 2001, 13, 134-140.
4. De Temmerman, M.-L.; Rejman, J.; Demeester, J.; Irvine, D. J.; Gander, B.; De Smedt, S. C. Particulate vaccines: on the quest for optimal delivery and immune response. *Drug Discov Today* 2011, 16, 569-582.
5. Heo, M. B.; Lim, Y. T. Programmed nanoparticles for combined immunomodulation, antigen presentation and tracking of immunotherapeutic cells. *Biomaterials* 2014, 35, 590-600.
6. Thomann-Harwood, L. J.; Kaeuper, P.; Rossi, N.; Milona, P.; Herrmann, B.; McCullough, K. C. Nanogel vaccines targeting dendritic cells: Contributions of the surface decoration and vaccine cargo on cell targeting and activation. *J Control Release* 2013, 166, 95-105.
7. Gregory, A. E.; Titball, R.; Williamson, D. Vaccine delivery using nanoparticles. *Front Cell Infect Microbiol* 2013, 3, 13.
8. Zhang, Z.; Tongchusak, S.; Mizukami, Y.; Kang, Y. J.; Ioji, T.; Touma, M.; Reinhold, B.; Keskin, D. B.; Reinherz, E. L.; Sasada, T. Induction of anti-tumor cytotoxic T cell responses through PLGA-nanoparticle mediated antigen delivery. *Biomaterials* 2011, 32, 3666-3678.
9. De Koker, S.; Lambrecht, B. N.; Willart, M. A.; van Kooyk, Y.; Grooten, J.; Vervaet, C.; Remon, J. P.; De Geest, B. G. Designing polymeric particles for antigen delivery. *Chem Soc Rev* 2011, 40, 320-339.
10. De Geest, B. G.; Willart, M. A.; Hammad, H.; Lambrecht, B. N.; Pollard, C.; Bogaert, P.; De Filette, M.; Saelens, X.; Vervaet, C.; Remon, J. P.; Grooten, J.; De Koker, S. Polymeric multilayer capsule-mediated vaccination induces protective immunity against cancer and viral infection. *ACS Nano* 2012, 6, 2136-49.
11. Pattani, A.; Patravale, V. B.; Panicker, L.; Potdar, P. D. Immunological Effects and Membrane Interactions of Chitosan Nanoparticles. *Mol Pharm* 2009, 6, 345-352.
12. Dierendonck, M.; Fierens, K.; De Rycke, R.; Lybaert, L.; Maji, S.; Zhang, Z.; Zhang, Q.; Hoogenboom, R.; Lambrecht, B. N.; Grooten, J.; Remon, J. P.; De Koker, S.; De Geest, B. G.

Nanoporous hydrogen bonded polymeric microparticles: facile and economic production of cross presentation promoting vaccine carriers. *Adv Func Mater* 2014, 24, 4634-4644.

13. Akagi, T.; Wang, X.; Uto, T.; Baba, M.; Akashi, M. Protein direct delivery to dendritic cells using nanoparticles based on amphiphilic poly(amino acid) derivatives. *Biomaterials* 2007, 28, 3427-3436.
14. Xiang, S. D.; Scholzen, A.; Minigo, G.; David, C.; Apostolopoulos, V.; Mottram, P. L.; Plebanski, M. Pathogen recognition and development of particulate vaccines: Does size matter? *Methods* 2006, 40, 1-9.
15. Manolova, V.; Flace, A.; Bauer, M.; Schwarz, K.; Saudan, P.; Bachmann, M. F. Nanoparticles target distinct dendritic cell populations according to their size. *Eur J Immunol* 2008, 38, 1404-1413.
16. Foged, C.; Brodin, B.; Frokjaer, S.; Sundblad, A. Particle size and surface charge affect particle uptake by human dendritic cells in an in vitro model. *Int J Pharm* 2005, 298, 315-322.
17. Fifis, T.; Gamvrellis, A.; Crimeen-Irwin, B.; Pietersz, G. A.; Li, J.; Mottram, P. L.; McKenzie, I. F.; Plebanski, M. Size-dependent immunogenicity: therapeutic and protective properties of nano-vaccines against tumors. *J Immunol* 2004, 173, 3148-54.
18. Joshi, V. B.; Geary, S. M.; Salem, A. K. Biodegradable particles as vaccine delivery systems: size matters. *AAPS J* 2013, 15, 85-94.
19. Silva, A. L.; Rosalia, R. A.; Sazak, A.; Carstens, M. G.; Ossendorp, F.; Oostendorp, J.; Jiskoot, W. Optimization of encapsulation of a synthetic long peptide in PLGA nanoparticles: Low-burst release is crucial for efficient CD8+ T cell activation. *Eur J Pharm Biopharm* 2013, 83, 338-345.
20. Sasaki, Y.; Akiyoshi, K. Nanogel engineering for new nanobiomaterials: From chaperoning engineering to biomedical applications. *Chemical Record* 2010, 10, 366-376.
21. Vermonden, T.; Censi, R.; Hennink, W. E. Hydrogels for Protein Delivery. *Chem Rev* 2012, 112, 2853-2888.
22. Kearney, C. J.; Mooney, D. J. Macroscale delivery systems for molecular and cellular payloads. *Nat Mater* 2013, 12, 1004-1017.
23. Valdebenito, A.; Espinoza, P.; Lissi, E. A.; Encinas, M. V. Bovine serum albumin as chain transfer agent in the acrylamide polymerization. Protein-polymer conjugates. *Polymer* 2010, 51, 2503-2507.
24. Cadee, J. A.; van Steenbergen, M. J.; Versluis, C.; Heck, A. J.; Underberg, W. J.; den Otter, W.; Jiskoot, W.; Hennink, W. E. Oxidation of recombinant human interleukin-2 by potassium peroxodisulfate. *Pharm Res* 2001, 18, 1461-7.
25. Huang, X.; Brazel, C. S. On the importance and mechanisms of burst release in matrix-controlled drug delivery systems. *J Control Release* 2001, 73, 121-136.
26. Schillemans, J. P.; Verheyen, E.; Barendregt, A.; Hennink, W. E.; Van Nostrum, C. F. Anionic and cationic dextran hydrogels for post-loading and release of proteins. *J Control Release* 2011,

150, 266-271.

27. Lin, C.-C.; Metters, A. T. Hydrogels in controlled release formulations: Network design and mathematical modeling. *Adv Drug Delivery Rev* 2006, 58, 1379-1408.
28. Verheyen, E.; van der Wal, S.; Deschout, H.; Braeckmans, K.; de Smedt, S.; Barendregt, A.; Hennink, W. E.; van Nostrum, C. F. Protein macromonomers containing reduction-sensitive linkers for covalent immobilization and glutathione triggered release from dextran hydrogels. *J Control Release* 2011, 156, 329-336.
29. Verheyen, E.; Delain-Bioton, L.; van der Wal, S.; el Morabit, N.; Barendregt, A.; Hennink, W. E.; van Nostrum, C. F. Conjugation of Methacrylamide Groups to a Model Protein via a Reducible Linker for Immobilization and Subsequent Triggered Release from Hydrogels. *Macromol Biosci* 2010, 10, 1517-1526.
30. Matsumoto, N. M.; Gonzalez-Toro, D. C.; Chacko, R. T.; Maynard, H. D.; Thayumanavan, S. Synthesis of Nanogel-Protein Conjugates. *Polym Chem* 2013, 4, 2464-2469.
31. Meister, A.; Anderson, M. E. Glutathione. *Annu Rev Biochem* 1983, 52, 711-760.
32. Jones, D. P.; Carlson, J. L.; Samiec, P. S.; Sternberg Jr, P.; Mody Jr, V. C.; Reed, R. L.; Brown, L. A. S. Glutathione measurement in human plasma: Evaluation of sample collection, storage and derivatization conditions for analysis of dansyl derivatives by HPLC. *Clin Chimi Acta* 1998, 275, 175-184.
33. Meng, F.; Hennink, W. E.; Zhong, Z. Reduction-sensitive polymers and bioconjugates for biomedical applications. *Biomaterials* 2009, 30, 2180-2198.
34. Brülisauer, L.; Gauthier, M. A.; Leroux, J.-C. Disulfide-containing parenteral delivery systems and their redox-biological fate. *J Control Release* 2014, 195, 147-154.
35. Brulisauer, L.; Kathriner, N.; Prenrecaj, M.; Gauthier, M. A.; Leroux, J. C. Tracking the bioreduction of disulfide-containing cationic dendrimers. *Angew Chem Int Ed Engl* 2012, 51, 12454-8.
36. Kidwai, S. A.; Ansari, A. A.; Salahuddin, A. Effect of succinylation (3-carboxypropionylation) on the conformation and immunological activity of ovalbumin. *Biochem J* 1976, 155, 171-80.
37. van Dijk-Wolthuis, W. N. E.; Franssen, O.; Talsma, H.; van Steenbergen, M. J.; Kettenes-van den Bosch, J. J.; Hennink, W. E. Synthesis, Characterization, and Polymerization of Glycidyl Methacrylate Derivatized Dextran. *Macromolecules* 1995, 28, 6317-6322.
38. van Dijk-Wolthuis, W. N. E.; Hoogeboom, J. A. M.; van Steenbergen, M. J.; Tsang, S. K. Y.; Hennink, W. E. Degradation and Release Behavior of Dextran-Based Hydrogels. *Macromolecules* 1997, 30, 4639-4645.
39. van Dijk-Wolthuis, W. N. E.; Kettenes-van den Bosch, J. J.; van der Kerk-van Hoof, A.; Hennink, W. E. Reaction of Dextran with Glycidyl Methacrylate: An Unexpected Transesterification. *Macromolecules* 1997, 30, 3411-3413.
40. Cadee, J. A.; van Luyn, M. J.; Brouwer, L. A.; Plantinga, J. A.; van Wachem, P. B.; de Groot, C.

J.; den Otter, W.; Hennink, W. E. In vivo biocompatibility of dextran-based hydrogels. *J Biomed Mater Res* 2000, 50, 397-404.

41. Zhang, X.; Wu, D.; Chu, C.-C. Synthesis and characterization of partially biodegradable, temperature and pH sensitive Dex–MA/PNIPAAm hydrogels. *Biomaterials* 2004, 25, 4719-4730.
42. Stenekes, R. J. H.; De Smedt, S. C.; Demeester, J.; Sun, G.; Zhang, Z.; Hennink, W. E. Pore Sizes in Hydrated Dextran Microspheres. *Biomacromolecules* 2000, 1, 696-703.
43. Raemdonck, K.; Naeye, B.; Buyens, K.; Vandenbroucke, R. E.; Høgset, A.; Demeester, J.; De Smedt, S. C. Biodegradable Dextran Nanogels for RNA Interference: Focusing on Endosomal Escape and Intracellular siRNA Delivery. *Adv Func Mater* 2009, 19, 1406-1415.
44. Ito, Y.; Kusawake, T.; Ishida, M.; Tawa, R.; Shibata, N.; Takada, K. Oral solid gentamicin preparation using emulsifier and adsorbent. *J Control Release* 2005, 105, 23-31.
45. Wu, W.; Wang, Y.; Que, L. Enhanced bioavailability of silymarin by self-microemulsifying drug delivery system. *Eur J Pharm Biopharm* 2006, 63, 288-294.
46. Ito, Y.; Arai, H.; Uchino, K.; Iwasaki, K.; Shibata, N.; Takada, K. Effect of adsorbents on the absorption of lansoprazole with surfactant. *Int J Pharm* 2005, 289, 69-77.
47. Steven, F. S.; Tristram, G. R. The reactivity of free amino groups in native and denatured ovalbumin towards fluorodinitrobenzene. *Biochem J* 1958, 70, 179-82.
48. Duncan, R. J. S.; Weston, P. D.; Wrigglesworth, R. A new reagent which may be used to introduce sulfhydryl groups into proteins, and its use in the preparation of conjugates for immunoassay. *Anal Biochem* 1983, 132, 68-73.
49. Franssen, O.; Hennink, W. E. A novel preparation method for polymeric microparticles without the use of organic solvents. *Int J Pharm* 1998, 168, 1-7.
50. Stenekes, R. J.; Franssen, O.; van Bommel, E. M.; Crommelin, D. J.; Hennink, W. E. The preparation of dextran microspheres in an all-aqueous system: effect of the formulation parameters on particle characteristics. *Pharm Res* 1998, 15, 557-61.
51. Karttunen, J.; Sanderson, S.; Shastri, N. Detection of rare antigen-presenting cells by the lacZ T-cell activation assay suggests an expression cloning strategy for T-cell antigens. *Proc Natl Acad Sci* 1992, 89, 6020-6024.
52. Heemels, M. T.; Ploegh, H. Generation, translocation, and presentation of MHC class I-restricted peptides. *Annu Rev Biochem* 1995, 64, 463-91.

Supporting Information

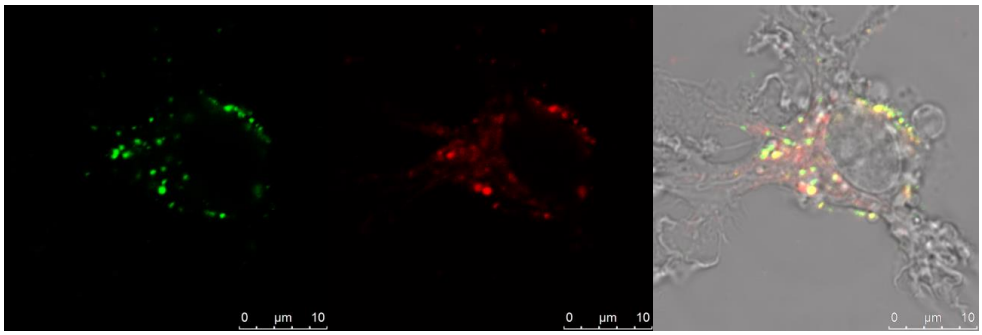

Figure S1. Intracellular release of conjugated OVA nanogels. The nanogels were labelled with AF488 (green), and AF647 (red) labelled OVA was loaded. D1 dendritic cells were incubated with nanogels for 24h at 37 ℃ and the images were taken (left: AF 488-nanogels, middle: AF647-OVA, right: merged image of AF488, AF647 and differential interference contrast image).

Chapter 4

Strong in vivo antitumor responses induced by antigen immobilized in nanogels via reducible bonds

Dandan Li [a], Feilong Sun [a], Meriem Bourajjaj [a], Yinan Chen [a], Ebel H. Pieters [a], Jian Chen [a], Joep B. van den Dikkenberg [a], Bo Lou [a], Marcel G. M. Camps [b], Ferry Ossendorp [b], Wim E. Hennink [a], Tina Vermonden [a], and Cornelus F. van Nostrum [a]

[a]Department of Pharmaceutics, Utrecht Institute for Pharmaceutical Sciences, Utrecht University. [b]Department of Immunohematology and Blood Transfusion, Leiden University Medical Center.

Nanoscale, 2016, DOI: 10.1039/C6NR05583D

Abstract: Cancer vaccines are at present mostly based on tumor associated protein antigens but fail to elicit strong cell-mediated immunity in their free form. For protein-based vaccines, the main challenges to overcome are the delivery of sufficient proteins into the cytosol of dendritic cells (DCs), the processing by, and the presentation through the MHC class I pathway. Recently, we developed a cationic dextran nanogel in which a model antigen (ovalbumin, OVA) is reversibly conjugated via disulfide bonds to the nanogel network to enable redox-sensitive intracellular release. In the present study, it is demonstrated that these nanogels, with the bound OVA, were efficiently internalized by DCs and capable to maturate them. On the other hand, when the antigen was just physically entrapped in the nanogels, OVA was prematurely released before the particles were taken up by cells. When combined with an adjuvant (polyinosinic-polycytidylic acid, poly(I:C)), nanogels with conjugated OVA induced strong protective and curative effect against melanoma in vivo. In a prophylactic vaccination setting, 90% of the mice vaccinated with nanogels with conjugated OVA + poly(I:C) did not develop a tumor. Moreover, in a therapeutic model, 40% of the mice cleared their established tumors and survived for the duration of the experiment (80 days) while the remaining mice showed substantial delay of tumor progression. In conclusion, our results demonstrate that conjugation of antigens to nanogels via reducible covalent bonds for intracellular delivery is a promising strategy to induce effective antigen-specific immune responses against cancer.

1. Introduction

With increasing interests of immunotherapy as a potential strategy against cancers, specific subunits, such as protein antigens, are used to develop safe and well-defined vaccines.[1-3] Moreover, these subunits are suited for GMP production. However, because of their poor immunogenicity, these protein antigens on their own often evoke weak and short-lived humoral and cellular immune responses, and particularly fail to elicit a $CD8^+$ cytotoxic T cell response.[4-7] Currently, there is still a lack of efficacious vaccines against many types of cancer and infections that require both humoral and cellular immunity for proper therapeutic effects. Soluble protein antigens are endocytosed by APCs (antigen presenting cells) and subsequently degraded into antigenic peptides in endo/lysosomal compartments.[4-7] Those antigenic peptides in lysosomes can be presented by MHC (major histocompatibility complex) class II molecules to $CD4^+$ T-helper cells, which can induce both cellular and humoral immunity i.e. helping B cells to produce antibodies.[4] However, for effective vaccination against cancer, it is crucial that APCs present antigenic peptides through the MHC class I pathway to $CD8^+$ cytotoxic T cells (CTLs), and these activated CTLs in turn attack tumor cells that express the same antigenic peptide determinants.[8, 9] The key challenges for optimal vaccine design are to deliver antigens to the correct APCs, which are known as dendritic cells (DCs),[9-11] and transport antigenic peptides to the cytosol of DCs resulting in subsequent presentation in MHC class II and class I pathway (so-called cross-presentation).[12-14]

Recent efforts to make effective and safe vaccines against cancer have focused on developing particulate delivery systems for antigens to induce robust CTL responses. Among the nano/micro particulate vaccines, they all showed more or less increase of immune efficacy of the loaded antigen.[15-25] To achieve effective vaccination, the first step is to ensure that the antigen remains associated with the carrier and that sufficient antigen loaded particles are taken up by DCs. After internalization, the second required step is the release and processing of the loaded antigen. Particulate carriers are usually internalized by APC and end up in compartments such as endo/lysosomes in which the antigens are mostly degraded and subsequently enter the MHC class II antigen presentation pathway. To enable MHC class I antigen presentation, some delivery systems have been designed to escape from endosomes (pH-responsive polymeric particles and particles modified with fusion peptides) to facilitate antigen cross-presentation.[26-28] In addition, some carriers, such as virus-like particles and cationic particles, display excellent adjuvant properties.[29-32] They provide sufficient danger signals to alert DCs and are capable to induce both innate and cognate immune responses.

In our previous study,[33] we designed and synthesized reduction-sensitive cationic dextran nanogels to control antigen release after their uptake by APCs. A protein antigen (ovalbumin, OVA) was reversibly immobilized in the nanogels via disulfide bonds with relative high loading capacity. An important advantage of this system is that the antigen remained stably entrapped in a non-reducing environment, whereas triggered release in reductive environments occurred. These nanogels showed intracellular release of the antigen in DCs and boost MHC class I antigen presentation. In the present paper, we will show the results of the influence of nanogel size and surface charge on the uptake by DCs, the capability of the nanogels to maturate DCs, the intracellular delivery, transportation and processing of antigen by DCs *in vitro*, and therapeutic and prophylactic vaccination with nanogels with conjugated antigen *in vivo*.

2. Experimental section

2.1 Materials.

Egg albumin (OVA) was obtained from Worthington (USA). Trimethyl aminoethyl methacrylate 80% aqueous solution (TMAEMA), 2-aminoethyl methacrylate hydrochloride, ethylenediamine tetraacetic acid (EDTA) and hydroxylamine were purchased from Sigma Aldrich. Methacrylated dextran (dex-MA, M_w 40,000 Da, degree of methacrylate substitution=8) and *N*-(4-(2-(pyridine-2-yldisulfanyl)ethyl)-amidobutyl) methacrylamide were synthesized as previously reported.[33-35] All the fluorescent dyes and markers were provided by Invitrogen.

2.2 Cell line, cell culture, and animals.

The D1 cell line,[36] a long-term growth factor-dependent immature myeloid dendritic cell line of splenic origin derived from a female C57BL/6 mouse, was cultured in IMDM (Iscove's Modified Dulbecco's Medium, Lonza) containing 10% heat-inactivated FBS (Sigma), 2 mM GlutaMax (GIBCO), 50 μM β-mercaptoethanol and 30% supernatant from R1 cells (mouse fibroblast NIH/3T3 cells transfected with mouse GM-CSF gene), which was collected from confluent cultures and filtered. The B16-OVA cell line,[37] a stable OVA-transfectant derived from the murine melanoma cell line B16, was maintained in RPMI 1640 medium (Sigma) supplemented with 10% fetal bovine serum (Sigma) and 1 mg/mL of G418 (Sigma). Inbred, 5-7-week old female C57BL/6 mice were obtained from Charles River Laboratories (Maastricht, Netherlands). All mice were housed at the Laboratory Animal Facility of the Utrecht University and treated according to the regulations of animal ethics committee of the Netherlands. All experiments were approved

by the animal experimental committee of Utrecht University, the Netherlands.

2.3 Preparation and characterization of OVA-loaded nanogels.

The cationic dextran nanogels were prepared by inverse mini-emulsion photo-polymerization of methacrylated dextran (120 mg), trimethyl aminoethyl methacrylate (160 μL) and a pyridyldisulfide-containing methacrylamide monomer, N-(4-(2-(pyridine-2-yldisulfanyl)ethyl)-amidobutyl) methacrylamide (5 mg), as previously reported.[33] To label the particles, amino groups were introduced by preparing them in the presence of 2 mol% (of dextran and TMAEMA) 2-aminoethyl methacrylate hydrochloride.[38] The latter particles (20 mg) were incubated with Alexa 488 dye (Alexa Fluor 488 NHS Ester (succinimidyl ester), 1 mg/ml, 15 μL) in sodium bicarbonate solution (100 mM, pH 8.4) for 2 h. Subsequently, the particles were washed with water and spun down until no free dye was found in the supernatant (determined by FLUOstar OPTIMA (BMG LABTECH), and the washing was repeated 3 times). OVA solution (native or derivatized with SATA (on the average 2.7 modifications on one OVA molecule as previously reported),[33] 2 mg/mL, 7.5 mL) was mixed with nanogels suspension (2 mg/mL, 42.5 mL) in HEPES buffer (20 mM, pH 7.4). The mixture was incubated at room temperature for 1 h to allow OVA loading into the particles. Subsequently, a deacetylation solution (1.72 g hydroxylamine 50% aqueous solution, 0.365 g EDTA in 50 mL HEPES buffer (20mM, pH 7.4), 5 mL) was added and the mixture was incubated for 2 h at room temperature. The OVA loaded particles were collected and purified by multiple washing (with 20 mM HEPES for native OVA or PBS for SATA-derivatized OVA) and centrifugation steps, and then lyophilized. Size and zeta-potential of the nanogels were measured in HEPES (20 mM) using DLS (Malvern ALV/CGS-3 Goniometer, Malvern Instruments, Malvern, UK) and Zetasizer (Zetasizer Nano, Malvern instrument, USA), respectively. The loading capacity was determined by measuring the OVA concentration in the washing fluids with a UPLC system (Waters, USA) as described.[33]

2.4 Interaction between OVA loaded particles and DCs.

Nanogels loaded with native or SATA-modified DQ-OVA (OVA labeled with BODIPY (boron-dipyrromethene) dyes, Invitrogen) were prepared as described above. D1 cells (70,000 cells in 200 μL medium per well) were incubated with the DQ-OVA loaded nanoparticles (final concentration of nanogel-associated OVA was 2.5 μg/mL), or with Alexa-labeled dextran particles (as shown in Table 1, having a final concentration of 25 μg/mL) for various times (2, 5, or 24 h at 37 or at 4 ºC). The viability of D1 cells incubated with these dextran particles were reported previously and no cytotoxicity was observed at

the particle concentration used in this study.[33] Subsequently, images were taken by confocal laser scanning microscopy (CLSM, Confocal Leica SPE-II, Leica Microsystems) before and after quenching with trypan blue (1 mg/mL, 30 μL per dish, confocal images were taken within 30 min after addition of trypan blue to cells).[39] For lysosome staining, lysotraker-red was added 1 h before imaging.

For quantification of the uptake, the D1 cells were detached (with 2 mM EDTA PBS buffer) after incubation with particles for 24 h, and detected for fluorescence intensity with or without quenching with trypan blue using flow cytometry (BD FACSCANTO II, BD Biosciences). To measure the maturation level of D1 cells after incubation with different particles for 24 h, the cells were washed with FACS buffer and subsequently stained with anti-CD40-FITC and anti-CD86-PE antibodies (2 μg/mL, 25 uL per well, eBioscience) for 30 min on ice. These D1 cells were subsequently analyzed by flow cytometry after being washed with FACS buffer. The cell culture supernatant was diluted (from 250 up to 32000 times) for analysis for interleukin 12 (IL-12 p40) with a cytokine-specific ELISA kit (NOVEX).[40]

2.5 Prophylactic vaccination.

For the prophylactic treatment study, 8 groups of mice (n=10) were immunized twice (prime and boost) at an interval of 2 weeks s.c. in the left flank with different vaccine formulations, comprising 50 μg of OVA (and 20 μg of poly(I:C)) in 100 uL PBS. These 8 groups included mice treated with 1) PBS only, 2) empty cationic nanogels, 3) native OVA, 4) native OVA+ poly(I:C), 5) nanogels with native OVA, 6) nanogels with native OVA + poly(I:C), 7) nanogels with conjugated OVA, and 8) nanogels with conjugated OVA+ poly(I:C). Two weeks after the last vaccination, $1.5*10^5$ OVA-expressing melanoma cells (B16-OVA) suspended in 100 μL PBS were inoculated s.c. on the opposite flank.[41, 42] The tumor size was measured every other day using a caliper in two vertical dimensions, and tumor size (mm^3) was calculated by (length × width2 /2). Mice were euthanized when the volume reached 2000 mm3 according to ethical guidelines. One week after prime and boost vaccination, blood samples were collected via submandibular bleeding in heparinized tubes for detecting OVA specific $CD8^+$ cells and in Eppendorf tubes for measuring OVA-specific antibody.[17, 37, 43]

2.6 Therapeutic vaccination.

For therapeutic immunization, $1.5*10^5$ B16-OVA tumor cells (in 100 μL PBS) were first injected s.c. into the mouse right flank.[44, 45] Tumors were monitored every other day for

tumor onset and upon the appearance of palpable tumors (~2×2 mm, around day 6), the various formulations were injected s.c on the opposite flank (groups and doses are as mentioned in prophylactic vaccination). Ten days after prime, mice within each group received boost injections with the same formulation as the prime. The tumor size of each mouse was measured every other day and tumor volumes were calculated as described above. Mice were sacrificed when humane end-points (tumor volume >2000 mm^3) were met. One week after prime and boost vaccination, blood was taken via submandibular bleeding for measuring OVA specific $CD8^+$ cells and OVA-specific antibody.

2.7 Tetramer staining.

Blood samples collected via submandibular bleeding in heparinized tubes were analyzed for OVA specific $CD8^+$ T cells.[44, 45] Red blood cells were lysed by red blood cell lysis buffer (Roche) and the remaining cells (mainly leukocytes) were washed with 2% BSA in PBS (FACS buffer) and spun down. T cells then were stained with APC-conjugated SIINFEKL/H2-Kb tetramers (Leiden University Medical Center, the Netherlands) and PE-conjugated anti-mouse CD8a mAb (BD Bioscience) for 1 h on ice. After tetramer staining, cells were washed with FACS buffer and suspended in 100 μL of FACS buffer. Data were acquired using flow cytometry. Gating strategy for analysis of % H-2Kb OVA tetramer $CD8^+$ T cells is described in supporting information Figure S2.

2.8 Determination of anti-OVA antibody titers in serum.

For the detection of anti-OVA antibody titers in immunized mice, serum was separated from clotted blood after overnight storage at 4 ℃ and subsequent centrifugation (2000×g, 10 min). The titers of OVA specific antibodies in the different serum samples of the mice were quantitatively determined by ELISA. Briefly, microtiter plates (Maxisorp, Nunc) were incubated with OVA solution in PBS (10 μg/mL, 100 μL) and incubated overnight at 4 °C. Subsequently, the plates were blocked with 4% milk (elk-milk, Campina, the Netherlands) and 0.1% Tween20 in PBS solution (blocking buffer). Serial dilutions of serum (100 μL) from each mouse were loaded on the OVA-coated plates. Then, 100 μL of goat anti-mouse total lgG-HRP conjugate (1:4000 dilution, Invitrogen) was added to each well after washing. The plates were incubated for 60 min at room temperature, washed with blocking buffer and subsequently incubated with 100 μL of 3,3',5,5'- tetramethylbenzidine substrate solution (Sigma) in the dark for 10 min at room temperature. The enzyme reaction was stopped by adding 100 μL of 0.18 M H_2SO_4 to each well, and the absorbance was measured at 450 nm using SPECTROstar (BMG Labtech).

2.9 Statistical analysis.

Graph Pad Prism software version 6 (GraphPad Software, Inc.) was used for statistical analysis. Comparison between groups was conducted with Student's t test. Differences in animal survival were calculated using Log-rank (ManteleCox) test. Statistical significance was considered when $p < 0.05$. Statistical analyses were done by comparison with the untreated group unless specified with markings.

3. Results and discussion

3.1 Preparation of OVA-loaded dextran particles and their interaction with DCs *in vitro*.

Dextran-based cationic nanogels containing a pyridyldisulfide linker were prepared by inverse mini-emulsion photo-polymerization (as described in Materials and Methods section, Figure 1).[33] When OVA, either native or derivatized with succinimidyl S-acetylthioacetate (SATA) groups, was incubated with a dispersion of the cationic nanogels in aqueous buffer of low ionic strength (HEPES, 20 mM, pH 7.4), the protein was almost quantitatively absorbed in these particles due to electrostatic interactions. Subsequently, SATA-derivatized OVA after deprotection of the SATA groups using hydroxyl amine, was conjugated to the linker units in the nanogel via a thiol-disulfide exchange reaction. Non-reacted OVA was removed by washing with a high (physiological) ionic strength buffer (PBS, 167 mM, pH7.4). Indeed, it was shown in our previous study that nanogels loaded with native OVA released the protein rapidly when the particles were dispersed in PBS. However, by conjugating OVA to the nanogels via disulfide bonds, the release of OVA in PBS only occurred in the presence of a reducing agent such as glutathione.[33] To get insight into the interaction between dextran gels and DCs, particle with various surface charge density (zeta potential) and size (around 0.2 and 2.5 micrometer diameter) were prepared (Table 1). While the microgels had a rather broad size distribution, the nanogels had a relatively low PDI.

It is known that DCs play a crucial role in activating the immune response because of their ability to take up and process antigens and subsequently present antigenic peptides to T cells.[9, 13] In light of these DC functions, the capability of DCs to internalize Alexa 488 labeled dextran nanoparticles was visualized with confocal microscopy (Figure 2A) and quantified using FACS (fluorescence-activated cell sorting, Figure 2B). The binding and uptake studies were performed by incubation of labeled particles (and covalently loaded

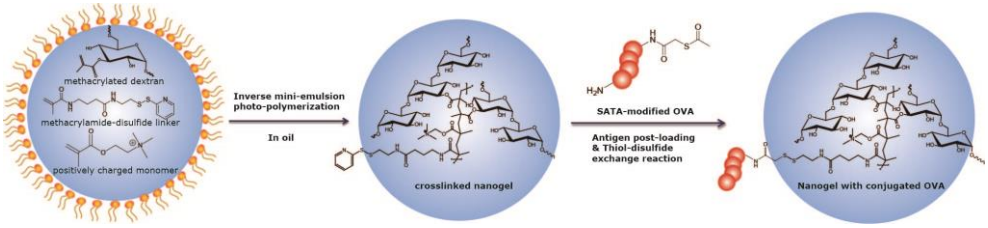

Figure 1. Schematic representation of reduction-sensitive cationic dextran nanogels and conjugation of SATA-modified OVA.

Table 1. Characterization (Z-average hydrodynamic diameter (Z_{ave}), polydispersity index (PDI), zeta potential, and loading capacity) of dextran particles dispersed in HEPES buffer (20 mM, pH 7.4). Mean values with corresponding standard deviations are shown (n=3).

Dextran particles	Z_{ave} (nm)	PDI	Size (µm) ± SD	ζ-potential (mV)	Loading capacity (wt%)
Nanogels with conjugated OVA	207 ±3	0.07 ±0.01		20.6 ±0.7	11.7 ±0.1
Nanogels with native OVA	198 ±6	0.13 ±0.02		20.6 ±0.3	11.1 ±0.1
Nanogels (low charge) with conjugated OVA	225 ±7	0.12 ±0.04		12.2 ±0.6	10.5 ±0.3
Nanogels (neutral)	213 ±8	0.17 ±0.03		-0.2 ±0.1	-
Microgels with conjugated OVA			2.5 ±1.4	22.3 ±0.2	14.3 ±0.2

with modified OVA) with D1 dendritic cells for 24 h at 4 or 37 °C. Subsequently, the cells were treated with trypan blue (TB) to quench the Alexa488-labeled particles that were surface associated with the cells (TB can quench green fluorescence and does not penetrate through cell membranes[39, 46, 47]). As shown in Figure 2A, negligible binding and uptake was detected for (empty) neutral nanogels. On the other hand, positively charged nanogels and microgels, both loaded with conjugated OVA, showed strong association with the D1 cells. After incubation of D1 cells with TB, no significant decrease of fluorescence was found for nanogels with conjugated OVA, which indicates that they were internalized by D1 cells. However, both for nanogels of low charge and for microgels, the fluorescence signals on the cell surface was quenched by TB which demonstrates that although these cationic particles were associated with the cells, they were not internalized as efficiently as the nanogels likely because of the lower charge and bigger size.[48-51] Interestingly, images of the

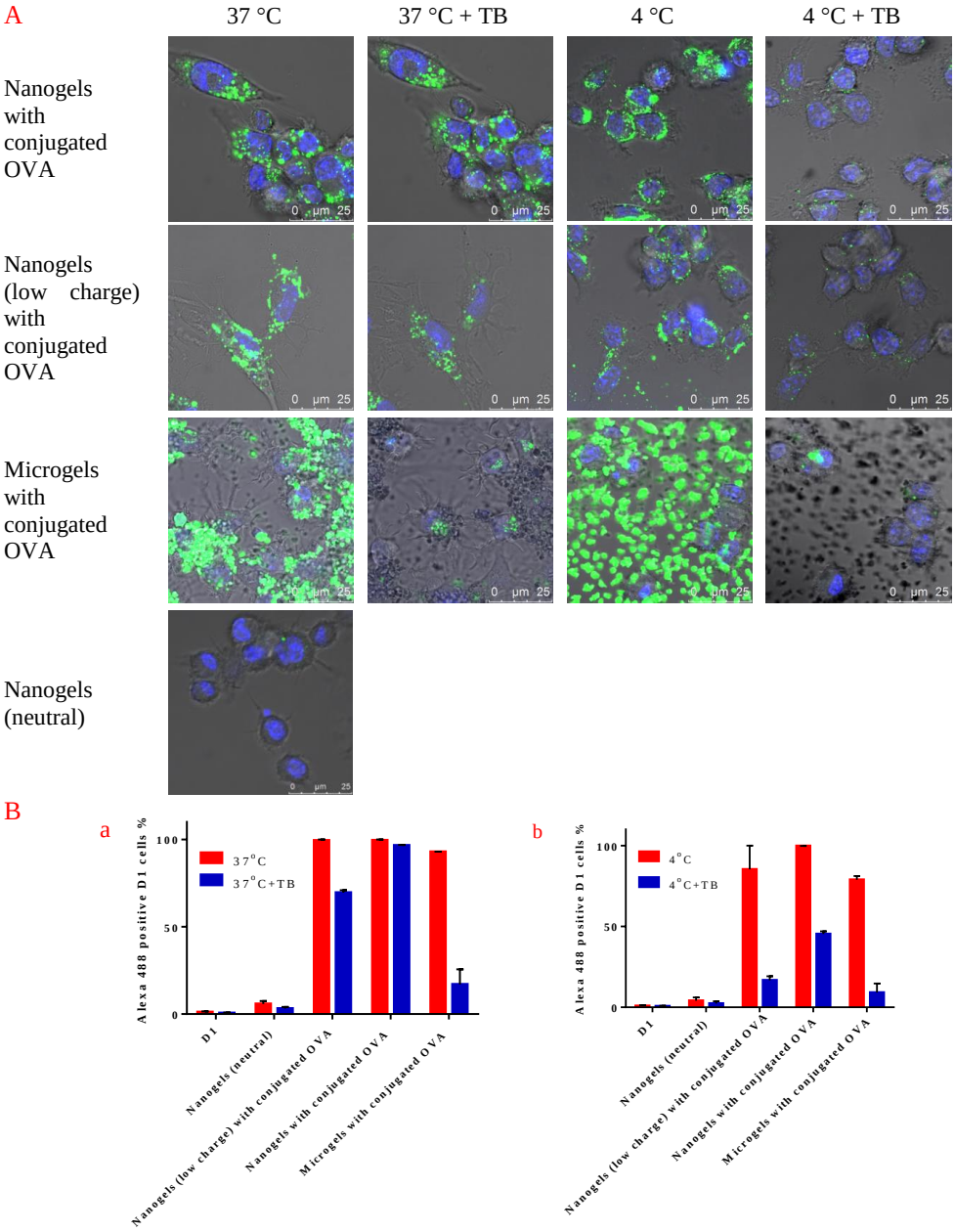

Figure 2. Binding and internalization of Alexa 488 labeled particles (25 µg/mL) to DCs for 24h at 4 or 37 °C before and after quenching with trypan blue (TB). (A) Confocal images of D1 cells after incubation with various Alexa 488 labeled particles. Nuclei were stained by Hoechst. (B) Binding and uptake of various Alexa 488 labeled particles to D1 cells quantified by flow cytometry at a) 37 °C and b) 4 °C.

cells incubated with the microgel formulation showed only small punctuate spots inside the cells, suggesting that only a fraction of smallest particles were taken up by the cells (keeping in mind the broad size distribution, Table 1), while the fluorescence of the larger particles was quenched outside the cells. Flow cytometry data (Figure 2Ba) showed that the cationic nanoparticles were indeed associated with almost all cells whereas only ~5% of the cells showed binding of neutral nanogels. After quenching with TB, the percentage positive cells previously incubated with nanogels with conjugated OVA did not change while these percentages dropped to 70% and 17 % for cells incubated with low charged nanogels and microgels, respectively. These data are consistent with the confocal images of Figure 2A. At 4 °C (Figure 2A), binding on the surface of the cells was clearly seen for all cationic particles, but only limited signals were detected intracellularly after quenching with TB demonstrating that at this temperature the particles are not internalized by DCs. The combined results of figure 2A and B demonstrate that the uptake of the particles at 37 °C requires energy as previously shown for the uptake of different types of nanoparticles and nanomedicines by living cells.[51] Taken together, these results are in agreement with other reports showing that relatively highly cationic and small sized particles are efficiently taken up by DCs.[31, 50-55] It should however be noted that the D1 cell line used for this uptake study is one subpopulation of DCs. The influence of particle size on the cell uptake may be varied in other DC populations with different properties.

The capture and internalization of an antigen by DCs is the first step to trigger an immune response, while maturation of DCs is necessary to enhance T-cell response and prevent immune tolerance in vivo.[56-58] The maturation of DCs is characterized by upregulation of co-stimulatory molecules (such as CD40, CD80, and CD86) on their membrane and secretion of cytokines (such as IL-12, a T-cell growth and stimulating factor).[40, 59, 60] Cationic particles are able to mature DCs although the exact mechanism is unknown at present.[31] To monitor DC maturation, D1 cells were incubated with and stimulated by the different dextran nanoparticles for 24 h and subsequently analyzed for cell expression of activated markers (CD40 and CD86) and cytokine production (IL-12). All samples used in this study were tested by limulus amebocyte lysate (LAL) assay, and the endotoxin contain was below detection level (0.1 EU/mL, supporting information Table S1). Poly(I:C) (1 μg/mL), a known immunostimulant of DCs,[61, 62] was used as a positive control. Flow cytometry data presented in Figure 3 (Aa and Ab) show that D1 cells incubated with cationic particles upregulated expression of both CD40 and CD86 and the percentage of matured DCs increased with the surface charge of the particles. Meanwhile, soluble OVA and neutral nanogels did not upregulate the expression of these markers on DCs. Taken

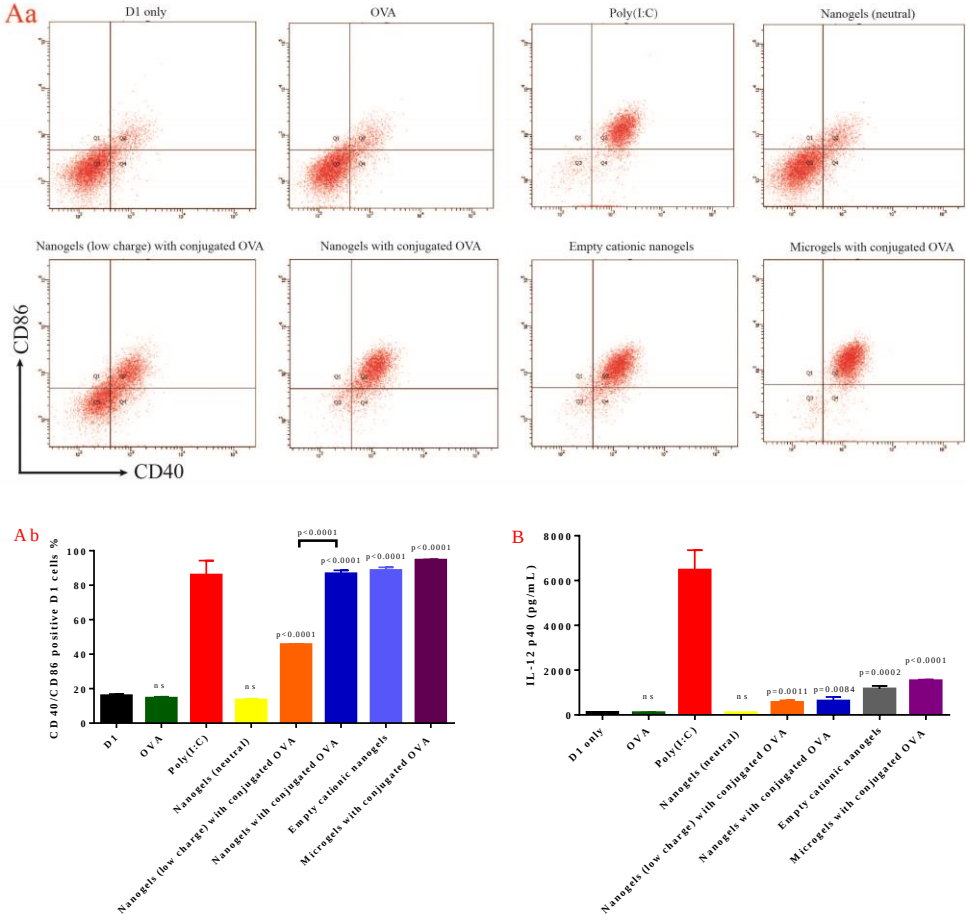

Figure 3. Flow cytometry analysis of DC maturation and cytokine secretion upon incubation with dextran particles. (Aa, Ab) Quantification of CD40 and CD86 expression after 24 h incubation with various particles. (B) Secretion of IL-12. Poly(I:C) was used as positive control. Statistical analyses were done by comparison with the untreated group (D1 only). ns, not significant.

together, the maturation of DCs is due to the charge of the particles. Moreover, relatively highly cationic particles demonstrated increased IL-12 secretion when compared to neutral/low charge nanogels, though not as efficiently as poly(I:C) (Figure 3B).

Further studies were focused on the localization of the best performing nanogels (i.e. with conjugated OVA) in DCs and the subsequent processing of OVA from these nanogels. Nanogels with conjugated OVA and labeled with Alexa 488 were incubated with D1 cells

for 2, 5 and 24 h before taking confocal images, and lysotracker-red was used to label lysosomes. Already after 2h, most of the nanogels were bound or taken up by D1 cells and the internalized nanogels colocalized with lysotracker (Figure 4A, yellow spots). Signals from the nanogels inside the cells still overlapped with lysotracker at 5 and 24 h, which

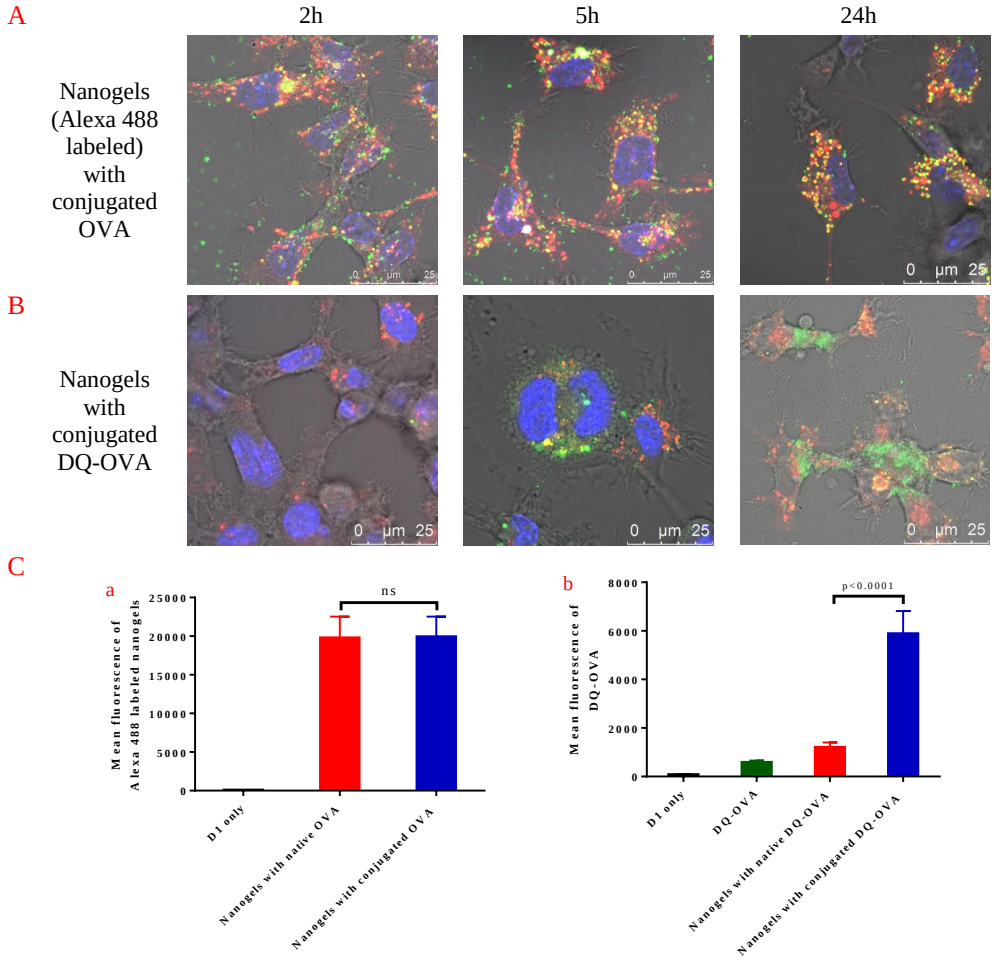

Figure 4. In vitro uptake and processing of OVA loaded nanogels by D1 cells. Confocal images of D1 cells incubated with, respectively, (A) Alexa 488 labeled nanogels (green) and (B) nanogels with conjugated DQ-OVA (green) for 2, 5 and 24 h. Lysosomes (red) were labeled by incubation with lysotracker-red 1h before taking images and nuclei were stained by Hoechst in blue. (C) a) Nanogel uptake and b) DQ-OVA processing after 24h incubation with D1 cells measured by flow cytometry. ns, not significant.

indicates that internalized nanogel particles remained in the lysosomes. To investigate the processing of the antigen by DCs, DQ-OVA was conjugated in the nanogels and subsequently incubated with D1 cells. DQ-OVA is heavily labeled with BODIPY (boron-dipyrromethene) dyes which leads to strong fluorescence quenching.[63] Once DQ-OVA is processed by DCs into single, dye-labeled peptides, the quenching is relieved resulting in bright fluorescence signals. Figure 4B shows that barely any green fluorescence signal from DQ-OVA was observed after 2h. However, fluorescence signals of this label were detected but not colocalized with lysotracker-red after 5 h and the signals became stronger after 24 h. These signals were homogenously distributed, which demonstrated that DQ-OVA was digested by D1 cells into small peptides which localized in the cytosol. Taken together, these images indicate although the nanogels were trapped in the endo/lysosomes, the released and processed antigen was transported to the cytosol, which is crucial for MHC class I antigen presentation to activate a T cell response.[4, 12, 13, 26] It is also revealed (Figure 4Ca) that nanogels were equally taken up no matter if OVA was conjugated or just physically loaded. However, the processed fragments of DQ-OVA were dramatically enhanced by nearly 5-fold when modified DQ-OVA was conjugated to nanogels via disulfide bonds compared to when native DQ-OVA was encapsulated but not conjugated (Figure 4Cb). This indicates that a higher amount of OVA was delivered intracellularly to DCs by conjugation to the reduction-sensitive linkers.

The results presented above suggest that OVA is efficiently delivered into DCs by reduction-sensitive nanogels and that OVA or the antigenic peptides can be transported to the cytosol of DCs. Moreover, the cationic nanogels have the ability to stimulate and maturate DCs. From the above we selected nanogels with conjugated OVA for in vivo studies and used nanogels with native OVA as a control.

3.2 Preventive antitumor effect of nanogels with conjugated OVA by prophylactic vaccination.

To investigate the protective efficacy of the nanogels with conjugated OVA against cancer, we tested formulations (details of the particulate formulations see supporting information Table S2) in a prophylactic vaccination setting using the B16-OVA melanoma model (expressing OVA antigen).[45] It has been shown that the specific T cell immune response induced by tumor antigen recognizes antigenic peptide determinants presented by MHC molecules of the tumor and attack and kill tumor cells. In this study, the mice were immunized with nanogels with conjugated OVA and other 7 control groups to prove the feasibility of intracellular delivery of antigen. C57BL/6 mice (10 per group) received

various formulations subcutaneously (s.c.) on day 0 and 14 as prime and boost, and mice were challenged with 1.5 × 10^5 B16-OVA cells s.c. at 14 days post boost (Figure 5A). OVA specific $CD8^+$ T cells and antibodies were measured 7 days after prime and boost, and the volume of the developing tumor was monitored in time after challenge.

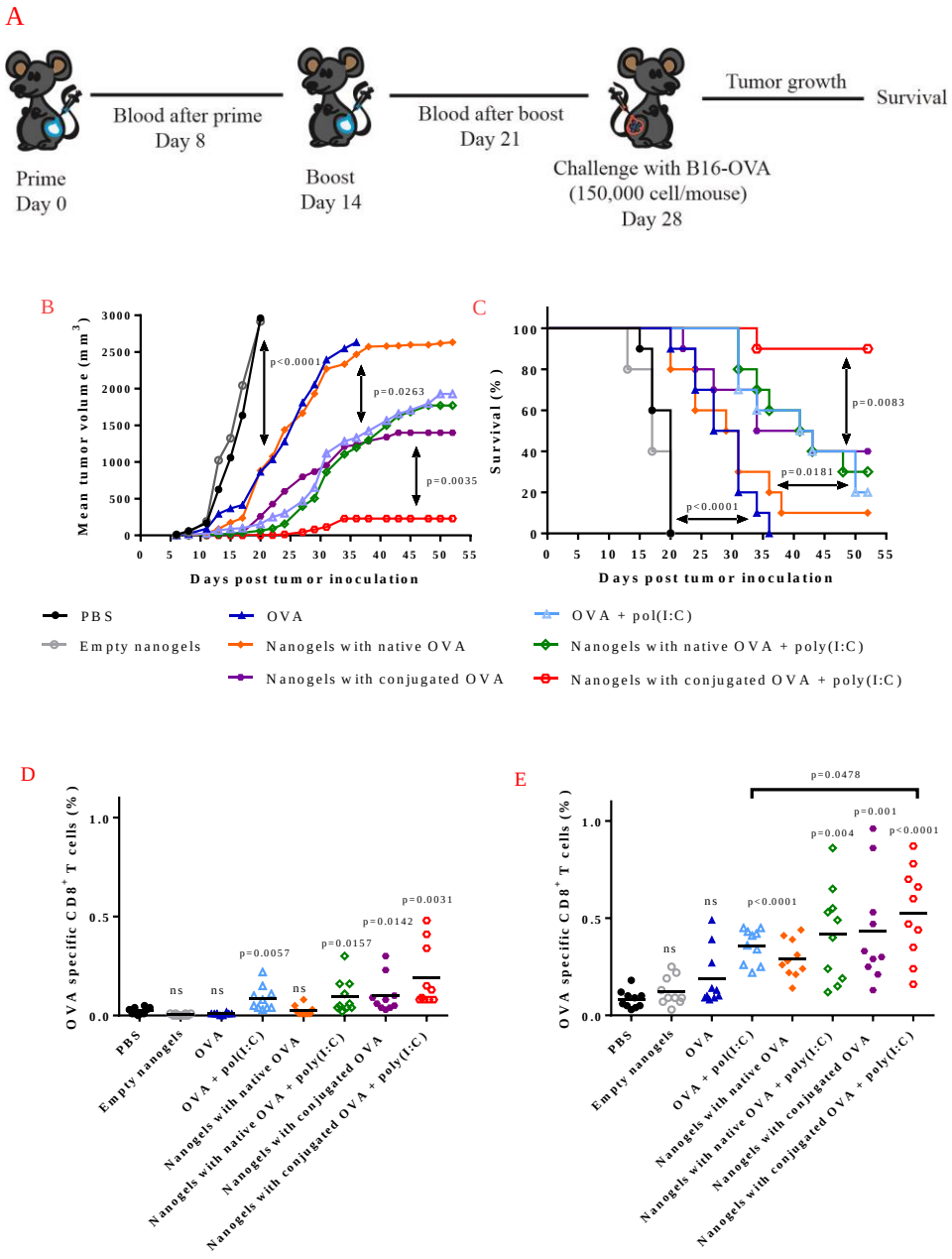

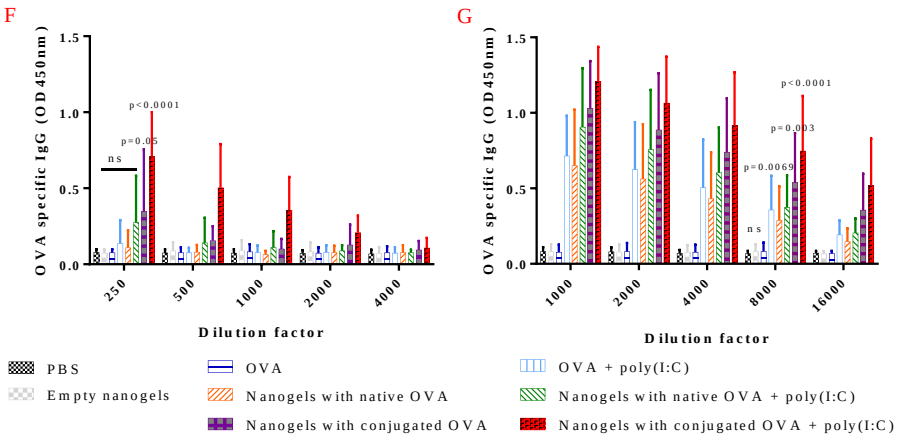

4

Figure 5. (A) Prophylactic vaccination scheme for OVA loaded nanogels formulations as prophylactic tumor vaccines in mice. Female C57BL/6 mice (n=10 per group) were immunized with various formulations (50 µg OVA (and 20 µg poly(I:C)) per mouse) according to the scheme A. (B) Tumor growth shown as mean (n=10) over 52 days post tumor challenge. SEM (standard error of the mean) are shown in the supporting information, Figure S1A. When one mouse was sacrificed, its end-point tumor size remained included in the calculations of the mean sizes after sacrificing. (C) Survival of mice (n=10). One week after (D) prime and (E) boost, blood samples were analyzed for OVA specific CD8+ T cells by tetramer staining using FACS. OVA specific total IgG was measured in the serum of diluted blood samples collected after (F) prime and (G) boost. Statistical analyses were done by comparison with the untreated group unless specified with markings. ns, not significant.

To assess the capacity of the various OVA formulations to raise specific $CD8^+$ T cell levels, blood samples of the mice 7 days after prime and boost vaccination were analyzed ex vivo. OVA specific $CD8^+$ T cells were identified with flow cytometry after tetramer staining using APC-conjugated SIINFEKL/H2-Kb tetramers and PE-conjugated anti-mouse CD8a mAb.[44, 45] Gating strategy for analysis of the percentage of H-2Kb-SIINFEKL tetramer $CD8^+$ T cells is described in the supporting information Figure S2. Figure 5D shows that prime vaccination with soluble OVA and nanogels with native OVA did not result in more antigen specific T cells than observed for the control groups. On the other hand, soluble OVA and nanogels with native OVA formulated with poly(I:C) did enhance the cellular response, and the number of antigen specific $CD8^+$ T cells detected in the blood was significantly higher than those in the non-adjuvanted group. Vaccination with nanogels with

conjugated OVA reached the same level of OVA specific $CD8^+$ T cells as the soluble OVA nanogels with native OVA supplemented with poly(I:C), which is in line with the above presented antitumor effect. The mice that were immunized with nanogels with conjugated OVA + poly(I:C) had the highest average number of OVA specific $CD8^+$ T cells. As shown in Figure 5E, also the boost vaccinations led to the highest level of OVA specific $CD8^+$ T cells. Overall, the conjugated OVA enhanced vaccine-induced CTLs responses more effectively than the other formulations did. The antitumor immunity observed in different groups correlated with the level of OVA specific $CD8^+$ T cells.

Whole protein is capable of inducing both $CD8^+$ and $CD4^+$ antigen-specific responses because it contains multiple epitopes which can be presented in both MHC class I and II pathways.[64] Since the whole protein was used as the antigen, we also evaluated the effect of the conjugates on the induction of a humoral immune response. OVA specific IgG antibodies were measured in the serum of the mice one week after prime and boost. In Figure 5F and G, the serum anti-OVA IgG titers shown for mice that received the same dose of OVA delivered with various formulations, and for the negative controls. No antibodies were detected in the blood of mice immunized with free OVA and negative controls. Nanogels with native OVA induced the production of IgG at notably low levels, while other formulations elicited higher levels of anti-OVA IgG with a similar trend as for the specific $CD8^+$ T cells; nanogels with conjugated OVA + poly(I:C) induced the highest levels of antibodies. The concentrations of OVA specific IgG measured in serum after the boost substantially increased except in serum of mice that received the negative controls and soluble OVA. Moreover, even though nanogels with native OVA produced remarkable higher antibody titers than soluble OVA after boost, the tumors of mice in these two groups showed similar growth after challenge. This indicates that antigen specific antibodies are not the determinant factor for antitumor immunity. This is in agreement with publications in which it is shown that T cells are considered to be the major immune cells involved in tumor clearance, and therefore an effective strategy for cancer immunotherapy is to activate specific T cells that recognize tumors.[12, 44, 56, 65]

3.3 Tumor growth inhibition of established melanoma by nanogels with conjugated OVA therapeutic vaccination.

The therapeutic potential of nanogels with conjugated OVA was evaluated according to the vaccination scheme of Figure 6A. B16-OVA cells were injected at day 0 and palpable tumors (~2×2 mm) were detected approximately 6 days post injection. Mice were then vaccinated with various formulations by giving prime and boost s.c. injections at day 6 and

16, respectively. As soon as palpable tumors appeared, tumor volumes increased rapidly in mice of the control groups (injected with PBS or empty nanogels) (Figure 6B). This figure also shows that no beneficial effect on tumor growth was found for mice receiving soluble OVA and nanogels with native OVA as compared to those of the control groups. Soluble OVA + polyI:C, nanogels with native OVA + polyI:C and nanogels with conjugated OVA slightly retarded the growth of the tumors when compared to the control groups. Importantly, we observed that following tumor onset, the mean tumor size of mice vaccinated with nanogels with conjugated OVA + poly(I:C) remained relatively small and it took a relatively long time for tumors to grow, so that the overall survival of this group (>80 days) was significantly better compared to all other groups (36 days when all mice were sacrificed). Although the mean tumor size increased continuously, the tumor growth was not the same for each mouse in the nanogels with conjugated OVA + poly(I:C) group (Figure 6D). Two mice out of ten displayed rapid tumor growth despite the treatment, while four mice showed a significant delay in tumor growth (i.e. the tumors started growing rapidly just after day 29). Strikingly, four mice completely eliminated these aggressive tumors and remained tumor free until the end of the 80-day study showing the potency of this vaccine formulation.

To analyze the antigen specific response raised by the vaccines in mice carrying established tumors, antigen specific $CD8^+$ T cells (Figure 6E and F) and antigen specific antibodies (Figure 6G and H) in blood were measured one week after prime and boost, respectively. In agreement with observations of the prophylactic experiment, soluble OVA and nanogels with native OVA raised similar levels of T cells and antibodies as observed for the negative control groups after prime and boost. Soluble OVA+ poly(I:C) and nanogels with native OVA + poly(I:C) vaccines induced stronger proliferation of antigen specific $CD8^+$ T cells and resulted in higher OVA specific antibodies, while nanogels with conjugated OVA + poly(I:C) showed substantially higher activation and proliferation of T cells and antibodies production. Interestingly, antigen specific T cells and IgG reached significantly higher levels (~4 times) than those detected in the prophylactic model after prime. This is in agreement with those reported in literature,[29, 66, 67] and it is likely because the immune

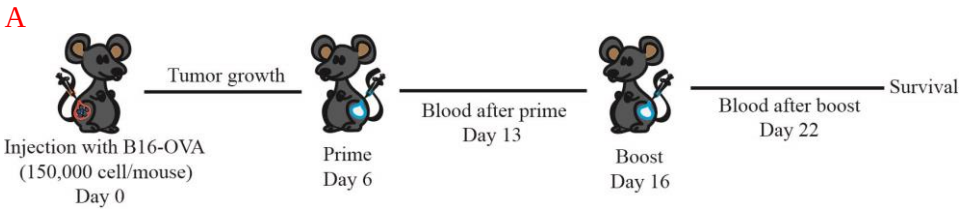

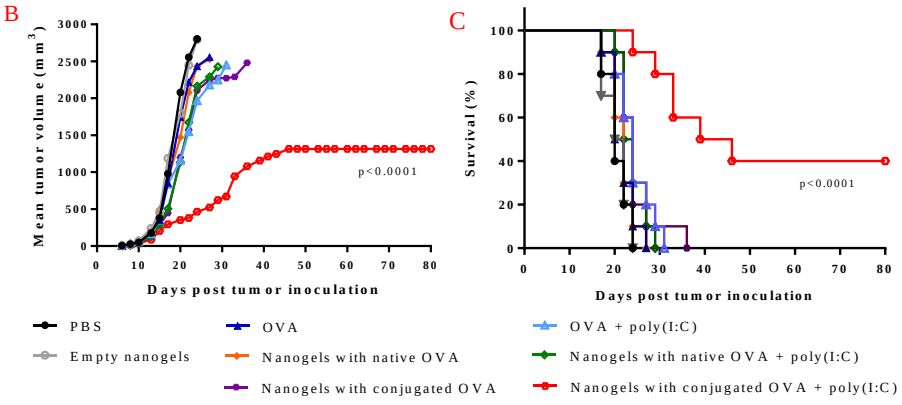
B
Mean tumor volume (mm3)
Days post tumor inoculation
p<0.0001
C
Survival (%)
Days post tumor inoculation
p<0.0001
PBS
Empty nanogels
OVA
Nanogels with native OVA
Nanogels with conjugated OVA
OVA + poly(I:C)
Nanogels with native OVA + poly(I:C)
Nanogels with conjugated OVA + poly(I:C)

D

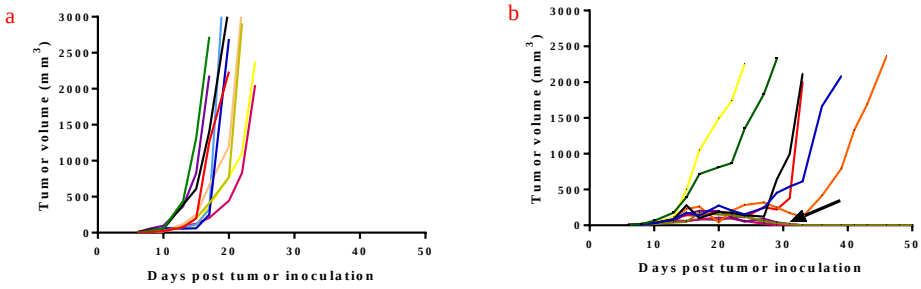
a
Tumor volume (mm3)
Days post tumor inoculation
b
Tumor volume (mm3)
Days post tumor inoculation

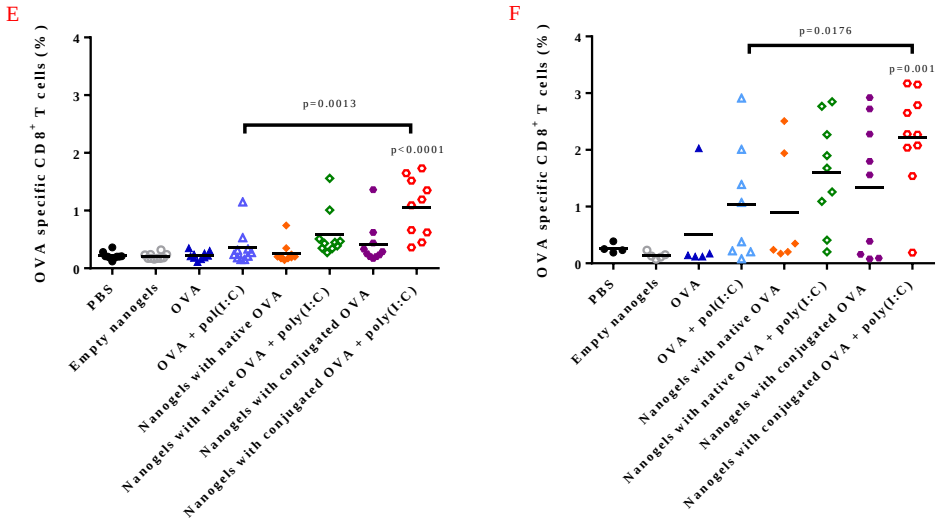
E
OVA specific CD8+ T cells (%)
p=0.0013
p<0.0001
PBS
Empty nanogels
OVA
OVA + pol(I:C)
Nanogels with native OVA
Nanogels with native OVA + poly(I:C)
Nanogels with conjugated OVA
Nanogels with conjugated OVA + poly(I:C)
F
OVA specific CD8+ T cells (%)
p=0.0176
p=0.001
PBS
Empty nanogels
OVA
OVA + pol(I:C)
Nanogels with native OVA
Nanogels with native OVA + poly(I:C)
Nanogels with conjugated OVA
Nanogels with conjugated OVA + poly(I:C)

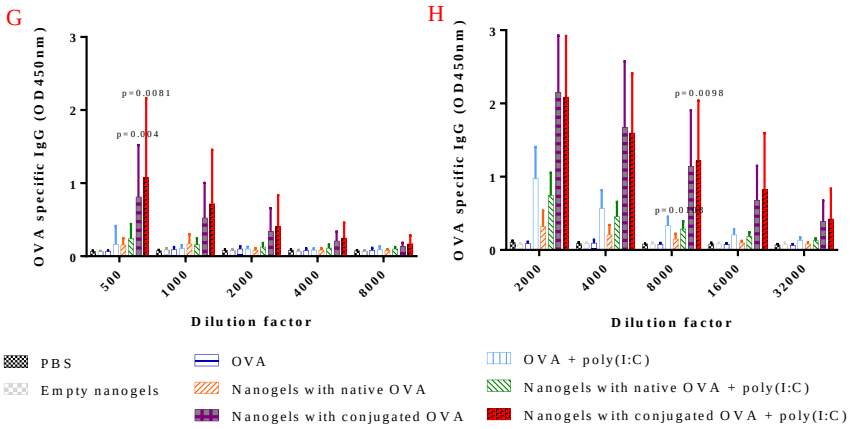

4

Figure 6. (A) Therapeutic vaccination for OVA-loaded nanogels in a tumor model. (B) Tumor growth in an established B16-OVA tumor model following treatment with various vaccine formulations. The mean tumor size was calculated from 10 mice in each group, SEM (standard error of the mean) are shown in supporting information Figure S1B. When one mouse was sacrificed, its end-point tumor size remained included in the calculations of the mean sizes after sacrificing. (C) Survival following treatment. (D) Tumor growth of each individual mouse treated with (a) PBS and (b) nanogels with conjugated OVA + poly(I:C). The black arrow (Figure Db) points out the curves of four mice in the base line which are tumor-free. Expansion of OVA specific CD8+ T cells in the blood (E) 7 days after prime and (F) 6 days after boost. Anti-OVA IgG concentrations in sera after (G) prime and (H) boost. Different numbers of mice in each group were sacrificed before the second blood sampling and the data are collected from the remaining mice. Statistical analyses were done by comparison with the untreated group. ns, not significant.

response was already activated by the presence of antigen-expressing tumor cells in these mice and reactivated by the vaccines. It should be noted that B16-OVA is an aggressive cell line and efficient treatment at early stage is needed. [42, 65, 68] Among all 8 groups, only mice immunized with nanogels with conjugated OVA + poly(I:C) showed reduction of tumors, likely because the antigen specific T cell levels in these mice were significantly higher than those other groups which is sufficient to inhibit the tumor growth already after the first vaccination.

4. Conclusion

This study demonstrates that cationic dextran nanogels are efficiently internalized by DCs, and able to maturate DCs in vitro. They facilitated the disulfide-linked OVA to be delivered to DCs, and subsequently processed and transported to the cytosol of the cells. Furthermore, these OVA-nanogel conjugates increased antigen specific T cell levels and antibody production, and thus induced strong protective and curative effect against melanoma in vivo. 4/10 mice showed complete regression of the aggressive melanoma tumor and remained tumor free for a period of at least 80 days. Collectively, the investigations presented in this paper demonstrate that intracellular delivery of antigens by the novel nanogels is a promising strategy to induce effective antigen specific immunity against cancer.

References

1. Couzin-Frankel, J. Cancer Immunotherapy. *Science* 2013, 342, 1432-1433.
2. Wong, K. K.; Li, W. A.; Mooney, D. J.; Dranoff, G. Chapter Five - Advances in Therapeutic Cancer Vaccines. *Advances Immunol*, 2016, 130, 191-249.
3. Mehta, N. K.; Moynihan, K. D.; Irvine, D. J. Engineering New Approaches to Cancer Vaccines. *Cancer Immunol Res* 2015, 3, 836-843.
4. Vyas, J. M.; Van der Veen, A. G.; Ploegh, H. L. The known unknowns of antigen processing and presentation. *Nat Rev Immunol* 2008, 8, 607-618.
5. Dani, A.; Chaudhry, A.; Mukherjee, P.; Rajagopal, D.; Bhatia, S.; George, A.; Bal, V.; Rath, S.; Mayor, S. The pathway for MHCII-mediated presentation of endogenous proteins involves peptide transport to the endo-lysosomal compartment. *J Cell Sci* 2004, 117, 4219-4230.
6. Griffin, J. P.; Chu, R.; Harding, C. V. Early endosomes and a late endocytic compartment generate different peptide-class II MHC complexes via distinct processing mechanisms. *J Immunol* 1997, 158, 1523-32.
7. Roche, P. A.; Furuta, K. The ins and outs of MHC class II-mediated antigen processing and presentation. *Nat Rev Immunol* 2015, 15, 203-216.
8. Drake, C. G.; Lipson, E. J.; Brahmer, J. R. Breathing new life into immunotherapy: review of melanoma, lung and kidney cancer. *Nat Rev Clin Oncol* 2014, 11, 24-37.
9. Palucka, K.; Banchereau, J. Dendritic-Cell-Based Therapeutic Cancer Vaccines. *Immunity* 2013, 39, 38-48.
10. Glass, J. J.; Yuen, D.; Rae, J.; Johnston, A. P.; Parton, R. G.; Kent, S. J.; De Rose, R. Human immune cell targeting of protein nanoparticles - caveospheres. *Nanoscale* 2016, 8, 8255-65.
11. Phua, K. K.; Nair, S. K.; Leong, K. W. Messenger RNA (mRNA) nanoparticle tumour vaccination. *Nanoscale* 2014, 6, 7715-29.
12. Joffre, O. P.; Segura, E.; Savina, A.; Amigorena, S. Cross-presentation by dendritic cells. *Nat*

Rev Immunol 2012, 12, 557-569.

13. Nierkens, S.; Tel, J.; Janssen, E.; Adema, G. J. Antigen cross-presentation by dendritic cell subsets: one general or all sergeants? *Trends Immunol* 2013, 34, 361-370.
14. Yue, H.; Wei, W.; Gu, Z.; Ni, D.; Luo, N.; Yang, Z.; Zhao, L.; Garate, J. A.; Zhou, R.; Su, Z.; Ma, G. Exploration of graphene oxide as an intelligent platform for cancer vaccines. *Nanoscale* 2015, 7, 19949-57.
15. Rahimian, S.; Fransen, M. F.; Kleinovink, J. W.; Christensen, J. R.; Amidi, M.; Hennink, W. E.; Ossendorp, F. Polymeric nanoparticles for co-delivery of synthetic long peptide antigen and poly IC as therapeutic cancer vaccine formulation. *J Control Release* 2015, 203, 16-22.
16. Ahmed, K. K.; Geary, S. M.; Salem, A. K. Development and Evaluation of Biodegradable Particles Coloaded With Antigen and the Toll-Like Receptor Agonist, Pentaerythritol Lipid A, as a Cancer Vaccine. *J Pharm Sci* 2016, 105, 1173-1179.
17. Geary, S. M.; Hu, Q.; Joshi, V. B.; Bowden, N. B.; Salem, A. K. Diaminosulfide based polymer microparticles as cancer vaccine delivery systems. *J Control Release* 2015, 220, 682-690.
18. Li, H.; Fierens, K.; Zhang, Z.; Vanparijs, N.; Schuijs, M. J.; Van Steendam, K.; Feiner Gracia, N.; De Rycke, R.; De Beer, T.; De Beuckelaer, A.; De Koker, S.; Deforce, D.; Albertazzi, L.; Grooten, J.; Lambrecht, B. N.; De Geest, B. G. Spontaneous Protein Adsorption on Graphene Oxide Nanosheets Allowing Efficient Intracellular Vaccine Protein Delivery. *ACS Appl Mater Interfaces* 2016, 8, 1147-1155.
19. De Koker, S.; Fierens, K.; Dierendonck, M.; De Rycke, R.; Lambrecht, B. N.; Grooten, J.; Remon, J. P.; De Geest, B. G. Nanoporous polyelectrolyte vaccine microcarriers. A formulation platform for enhancing humoral and cellular immune responses. *J Control Release* 2014, 195, 99-109.
20. Gu, L.; Mooney, D. J. Biomaterials and emerging anticancer therapeutics: engineering the microenvironment. *Nat Rev Cancer* 2016, 16, 56-66.
21. Cheung, A. S.; Koshy, S. T.; Stafford, A. G.; Bastings, M. M. C.; Mooney, D. J. Adjuvant-Loaded Subcellular Vesicles Derived From Disrupted Cancer Cells for Cancer Vaccination. *Small* 2016, 12, 2321-2333.
22. Irvine, D. J.; Hanson, M. C.; Rakhra, K.; Tokatlian, T. Synthetic Nanoparticles for Vaccines and Immunotherapy. *Chem Rev* 2015, 115, 11109-11146.
23. Mody, K. T.; Popat, A.; Mahony, D.; Cavallaro, A. S.; Yu, C.; Mitter, N. Mesoporous silica nanoparticles as antigen carriers and adjuvants for vaccine delivery. *Nanoscale* 2013, 5, 5167-79.
24. Tao, Y.; Zhang, Y.; Ju, E.; Ren, H.; Ren, J. Gold nanocluster-based vaccines for dual-delivery of antigens and immunostimulatory oligonucleotides. *Nanoscale* 2015, 7, 12419-26.
25. Zhu, G.; Liu, Y.; Yang, X.; Kim, Y. H.; Zhang, H.; Jia, R.; Liao, H. S.; Jin, A.; Lin, J.; Aronova, M.; Leapman, R.; Nie, Z.; Niu, G.; Chen, X. DNA-inorganic hybrid nanovaccine for cancer

immunotherapy. *Nanoscale* 2016, 8, 6684-92.

26. Molino, N. M.; Anderson, A. K. L.; Nelson, E. L.; Wang, S.-W. Biomimetic Protein Nanoparticles Facilitate Enhanced Dendritic Cell Activation and Cross-Presentation. *ACS Nano* 2013, 7, 9743-9752.
27. Goldberg, Michael S. Immunoengineering: How Nanotechnology Can Enhance Cancer Immunotherapy. *Cell* 2015, 161, 201-204.
28. Derouazi, M.; Di Berardino-Besson, W.; Belnoue, E.; Hoepner, S.; Walther, R.; Benkhoucha, M.; Teta, P.; Dufour, Y.; Yacoub Maroun, C.; Salazar, A. M.; Martinvalet, D.; Dietrich, P.-Y.; Walker, P. R. Novel Cell-Penetrating Peptide-Based Vaccine Induces Robust CD4+ and CD8+ T Cell–Mediated Antitumor Immunity. *Cancer Res* 2015, 75, 3020-3031.
29. Håkerud, M.; Selbo, P. K.; Waeckerle-Men, Y.; Contassot, E.; Dziunycz, P.; Kündig, T. M.; Høgset, A.; Johansen, P. Photosensitisation facilitates cross-priming of adjuvant-free protein vaccines and stimulation of tumour-suppressing CD8 T cells. *J Control Release* 2015, 198, 10-17.
30. Jain, N. K.; Sahni, N.; Kumru, O. S.; Joshi, S. B.; Volkin, D. B.; Russell Middaugh, C. Formulation and stabilization of recombinant protein based virus-like particle vaccines. *Adv Drug Deliv Rev* 2015, 93, 42-55.
31. Ma, Y.; Zhuang, Y.; Xie, X.; Wang, C.; Wang, F.; Zhou, D.; Zeng, J.; Cai, L. The role of surface charge density in cationic liposome-promoted dendritic cell maturation and vaccine-induced immune responses. *Nanoscale* 2011, 3, 2307-2314.
32. Hanson, M. C.; Crespo, M. P.; Abraham, W.; Moynihan, K. D.; Szeto, G. L.; Chen, S. H.; Melo, M. B.; Mueller, S.; Irvine, D. J. Nanoparticulate STING agonists are potent lymph node-targeted vaccine adjuvants. *J Clin Invest* 2015, 125, 2532-46.
33. Li, D.; Kordalivand, N.; Fransen, M. F.; Ossendorp, F.; Raemdonck, K.; Vermonden, T.; Hennink, W. E.; van Nostrum, C. F. Reduction-Sensitive Dextran Nanogels Aimed for Intracellular Delivery of Antigens. *Adv Func Mater* 2015, 25, 2993-3003.
34. van Dijk-Wolthuis, W. N. E.; Franssen, O.; Talsma, H.; van Steenbergen, M. J.; Kettenes-van den Bosch, J. J.; Hennink, W. E. Synthesis, Characterization, and Polymerization of Glycidyl Methacrylate Derivatized Dextran. *Macromolecules* 1995, 28, 6317-6322.
35. Verheyen, E.; Delain-Bioton, L.; van der Wal, S.; el Morabit, N.; Barendregt, A.; Hennink, W. E.; van Nostrum, C. F. Conjugation of Methacrylamide Groups to a Model Protein via a Reducible Linker for Immobilization and Subsequent Triggered Release from Hydrogels. *Macromol Biosci* 2010, 10, 1517-1526.
36. Winzler, C.; Rovere, P.; Rescigno, M.; Granucci, F.; Penna, G.; Adorini, L.; Zimmermann, V. S.; Davoust, J.; Ricciardi-Castagnoli, P. Maturation Stages of Mouse Dendritic Cells in Growth Factor–dependent Long-Term Cultures. *J Exp Med* 1997, 185, 317-328.
37. Pulaski, B. A.; Yeh, K. Y.; Shastri, N.; Maltby, K. M.; Penney, D. P.; Lord, E. M.; Frelinger, J. G.

Interleukin 3 enhances cytotoxic T lymphocyte development and class I major histocompatibility complex "re-presentation" of exogenous antigen by tumor-infiltrating antigen-presenting cells. *Proc Natl Acad Sci USA* 1996, 93, 3669-3674.

38. Naeye, B.; Raemdonck, K.; Remaut, K.; Sproat, B.; Demeester, J.; De Smedt, S. C. PEGylation of biodegradable dextran nanogels for siRNA delivery. *Eur J Pharm Sci* 2010, 40, 342-351.
39. Srivastava, G. K.; Reinoso, R.; Singh, A. K.; Fernandez-Bueno, I.; Hileeto, D.; Martino, M.; Garcia-Gutierrez, M. T.; Pigazo Merino, J. M.; Alonso, N. F.; Corell, A.; Pastor, J. C. Trypan Blue staining method for quenching the autofluorescence of RPE cells for improving protein expression analysis. *Exp Eye Res* 2011, 93, 956-962.
40. Hsieh, C.; Macatonia, S.; Tripp, C.; Wolf, S.; O'Garra, A.; Murphy, K. Development of TH1 CD4+ T cells through IL-12 produced by Listeria-induced macrophages. *Science* 1993, 260, 547-549.
41. Aranda, F.; Llopiz, D.; Díaz-Valdés, N.; Riezu-Boj, J. I.; Bezunartea, J.; Ruiz, M.; Martínez, M.; Durantez, M.; Mansilla, C.; Prieto, J.; Lasarte, J. J.; Borrás-Cuesta, F.; Sarobe, P. Adjuvant Combination and Antigen Targeting as a Strategy to Induce Polyfunctional and High-Avidity T-Cell Responses against Poorly Immunogenic Tumors. *Cancer Res* 2011, 71, 3214-3224.
42. Phua, K. K.; Staats, H. F.; Leong, K. W.; Nair, S. K. Intranasal mRNA nanoparticle vaccination induces prophylactic and therapeutic anti-tumor immunity. *Sci Rep* 2014, 4, 5128.
43. Yang, C.; Ren, X.; Ding, D.; Wang, L.; Yang, Z. Enzymatic induction of supramolecular order and bioactivity. *Nanoscale* 2016, 8, 10768-73.
44. Rosalia, R. A.; Cruz, L. J.; van Duikeren, S.; Tromp, A. T.; Silva, A. L.; Jiskoot, W.; de Gruijl, T.; Löwik, C.; Oostendorp, J.; van der Burg, S. H.; Ossendorp, F. CD40-targeted dendritic cell delivery of PLGA-nanoparticle vaccines induce potent anti-tumor responses. *Biomaterials* 2015, 40, 88-97.
45. Mandl, S.; Sigal, L. J.; Rock, K. L.; Andino, R. Poliovirus vaccine vectors elicit antigen-specific cytotoxic T cells and protect mice against lethal challenge with malignant melanoma cells expressing a model antigen. *Proc Natl Acad Sci* 1998, 95, 8216-8221.
46. Nuutila, J.; Lilius, E.-M. Flow cytometric quantitative determination of ingestion by phagocytes needs the distinguishing of overlapping populations of binding and ingesting cells. *Cytometry A* 2005, 65A, 93-102.
47. Mahony, D.; Cavallaro, A. S.; Mody, K. T.; Xiong, L.; Mahony, T. J.; Qiao, S. Z.; Mitter, N. In vivo delivery of bovine viral diahorrea virus, E2 protein using hollow mesoporous silica nanoparticles. *Nanoscale* 2014, 6, 6617-26.
48. Shima, F.; Uto, T.; Akagi, T.; Baba, M.; Akashi, M. Size effect of amphiphilic poly(γ-glutamic acid) nanoparticles on cellular uptake and maturation of dendritic cells in vivo. *Acta Biomat* 2013, 9, 8894-8901.
49. Cheng, L.-C.; Jiang, X.; Wang, J.; Chen, C.; Liu, R.-S. Nano-bio effects: interaction of

nanomaterials with cells. *Nanoscale* 2013, 5, 3547-3569.

50. Blank, F.; Stumbles, P. A.; Seydoux, E.; Holt, P. G.; Fink, A.; Rothen-Rutishauser, B.; Strickland, D. H.; von Garnier, C. Size-Dependent Uptake of Particles by Pulmonary Antigen-Presenting Cell Populations and Trafficking to Regional Lymph Nodes. *Am J Respir Cell Mol Biol* 2013, 49, 67-77.
51. Jin, H.; Heller, D. A.; Sharma, R.; Strano, M. S. Size-Dependent Cellular Uptake and Expulsion of Single-Walled Carbon Nanotubes: Single Particle Tracking and a Generic Uptake Model for Nanoparticles. *ACS Nano* 2009, 3, 149-158.
52. Xiang, S. D.; Scholzen, A.; Minigo, G.; David, C.; Apostolopoulos, V.; Mottram, P. L.; Plebanski, M. Pathogen recognition and development of particulate vaccines: Does size matter? *Methods* 2006, 40, 1-9.
53. Joshi, V. B.; Geary, S. M.; Salem, A. K. Biodegradable particles as vaccine delivery systems: size matters. *AAPS J* 2013, 15, 85-94.
54. Benne, N.; van Duijn, J.; Kuiper, J.; Jiskoot, W.; Slütter, B. Orchestrating immune responses: How size, shape and rigidity affect the immunogenicity of particulate vaccines. *J Control Release* 2016, 234, 124-134.
55. Foged, C.; Brodin, B.; Frokjaer, S.; Sundblad, A. Particle size and surface charge affect particle uptake by human dendritic cells in an in vitro model. *Int J Pharm* 2005, 298, 315-322.
56. Sakaguchi, S.; Yamaguchi, T.; Nomura, T.; Ono, M. Regulatory T Cells and Immune Tolerance. *Cell* 2008, 133, 775-787.
57. Fallarini, S.; Paoletti, T.; Battaglini, C. O.; Ronchi, P.; Lay, L.; Bonomi, R.; Jha, S.; Mancin, F.; Scrimin, P.; Lombardi, G. Factors affecting T cell responses induced by fully synthetic glyco-gold-nanoparticles. *Nanoscale* 2013, 5, 390-400.
58. Haughney, S. L.; Ross, K. A.; Boggiatto, P. M.; Wannemuehler, M. J.; Narasimhan, B. Effect of nanovaccine chemistry on humoral immune response kinetics and maturation. *Nanoscale* 2014, 6, 13770-8.
59. Slawek, A.; Maj, T.; Chelmonska-Soyta, A. CD40, CD80, and CD86 Costimulatory Molecules are Differentially Expressed on Murine Splenic Antigen-presenting Cells During the Pre-implantation Period of Pregnancy, and they Modulate Regulatory T-cell Abundance, Peripheral Cytokine Response, and Pregnancy Outcome. *Am J Reprod Immunol* 2013, 70, 116-126.
60. Van Gool, S. W.; Vandenberghe, P.; Boer, M. d.; Ceuppens, J. L. CD80, CD86 and CD40 Provide Accessory Signals in a Multiple-Step T-Cell Activation Model. *Immunol Rev* 1996, 153, 47-83.
61. Ammi, R.; De Waele, J.; Willemen, Y.; Van Brussel, I.; Schrijvers, D. M.; Lion, E.; Smits, E. L. J. Poly(I:C) as cancer vaccine adjuvant: Knocking on the door of medical breakthroughs. *Pharmacol Ther* 2015, 146, 120-131.

62. Hafner, A. M.; Corthésy, B.; Merkle, H. P. Particulate formulations for the delivery of poly(I:C) as vaccine adjuvant. *Adv Drug Deliv Rev* 2013, 65, 1386-1399.
63. Young, L. J.; Wilson, N. S.; Schnorrer, P.; Mount, A.; Lundie, R. J.; La Gruta, N. L.; Crabb, B. S.; Belz, G. T.; Heath, W. R.; Villadangos, J. A. Dendritic cell preactivation impairs MHC class II presentation of vaccines and endogenous viral antigens. *Proc Natl Acad Sci* 2007, 104, 17753-17758.
64. Pouniotis, D. S.; Esparon, S.; Apostolopoulos, V.; Pietersz, G. A. Whole protein and defined CD8+ and CD4+ peptides linked to penetratin targets both MHC class I and II antigen presentation pathways. *Immunol Cell Biol* 2011, 89, 904-913.
65. Merad, M.; Sugie, T.; Engleman, E. G.; Fong, L. In vivo manipulation of dendritic cells to induce therapeutic immunity. *Blood* 2002, 99, 1676-1682.
66. Neumann, S.; Young, K.; Compton, B.; Anderson, R.; Painter, G.; Hook, S. Synthetic TRP2 long-peptide and α-galactosylceramide formulated into cationic liposomes elicit CD8+ T-cell responses and prevent tumour progression. *Vaccine* 2015, 33, 5838-5844.
67. Schuurhuis, D. H.; van Montfoort, N.; Ioan-Facsinay, A.; Jiawan, R.; Camps, M.; Nouta, J.; Melief, C. J.; Verbeek, J. S.; Ossendorp, F. Immune complex-loaded dendritic cells are superior to soluble immune complexes as antitumor vaccine. *J Immunol* 2006, 176, 4573-80.
68. Kottke, T.; Boisgerault, N.; Diaz, R. M.; Donnelly, O.; Rommelfanger-Konkol, D.; Pulido, J.; Thompson, J.; Mukhopadhyay, D.; Kaspar, R.; Coffey, M.; Pandha, H.; Melcher, A.; Harrington, K.; Selby, P.; Vile, R. Detecting and targeting tumor relapse by its resistance to innate effectors at early recurrence. *Nat Med* 2013, 19, 1625-1631.

Chapter 5

Reduction-sensitive polymer shell coated nanogels for intracellular delivery of antigens

Dandan Li, Yinan Chen, Enrico Mastrobattista, Cornelus F. van Nostrum, Wim E. Hennink, and Tina Vermonden

Department of Pharmaceutics, Utrecht Institute for Pharmaceutical Sciences, Utrecht University.

Submitted for publication

Abstract. Nowadays, layer-by-layer assembled microsized particles receive great interest as drug delivery systems. In the present study, we report nanosized hydrogels loaded with a protein antigen that are coated with a disulfide crosslinked polymer shell. These disulfide bonds are stable in the non-reducing extracellular environment, but are reduced in the intracellular environment. This in turn leads to disintegration of the polymer shell and subsequent intracellular antigen release. Furthermore, we demonstrate the ability of these core-shell nanogels to boost the MHC class I antigen presentation by dendritic cells to $CD8^+$ T cells.

Layer-by-Layer (LbL) technology has been used for the design of drug delivery systems with an appropriate coating for controlled release.[1, 2] Multilayer shells can be assembled based on almost any type of interaction, including electrostatics, hydrogen bonding and receptor-ligand interactions.[1-5] The LbL assembly process is usually performed in aqueous conditions and is well suited to maintain the biological activity of sensitive compounds. The major benefit of LbL assembly is its versatility in terms of materials that can be chosen as layer component to engineer colloidal objects with a wide variety of surface properties. However, most LbL assembled drug delivery systems developed thus far have micrometer dimensions.[5-8] Moreover, nanoscale systems have mainly been prepared by LbL coating of solid drugs or colloidal particles of silica, gold, metal oxides, etc, and removable core templates.[1, 2, 5, 9, 10]

An issue of LbL-based drug delivery systems is that the release rate of the encapsulated drugs is mainly governed by the shell thicknesses and prone to burst release due to rapid swelling and/or disintegration under physiological conditions.[11-13] Importantly, there is a need for nanocarriers that selectively release their payload at the site of action. To achieve triggered release of an encapsulated payload, the LbL shell should remain intact and impermeable under physiological conditions, but readily disassemble in response to a specific stimulus, preferably physiological triggers.[14-16] The reduction-sensitivity of disulfide bonds has received great attention for intracellular drug delivery.[17-20] Disulfides possess excellent stability in a non-reducing extracellular environment, but are prone to cleavage under reductive conditions in intracellular space. This phenomenon has been exploited by a variety of drug carriers including disulfide-crosslinked LbL films and microcapsules.[21-23]

Polymeric nanogels are known for their overall biocompatibility and can encapsulate relatively high amounts of hydrophilic compounds, such as biotherapeutics, within their polymeric mesh network.[24, 25] In the present paper, we report on a strategy that allows loading of protein antigens into nanogels followed by LbL coating with a reducible disulfide-crosslinked polymer shell. This shell keeps loaded antigen stably entrapped in nanogels in the non-reducing environment. In response to reductive conditions, this polymer shell can disassemble, resulting in the release of the protein payload (Scheme 1).

In the first step, cationic dextran nanogels with a diameter of approximately 200 nm and a zeta-potential of 22.6 mV were prepared from methacrylated dextran and

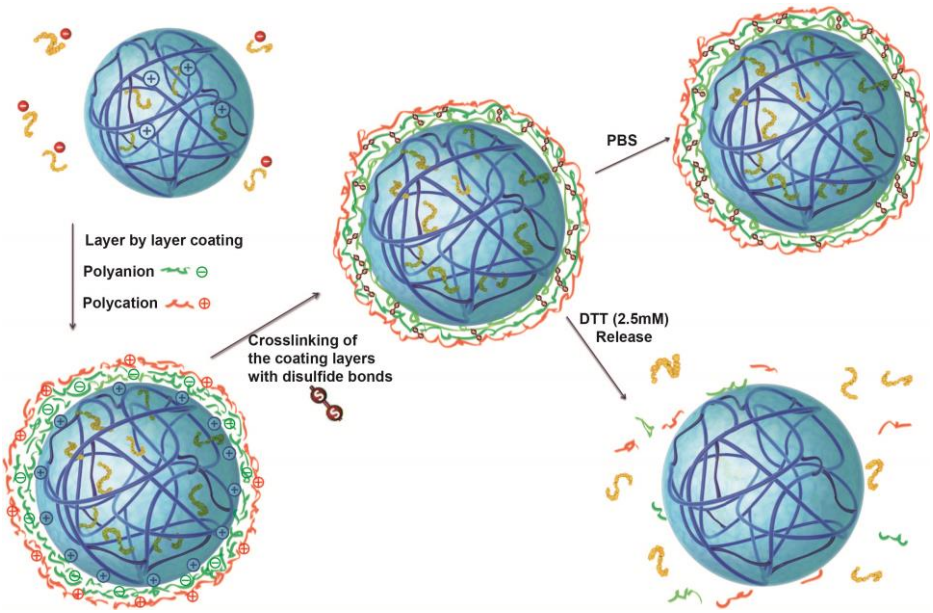

5

Scheme 1. Schematic representation of the LbL coating of protein loaded nanogels. Preformed cationic nanogels are first loaded with anionic proteins. After removal of the unbound protein, nanogels are coated with alternating layers of anionic and cationic polymers that will subsequently be cross-linked. Reduction-triggered disassembly of the coating induces release of the protein payload.

trimethyl aminoethyl methacrylate (TMAEMA) by inverse mini-emulsion photo-polymerization.[26] The model antigen ovalbumin (OVA) was subsequently post-loaded into the nanogels in a low ionic strength buffer (HEPES, 20 mM, pH 7.4) via electrostatic interaction as previously reported.[26] The nanogels maintained a positive surface charge of 21.3 mV and similar size of 200 nm after OVA loading.

Subsequently, oppositely charged polymers were used for LbL coating of the nanogels via electrostatic attraction.[27, 28] For this purpose, firstly, the polymers used for the LbL coating should not penetrate into the nanogel core as this would result in desorption of the loaded protein due to competition for binding sites. Secondly, the LbL coating should be impermeable for the loaded protein after crosslinking and thirdly, when non-crosslinked, the LbL coating should disassemble under physiological conditions. Therefore, polyanions and polycations with different molecular weights were prepared by free radical polymerization of respectively

methacrylic acid (MAA) or TMAEMA, and a neutral hydrophilic co-monomer, N-(2-hydroxypropyl) methacrylamide (HPMA) to tune the charge density (Scheme 2A-B, and Table S1 and S2, ESI†). The positively charged OVA loaded nanogels were alternately coated with the polyanion and polycation, and the zeta-potential and OVA loading during the coating process were monitored (Table S3, ESI†). The nanogels incubated with the homopolymers of MAA and TMAEMA showed substantial release of OVA during the coating process, whereas the copolymers with pHPMA of high molecular weight and with reduced charge density retained most of the protein in HEPES buffer. pHPMA-co-MAA reversed the surface charge to -22.7 mV, and to +31.8 mV after coating with pHPMA-co-TMAEMA, indicating the successful coating of the charged polymers on the nanogels. When the nanogels with non-crosslinked shell were exposed to physiological ionic strength (PBS, 164 mM), more than 98% of the encapsulated OVA was released within 1 hour (Table S3, ESI†). In conclusion, PHPMA-co-MAA (molar ratio 1:1, M_n=539kD, PDI=1.8) and pHPMA-co-TMAEMA (molar ratio1:1, M_n=302kD, PDI=2.2) were found suitable for the LbL coating.

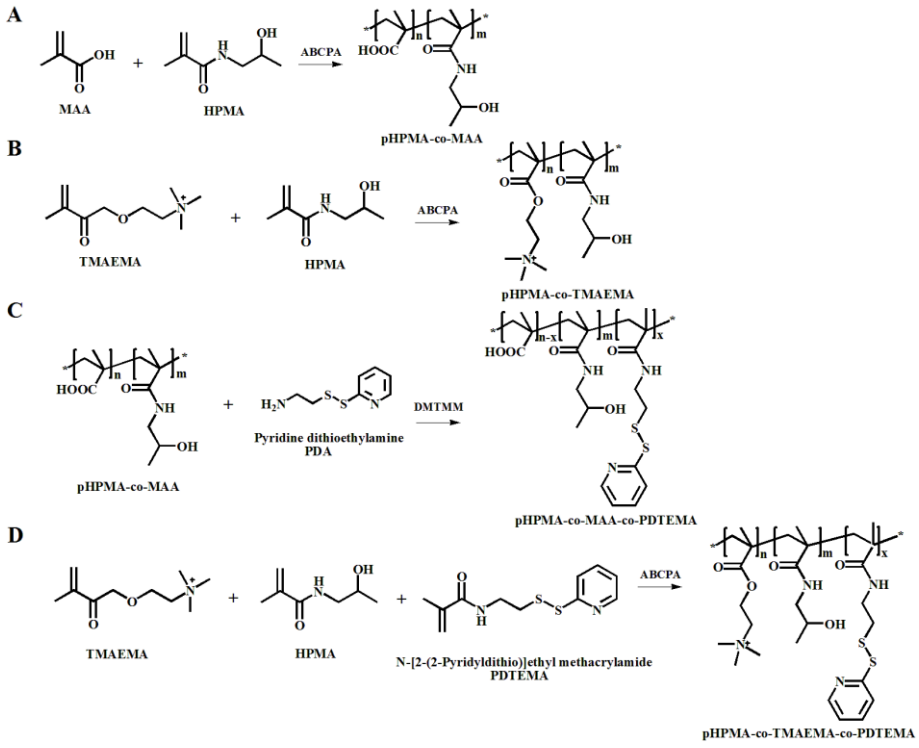

Scheme 2. Synthesis route of anionic and cationic polymers for LbL assembly.

In the next step, pyridyldisulfide groups were introduced in both the polyanion and polycation to enable oxidative crosslinking of the LbL coating and consequently retain the OVA stably entrapped within the nanogels at physiological ionic strength, while also enabling to trigger dissociation of the polymer shell and subsequently release of the OVA antigen under reducing conditions. pHPMA-co-MAA-co-PDTEMA (N-[2-(2-pyridyldithio)] ethyl methacrylamide) with 11 mol% of pyridyldisulfide containing units and pHPMA-co-TMAEMA-co-PDTEMA with 15 mol% of pyridyldisulfide units were prepared (Scheme 2c and 2d) and alternating layers of these polymers were adsorbed onto the OVA loaded nanogels. Next, dithiothreitol (DTT) corresponding to 0.5 molar equivalent of pyridyldisulfide groups of the coating polymers was added to cleave half of the pyridyldisulfide groups to yield thiol groups. Subsequently, these thiol groups reacted with the remaining 0.5 molar equivalent of pyridyldisulfide groups by thiol disulfide exchange, resulting in a disulfide-crosslinked LbL coating. The crosslinking efficiency was checked by measuring the released 2-mercaptopyridine, which corresponded to 99% of reacted pyridyldisulfide groups. OVA loaded nanogels coated with 1, 2 and 3 disulfide-crosslinked polymer layers were prepared and nanogels with 2 non-crosslinked layers (with positive surface charge) were used as a control. The coating of each layer resulted in reversal of the ζ-potential (Table 1). The size of nanogels increased from 200 to 263 nm after coating of the first layer and no significant increase of size was found upon deposition of the second and third layer. This could be attributed to a larger mass of polymer that is adsorbed as the first layer (Table 1). As listed in Table 1, more than 90 % of the loaded OVA remained in the nanogels after coating and crosslinking of the polymer shell.

The release of OVA from disulfide-crosslinked LbL coated nanogels was examined under physiological conditions (PBS, 164 mM, pH 7.4, 37 °C) and thereafter under reducing conditions (2.5 mM of DTT in PBS). Figure 1A shows that nanogels with a non-crosslinked shell release their payload rapidly within 1 h after incubation in PBS. In contrast, only ~10% of the loaded OVA was released from nanogels with a disulfide-crosslinked LbL coating upon incubation in PBS for 8 h. This means that the crosslinked coating is indeed impermeable for OVA. Interestingly, these nanogels showed a triggered release of OVA upon incubation in PBS containing DTT (2.5 mM), due to the reduction of the disulfide bridges and desorption of the polymers. No significant difference of OVA release was found for nanogels coated with 1, 2, or 3 crosslinked layers. To visualize the coating layers on the cationic gels

Tabel. 1 Z-average hydrodynamic diameter (Zave), zeta potential, mass of coated polymers, loading capacity (LC) and loading efficiency (LE) of OVA-loaded nanogels (n=3).

Nanogels coated with	Z_{ave} [a] (nm)	ζ-potential (mV)	Mass of polymer (mg/1 mg nanogels)[b]	LE (wt %)	LC (wt %)
1 disulfide-crosslinked layer	263 ±5	-18.8 ±0.5	0.35 ±0.00	99.2 ±0.1	22.6 ±0.1
2 disulfide-crosslinked layers	271 ±9	22.2 ±0.9	0.38 ±0.01	93.8 ±0.6	21.2 ±0.2
3 disulfide-crosslinked layers	278 ±9	-27.0 ±0.5	0.42 ±0.01	92.2 ±2.1	20.4 ±0.1
2 non-crosslinked layers	265 ±8	27.0 ±1.0	n.d.	83.3 ±3.0	19.3 ±0.1

[a] PDI for all formulations was <0.16. [b] The method of quantification of the amount of polymers coated on nanogels is described in the supporting information.

and the triggered release of OVA, confocal laser scanning microscopy (CLSM) experiments were performed using microgels rather than nanogels to avoid diffraction limitated resolution. Note that these microgels exhibit, apart from a larger size, similar properties as the nanogels.[26] The FITC-OVA loaded microgels were coated with either a 2 layer crosslinked or a 2 layer non-crosslinked LbL coating labelled with rhodamine B, followed by incubated in respectively HEPES, PBS with(out) DTT (2.5 mM in PBS). CLSM images (Figure 1Ba and Bc) demonstrate that microgels with both crosslinked and non-crosslinked shell show a clear ring of red fluorescence (originating from the rhodamine B-labelled polycation) surrounding the OVA (green fluorescence) loaded microgel, indicating a stable LbL coating onto the microgels in HEPES buffer of low ionic strength. When the particles were incubated with PBS, the higher ionic strength of this medium resulted in destabilisation of the non-crosslinked LbL coating and the release of OVA from the microgels (Figure 1Bb), while the crosslinked LbL coating remained intact upon exposure to PBS (Figure 1Bd). Importantly, incubation of these particles in the presence of 2.5 mM DTT led to destabilisation of the crosslinked LbL coating and triggered the release of OVA (Figure 1Be).

To visualize the intracellular delivery of entrapped OVA, Alexa Fluor 647 (AF647) labelled OVA was loaded in nanogels that were labelled with Alexa Fluor 488 (AF488), and coated with rhodamine B labelled polymer. CLSM images were taken after incubation of the particles with D1 cells, a growth factor dependent immature

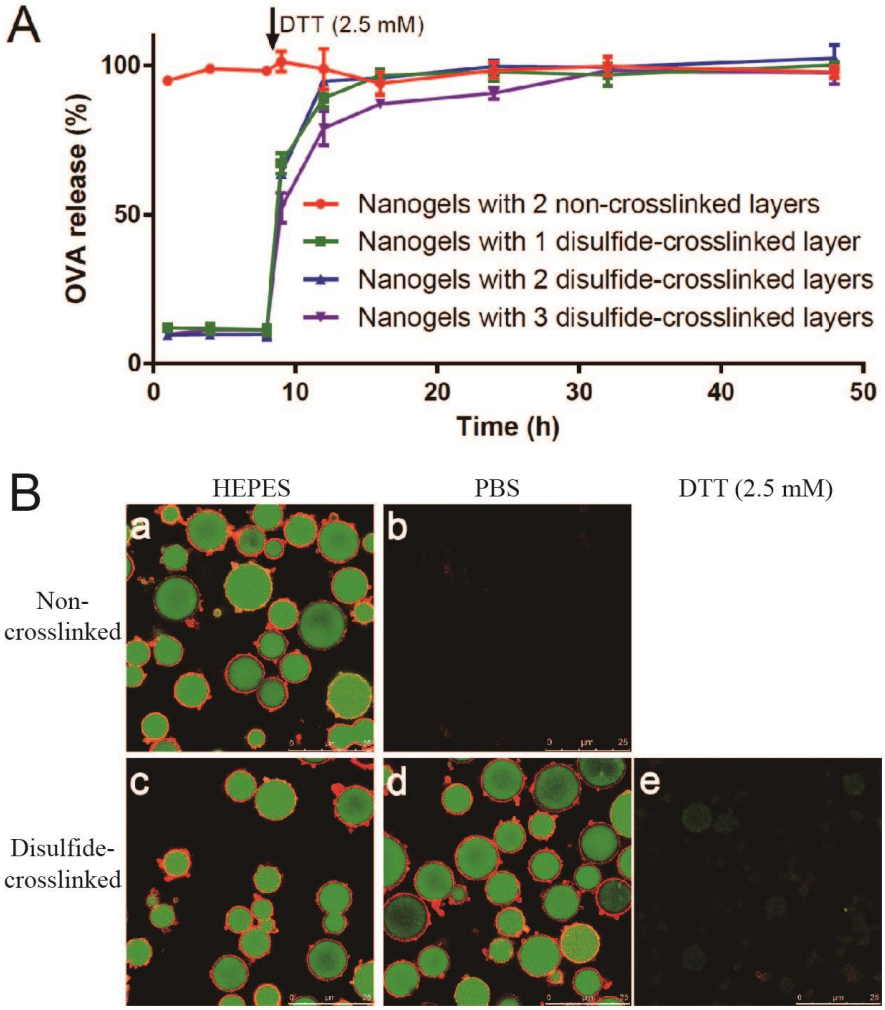

Figure 1. A) OVA release from nanogels coated with polymer shell in PBS pH 7.4 at 37 ℃; DTT was added to 2.5 mM final concentration at 8h. B) Confocal snapshots of FITC-OVA loaded microgels with 2 non-crosslinked layers and with 2 disulfide-crosslinked layers in HEPES, PBS and DTT (2.5 mM).

murine dendritic cell line, for 2 and 24 h (Figure 2). Images of cells incubated with nanogels coated with 2 disulfide-crosslinked layers having a positive surface charge showed colocalization of AF488-nanogels, AF647-OVA and rhodamine B-polycation after 2 h. After 24 h, barely any signal of AF647-OVA was observed

compared to the signal after 2 h incubation, while AF488-nanogels and rhodamine B-polycation were seen and overlapped. Likely, the entrapped OVA was released from the nanogels in reductive cellular compartments and subsequently processed by DCs.[29, 30] On the other hand, no fluorescence of OVA was observed in the pictures of nanogels with non-crosslinked shell after 2 and 24 h (Figure 2B), and the polycation was not colocalized with nanogels in the same compartments of cells, indicating that the coating polymers were disassociated from the nanogels (and subsequently taken up), while the protein was released before the nanogel particles were taken up by cells.

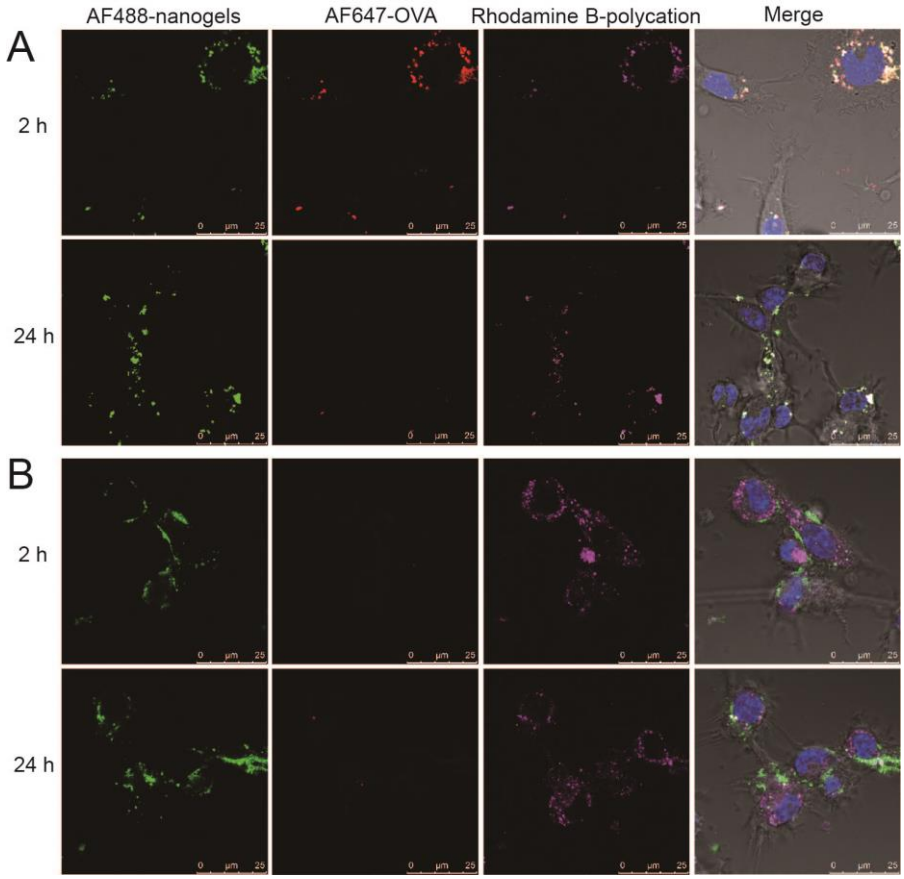

Figure 2. Intracellular release of OVA was studied by CLSM with AF647-OVA (red) loaded AF488-nanogels (green) coated with rhodamine B-polymer (magenta). The images were taken after D1 dendritic cells were incubated with nanogels coated with A) 2 layers of disulfide-crosslinked shell, and B) 2 layers of non-crosslinked shell for 2 and 24 h.

The ability of OVA loaded nanogels with disulfide-crosslinked shell to activate OVA-specific $CD8^+$ T cells (B3Z cells) was tested in vitro by an MHC class I antigen presentation assay (Figure 3, for cytotoxicity see Figure S3, ESI†). The nanogels with crosslinked shell activated OVA-specific $CD8^+$ T cells to a higher extent (factor of 2) than their non-crosslinked counterparts and bare nanogels. Non-crosslinked and non-coated nanogels enhanced T cell activation to the same extent similarly as cells incubated with soluble OVA. Noteworthy, nanogels with 1 crosslinked layer were less efficient in stimulating $CD8^+$ T cells presumably because of the negative surface charge, which resulted in low uptake by D1 cells.[31] The improved MHC class I antigen presentation by nanogels with crosslinked shell and cationic top layer indicates that relative high quantities of OVA were delivered and released into D1 cells and furthermore processed and presented in MHC class I molecules to $CD8^+$ T cells.

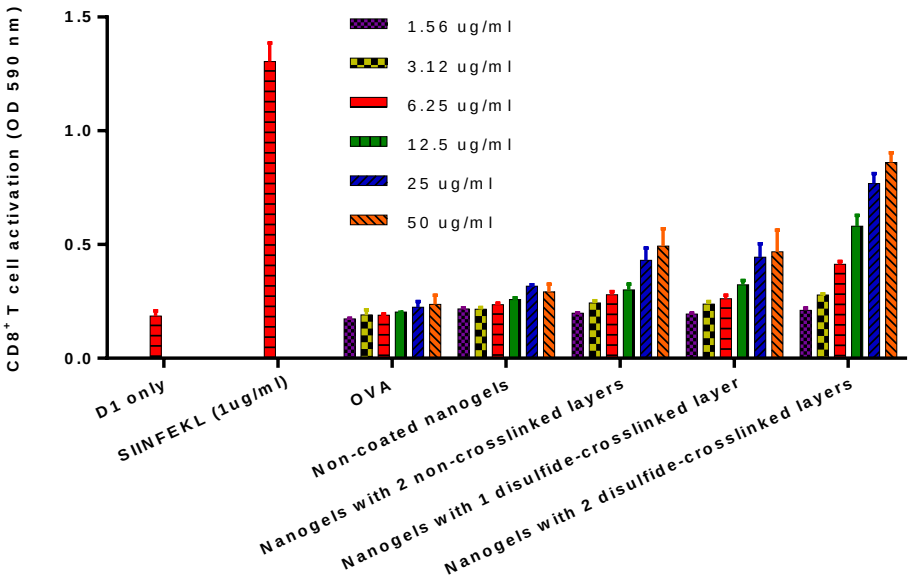

Figure 3. Activation of SIINFEKL-specific CD8+ T cells (B3Z) after co-culturing with DCs. DCs were incubated with various formulations for 24h with titrated amounts of OVA (n=3). SIINFEKL (1 μg/mL) was used as positive control. Representative results from one out of three experiments are shown.

To conclude, we have developed nanogels in which a protein antigen (OVA) was entrapped followed by deposition of a disulfide-crosslinked LbL coating. The antigen remained stably encapsulated under non-reducing conditions, but was readily released in response to a reductive environment. Furthermore, these particles showed intracellular release of the encapsulated antigen and boost the MHC class I antigen presentation *in vitro*. This technology can be broadly applied for encapsulating a wide variety of native biotherapeutics, thus making it a versatile drug delivery system.

References

1. Ariga, K.; Lvov, Y. M.; Kawakami, K.; Ji, Q.; Hill, J. P. Layer-by-layer self-assembled shells for drug delivery. *Adv Drug Deliv Rev* 2011, 63, 762-771.
2. De Cock, L. J.; De Koker, S.; De Geest, B. G.; Grooten, J.; Vervaet, C.; Remon, J. P.; Sukhorukov, G. B.; Antipina, M. N. Polymeric multilayer capsules in drug delivery. *Angew Chem Int Edit* 2010, 49, 6954-6973.
3. Kim, B.-S.; Park, S. W.; Hammond, P. T. Hydrogen-bonding layer-by-layer-assembled biodegradable polymeric micelles as drug delivery vehicles from surfaces. *ACS Nano* 2008, 2, 386-392.
4. Lee, S. W.; Kim, B.-S.; Chen, S.; Shao-Horn, Y.; Hammond, P. T. Layer-by-layer assembly of all carbon nanotube ultrathin films for electrochemical applications. *J Am Chem Soc* 2009, 131, 671-679.
5. Mohanta, V.; Madras, G.; Patil, S. Layer-by-layer assembled thin films and microcapsules of nanocrystalline cellulose for hydrophobic drug delivery. *ACS Appl Mater Interfaces* 2014, 6, 20093-20101.
6. Chiu, Y.-C.; Gammon, J. M.; Andorko, J. I.; Tostanoski, L. H.; Jewell, C. M. Modular vaccine design using carrier-free capsules assembled from polyionic immune signals. *ACS Biomater Sci Eng* 2015, 1, 1200-1205.
7. De Geest, B. G.; Willart, M. A.; Lambrecht, B. N.; Pollard, C.; Vervaet, C.; Remon, J. P.; Grooten, J.; De Koker, S. Surface-engineered polyelectrolyte multilayer capsules: synthetic vaccines mimicking microbial structure and function. *Angew Chem Int Edit* 2012, 51, 3862-3866.
8. De Geest, B. G.; Willart, M. A.; Hammad, H.; Lambrecht, B. N.; Pollard, C.; Bogaert, P.; De Filette, M.; Saelens, X.; Vervaet, C.; Remon, J. P.; Grooten, J.; De Koker, S. Polymeric multilayer capsule-mediated vaccination induces protective immunity against cancer and viral infection. *ACS Nano* 2012, 6, 2136-49.
9. Wang, Y.; Angelatos, A. S.; Caruso, F. Template Synthesis of nanostructured materials via

layer-by-layer assembly. *Chem Mater* 2008, 20, 848-858.

10. Dreaden, E. C.; Morton, S. W.; Shopsowitz, K. E.; Choi, J.-H.; Deng, Z. J.; Cho, N.-J.; Hammond, P. T. Bimodal tumor-targeting from microenvironment responsive hyaluronan layer-by-layer (LbL) nanoparticles. *ACS Nano* 2014, 8, 8374-8382.
11. Chen, P.; Wang, X.; Dong, Y.; Hu, X. Development of a layer-by-layer assembled film on hydrogel for ocular drug delivery. *Int J Polym Sci* 2015, 2015, 9.
12. Zhou, G.; Lu, Y.; Zhang, H.; Chen, Y.; Yu, Y.; Gao, J.; Sun, D.; Zhang, G.; Zou, H.; Zhong, Y. A novel pulsed drug-delivery system: polyelectrolyte layer-by-layer coating of chitosan-alginate microgels. *Int J Nanomedicine* 2013, 8, 877-87.
13. Hsu, B. B.; Hagerman, S. R.; Jamieson, K.; Castleberry, S. A.; Wang, W.; Holler, E.; Ljubimova, J. Y.; Hammond, P. T. Multifunctional self-assembled films for rapid hemostat and sustained anti-infective delivery. *ACS Biomater Sci Eng* 2015, 1, 148-156.
14. Xu, Q.; He, C.; Ren, K.; Xiao, C.; Chen, X. Thermosensitive polypeptide hydrogels as a platform for ros-triggered cargo release with innate cytoprotective ability under oxidative stress. *Adv Healt Mater* 2016, 5, 1979-1990.
15. Yao, X.; Chen, L.; Chen, X.; Xie, Z.; Ding, J.; He, C.; Zhang, J.; Chen, X. pH-responsive metallo-supramolecular nanogel for synergistic chemo-photodynamic therapy. *Acta Biomater* 2015, 25, 162-171.
16. Yu, C.; Qian, L.; Ge, J.; Fu, J.; Yuan, P.; Yao, S. C. L.; Yao, S. Q. Cell-penetrating poly(disulfide) assisted intracellular delivery of mesoporous silica nanoparticles for inhibition of miR-21 function and detection of subsequent therapeutic effects. *Angew Chem Int Edit* 2016, 55, 9272-9276.
17. Brülisauer, L.; Gauthier, M. A.; Leroux, J.-C. Disulfide-containing parenteral delivery systems and their redox-biological fate. *J Control Release* 2014, 195, 147-154.
18. De Koker, S.; Cui, J.; Vanparijs, N.; Albertazzi, L.; Grooten, J.; Caruso, F.; De Geest, B. G. Engineering polymer hydrogel nanoparticles for lymph node-targeted delivery. *Angew Chem Int Edit* 2016, 55, 1334-1339.
19. Cheng, R.; Feng, F.; Meng, F.; Deng, C.; Feijen, J.; Zhong, Z. Glutathione-responsive nano-vehicles as a promising platform for targeted intracellular drug and gene delivery. *J Control Release* 2011, 152, 2-12.
20. Akita, H.; Noguchi, Y.; Hatakeyama, H.; Sato, Y.; Tange, K.; Nakai, Y.; Harashima, H. Molecular tuning of a vitamin E-scaffold pH-sensitive and reductive cleavable lipid-like material for accelerated in vivo hepatic sirna delivery. *ACS Biomater Sci Eng* 2015, 1, 834-844.
21. Becker, A. L.; Orlotti, N. I.; Folini, M.; Cavalieri, F.; Zelikin, A. N.; Johnston, A. P. R.; Zaffaroni, N.; Caruso, F. Redox-active polymer microcapsules for the delivery of a survivin-specific sirna in prostate cancer cells. *ACS Nano* 2011, 5, 1335-1344.
22. Sexton, A.; Whitney, P. G.; Chong, S.-F.; Zelikin, A. N.; Johnston, A. P. R.; De Rose, R.; Brooks,

A. G.; Caruso, F.; Kent, S. J. A protective vaccine delivery system for in vivo T cell stimulation using nanoengineered polymer hydrogel capsules. *ACS Nano* 2009, 3, 3391-3400.

23. Xie, C.; Lu, X.; Wang, K.; Yuan, H.; Fang, L.; Zheng, X.; Chan, C.; Ren, F.; Zhao, C. Pulse electrochemical driven rapid layer-by-layer assembly of polydopamine and hydroxyapatite nanofilms via alternative redox in situ synthesis for bone regeneration. *ACS Biomater Sci Eng* 2016, 2, 920-928.
24. Kabanov, A. V.; Vinogradov, S. V. Nanogels as pharmaceutical carriers: finite networks of infinite capabilities. *Angew Chem Int Edit* 2009, 48, 5418-5429.
25. Kharkar, P. M.; Rehmann, M. S.; Skeens, K. M.; Maverakis, E.; Kloxin, A. M. Thiol–ene click hydrogels for therapeutic delivery. *ACS Biomater Sci Eng* 2016, 2, 165-179.
26. Li, D.; Kordalivand, N.; Fransen, M. F.; Ossendorp, F.; Raemdonck, K.; Vermonden, T.; Hennink, W. E.; van Nostrum, C. F. Reduction-sensitive dextran nanogels aimed for intracellular delivery of antigens. *Adv Func Mater* 2015, 25, 2993-3003.
27. De Geest, B. G.; Déjugnat, C.; Prevot, M.; Sukhorukov, G. B.; Demeester, J.; De Smedt, S. C. Self-rupturing and hollow microcapsules prepared from bio-polyelectrolyte-coated microgels. *Adv Func Mater* 2007, 17, 531-537.
28. Tan, J. P. K.; Wang, Q.; Tam, K. C. Control of burst release from nanogels via layer by layer assembly. *J Control Release* 2008, 128, 248-254.
29. Collins, D. S.; Unanue, E. R.; Harding, C. V. Reduction of disulfide bonds within lysosomes is a key step in antigen processing. *J Immunology* 1991, 147, 4054-9.
30. Brubaker, C. E.; Panagiotou, V.; Demurtas, D.; Bonner, D. K.; Swartz, M. A.; Hubbell, J. A. A cationic micelle complex improves $CD8^+$ T cell responses in vaccination against unmodified protein antigen. *ACS Biomater Sci Eng* 2016, 2, 231-240.
31. Frohlich, E. The role of surface charge in cellular uptake and cytotoxicity of medical nanoparticles. *Int J Nanomedicine* 2012, 7, 5577-91.

Supporting Information

Experimental Details

Materials

Egg albumin (OVA) was obtained from Worthington (USA). Methacrylic acid (MAA), trimethyl aminoethyl methacrylate 80% aqueous solution (TMAEMA), 4-(4,6-dimethoxy-1,3,5-triazin-2-yl)-4-methylmorpholinium chloride (DMTMM), 4,4'-Azobis(4-cyanovaleric acid) (ABCPA), 2-Aminoethyl methacrylate hydrochloride (AEMA), HEPES, 2-mercaptopyridine, sodium bisulfite, potassium persulfate (KPS), light mineral oil, dithiothreitol (DTT), rhodamine B isothiocyanate, β-mercaptoethanol, IGEPAL CA-630, chlorophenol red-β-D-galactopyranoside (CPRG), and H-2Kb-restricted OVA class I epitope SIINFEKL were purchased from Sigma Aldrich. Methacrylated dextran (dex-MA, Mw 40,000 Da, degree of methacrylate substitution=20),[1] *N*-(2-hydroxypropyl) methacrylamide (HPMA),[2] pyridine dithioethylamine[3] and *N*-[2-(2-pyridyldithio)]ethyl methacrylamide[3] were synthesized as previously reported. ABIL EM 90 was provided by Goldschmidt (France). Irgacure 2959 was purchased from Ciba Specialty Chemicals (USA). Ovalbumin fluorescein conjugate (FITC-OVA), Alexa Fluor 647 ovalbumin conjugate and Alexa Fluor 488 NHS ester were obtained from Invitrogen (The Netherlands). CellTiter 96 AQueous One Solution Cell Proliferation Assay (MTS) was purchased from Promega (USA).

Cells

D1 cells, a long-term growth factor-dependent immature myeloid dendritic cell line of splenic origin derived from a female C57BL/6 mouse,[4] were cultured in IMDM (Iscove's Modified Dulbecco's Medium, Lonza) containing 10% heat-inactivated FBS (Sigma), 2 mM GlutaMax (GIBCO), 50 mM β-mercaptoethanol and fibroblast supernatant (SN) from NIH/3T3 cells, which was collected from confluent cultures and filtered.

B3Z cells, a T cell hybridoma expressing a T-cell receptor that specifically recognizes H-2Kb-restricted OVA MHC class I epitope SIINFEKL, which carries a lacZ construct, were cultured in IMDM medium (Lonza, The Netherlands) containing 10% heat-inactivated

FBS (Sigma, Germany), 2 mM GlutaMax (GIBCO, The Netherlands), 50 mM β-mercaptoethanol (in IMDM).[5]

Preparation and characterization of nanogels/microgels

Cationic nanogels were prepared by inverse mini-emulsion photo-polymerization adapted from a previously published procedure.[3, 6] In short: 150 mg dex-MA was dissolved in 100 µL of distilled water to which subsequently 160 L of an aqueous stock solution TMAEMA was added. Subsequently, 120 µL photoinitiator solution (Irgacure 2959, 10 mg/mL in water) was added. This dextran solution was emulsified in the external phase (5 mL of light mineral oil, containing 10% v/v ABIL EM 90 surfactant) by ultrasonication for 2 minutes (cycle-0, amplitude 10%, Sonopuls HD 2200, BANDELIN). The emulsified nanodroplets were exposed to UV irradiation (15 minutes, Bluepoint UV source, Hönle UV technology) to polymerize dex-MA and TMAEMA. The crosslinked nanoparticles were purified by 5 times washing with acetone/hexane (50:50 v/v), then rehydrated and lyophilized (Yield: ~95%). The average size and zeta-potential of the nanogels dispersed in HEPES buffer (20mM, pH 7.4) was measured using DLS (Malvern ALV/CGS-3 Goniometer, Malvern Instruments) and Zetasizer (Zetasizer Nano, Malvern Instruments).

Microgels were obtained by dextran/PEG water-in-water emulsion polymerization.[3, 7, 8] Briefly, PEG (3.22 g), dex-MA (146 mg), and 1 mL of TMAEMA were added to 20 mL HEPES buffer (100 mM pH 7.4). After dissolution of PEG and dex-MA, the solution was transferred into a 50 mL tube and vortexed for 2 minutes at maximum intensity. A water-in-water emulsion was formed and then allowed to stabilize for 5 minutes. Next, a sodium bisulfite solution (720 µL, 20 mg/mL in HEPES buffer (100 mM pH 7.4)) and a KPS solution (720 µL, 50 mg/mL in HEPES buffer (100 mM pH 7.4)) were added to the mixture. Dex-MA and TMAEMA in the formed droplets were allowed to crosslink overnight at room temperature. The polymerized particles were purified by 3 times washing with water and then lyophilized (yield: ~80%). The particle size distribution and zeta-potential of the microgels dispersed in HEPES buffer (20mM, pH 7.4) were measured using AccuSizer (PSS-Nicomp, Santa Barbara) and Zetasizer, respectively.

Synthesis of pMAA, pHPMA-co-MAA, pTMAEMA and pHPMA-co-TMAEMA

Polymers were synthesized by free radical polymerization as follows. For the

polymerization, MAA (30-120 mg) or TMAEMA (91-363 mg), with or without HPMA (100-150 mg), and ABCPA (2-20 mg) were dissolved in water (1-10 mL) and transferred into glass vials. The composition of polymer, ratio of momomer and initiator, and concentration of monomer for synthesis of various polymers are described in table S1 and S2. Oxygen was removed by application of three vacuum purge/nitrogen flush cycles. Next the vials were incubated at 70 ℃ for 15 hours and the synthesized polymers were dialyzed (molecular weight cutoff of dialysis tubing 14 kDa) against water for 2 days to remove low molecular weight impurities. Polymers were obtained after lyophilization.

Molecular weights and molecular weight distribution of polymers were determined by Viscotek TDAmax (equipped with RI, light scattering and viscosity detectors, Malvern Instruments Ltd., UK) with a Shodex OH pak® SB-806M HQ column (Waters). A 0.1 M sodium hydrogen phosphate buffer (pH 9) for pMAA/pHPMA-co-MAA or a 0.5 M sodium acetate buffer (pH 2) for pTMAEMA/pHPMA-co-TMAEMA were used as eluents with a flow rate of 0.7 mL/min. Samples were dissolved in the mobile phase and injected onto the column (injection volume 50 μL). Results were analyzed by OmniSEC software (Malvern Instruments Ltd., UK) with poly(ethylene oxide) (M_n: 19 kDa, PDI: 1.04, Malvern Instruments Ltd.) as calibration standard. This method was checked by measuring a standard pMAA (M_w=483, PDI=1.12, Sigma). The measured molecular weight and PDI of standard pMMA were M_w=487 and PDI=1.12. The results are shown in table S1 and S2, and the chromatograms of various polymers in table S1 and S2 are shown in figure S1. It should be noted that the high molecular weight of the polymers can be explained by the free radical polymerization in aqueous solution.[9-12]

Table S1. Synthesis and characterization of pMAA and pHPMA-co-MAA.

	HPMA:MA (molar ratio)	Monomer: initiator (molar ratio)	Concentration of monomers (M)	Yield (%)	M_n (kDa)	M_w (kDa)	PDI	dn/dc
pMAA_high MW	0:1	200:1	1.4	96.9	466	817	1.8	0.184
pMAA_low MW	0:1	20:1	0.14	94.3	132	299	2.3	
pHPMA-co-MAA_high MW	1:1	200:1	1.4	96.5	539	986	1.8	0.163
pHPMA-co-MAA_low MW	1:1	20:1	0.14	98.8	134	317	2.4	
pHPMA-co-MAA_3:1	3:1	100:1	1.4	98.3	186	371	2.0	0.155

Table S2. Synthesis and characterization of pTMAEMA and pHPMA-co-TMAEMA.

	HPMA: TMAEMA (molar ratio)	Monomer: initiator (molar ratio)	Concentration of monomers (M)	Yield (%)	M_n (kDa)	M_w (kDa)	PDI	dn/dc
pTMAEMA _high MW	0:1	200:1	1.4	97.7	382	731	1.9	0.132
pTMAEMA _low MW	0:1	20:1	0.14	87.2	173	446	2.6	
pHPMA-co-TMAEMA _high MW	1:1	200:1	1.4	99.1	294	663	2.3	0.157
pHPMA-co-TMAEMA _low MW	1:1	20:1	0.14	86.6	94	186	2.0	
pHPMA-co-TMAEMA _3:1	3:1	100:1	1.4	93.7	240	496	2.1	0.163

pMAA standard from Sigma

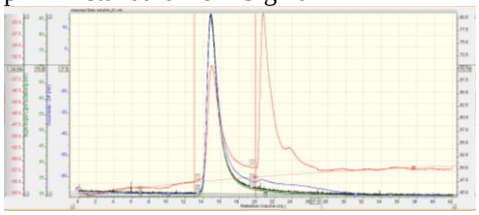

Polyanion

pMAA_high MW

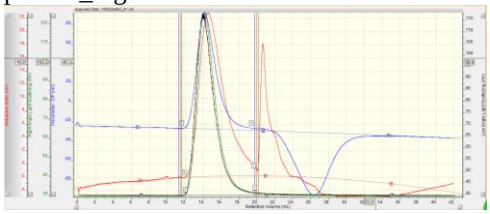

pMAA_low MW

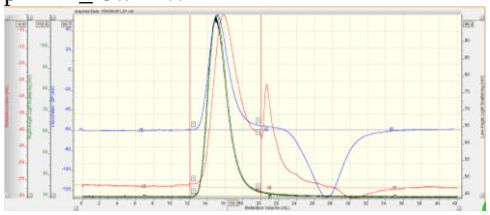

pHPMA-co-MAA_high MW

Polycation

pTMAEMA_high MW

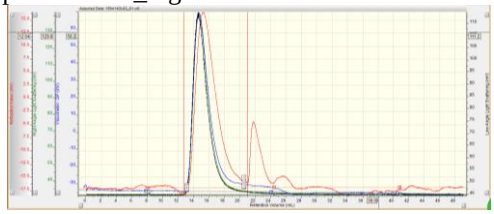

pTMAEMA _low MW

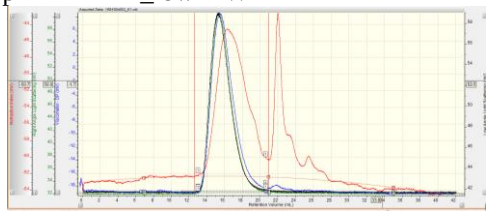

pHPMA-co-TMAEMA_high MW

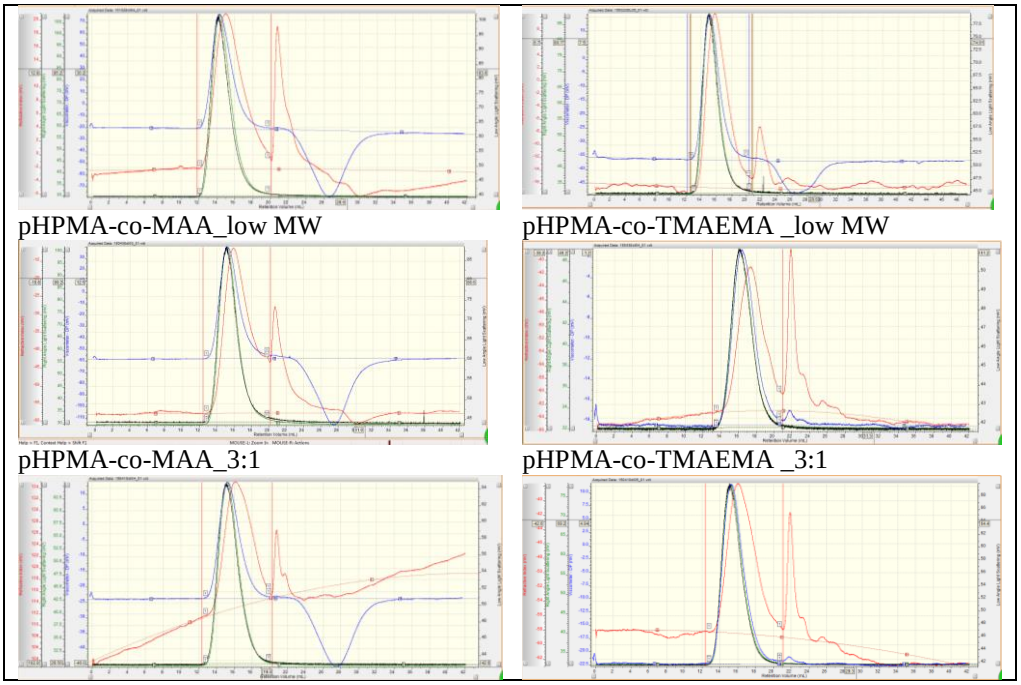

Figure S1. Chromatograms of standard pMAA and various polymers in table S1 and S2. Chromatogram of polymers showing the refractive index (red), right angle light scattering (green), low angle light scattering (black), and viscosity (blue) detector signals.

Preparation and characterization of OVA loaded nanogels/microgels with non-crosslinked LbL coating

An OVA solution (FITC-labelled, 2 mg/mL in HEPES buffer (20 mM, pH 7.4), 0.2 mL) was mixed with a particle suspension (2 mg/mL in HEPES buffer (20 mM, pH 7.4), 0.5 mL) and incubated at room temperature for 2 h to allow OVA loading into the particles. Subsequently, 0.4 mL of pMAA or pHPMA-co-MAA (2 mg/mL in HEPES buffer (20 mM, pH 7.4)) was added and the mixture was incubated for 10 min, followed by centrifugation (20000 g, 30 min) to remove non-coated/free polymers. The pellet after centrifugation was resuspended in 1 mL of HEPES by ultrasonication for 10 secs (cycle-0, amplitude 10%) and 0.4 mL of pTMAEMA or pHPMA-co-TMAEMA (2 mg/mL in HEPES buffer (20 mM, pH 7.4)) was added. Next, the coated particles with 2 layers were collected by centrifugation. The zeta-potential of the obtained coated nanogels (dispersed in HEPES buffer (20 mM, pH 7.4)) was measured by Zetasizer. After each centrifugation step, 200 µL of the supernatant was collected and placed in a 96-well plate. The OVA concentration in

the supernatant was determined by FLUOstar OPTIMA (BMG LABTECH) using FITC-OVA as the standard and the loading efficiency (LE) was calculated by (feed OVA-OVA in the supernatant)/feed OVA weight*100%. The FITC-OVA calibration curve was linear between 5 and 400 μg/mL. The release of FITC-OVA from the nanogels coated with non-crosslinked polymers was measured after 1 h incubation in PBS (Table S3).

For imaging, FITC-OVA loaded microgels coated with 2 layers of pMAA/pHPMA-co-MAA and rhodamine B labelled pTMAEMA/pHPMA-co-TMAEMA were prepared as described above. To label the pTMAEMA/pHPMA-co-TMAEMA, amine groups were introduced by adding 2 mol% of AEMA during polymerization. The pTMAEMA/pHPMA-co-TMAEMA with amine groups (20 mg dissolved in 1mL of sodium bicarbonate buffer (100 mM, pH 8.5), containing 114 μmol of amine groups) was incubated with rhodamine B isothiocyanate (10 mg/mL in DMSO, 35 μL, 0.65 μmol) for 2 h. The free dye was removed by PD-10 desalting column (GE Healthcare Life Sciences). After 1 h incubation of these FITC-OVA loaded microgels coated with various polymers (1 mg/mL) in HEPES (20 mM, pH 7.4) and PBS (164 mM, pH 7.4), CLSM images (Figure S2) were taken by confocal laser scanning microscopy (CLSM, Confocal Leica SPE-II, Leica Microsystems).

The table S3 shows that after coating with the first layer of pMAA or pHPMA-co-MAA, the ζ-potential of the nanogels reversed except the one coated with pHPMA-co-MAA_3:1, indicating that the charge density of this polyanion is not sufficient either to coat on the nanogels or to reverse the surface charge. Further, except nanogels coated with pHPMA-co-MAA_3:1 and pHPMA-co-TMAEMA_3:1, only nanogels coated with pHPMA-co-MAA_high MW and pHPMA-co-TMAEMA_high MW maintained most OVA encapsulated. Moreover, most of the encapsulated OVA was released within 1 hour when these nanogels were incubated in physiological ionic strength buffer (PBS). In agreement with these data, microgels coated with pHPMA-co-MAA_high MW and pHPMA-co-TMAEMA_high MW showed in CLSM a clear ring of red fluorescence of rhodamine labelled polycations (without polymer penetrating into the particles) in HEPES buffer of low ionic strength (Figure S2). When the particles were incubated with PBS, the higher ionic strength of this medium resulted in destabilisation of the non-crosslinked LbL coating and the release of OVA from the microgels (Figure S2). Based on the OVA loading and release data (Table S3) and confocal images (Figure S2) of particles coated with various polymers of table S1 and S2, pHPMA-co-MAA (molar ratio 1:1, Mn=539kD, PDI=1.8) and pHPMA-co-TMAEMA (molar ratio1:1, Mn=302kD, PDI=2.2) of optimized charge density and molecular weight were selected for further study.

Table S3. Characterization of OVA loaded nanogels coated with various polyanions/polycations (n=3). The nanogels were dispersed in HEPES buffer (20 mM, pH 7.4).

First coating layer	Second coating layer	ζ-potential after first coating layer (mV)	ζ-potential after second coating layer (mV)	LE (%)	Release of OVA in PBS in 1 h (%)
pMAA_high MW	pTMAEMA_high MW	-29.0 ±2.0	34.9 ±1.3	56.1 ±0.9	86.5 ±3.8
pMAA_low MW	pTMAEMA _low MW	-23.9 ±0.6	28.7 ±1.2	34.7 ±1.3	95.6 ±2.3
pHPMA-co-MAA_high MW	pHPMA-co-TMAEMA_high MW	-22.7 ±1.7	31.8 ±1.4	87.2 ±1.3	98.9 ±2.0
pHPMA-co-MAA_low MW	pHPMA-co-TMAEMA _low MW	-22.4 ±0.8	26.3 ±1.1	43.9 ±0.5	98.2 ±0.6
pHPMA-co-MAA_3:1	pHPMA-co-TMAEMA _3:1	3.9 ±0.3	12.9 ±0.8	90.8 ±0.3	100.0 ±0.9

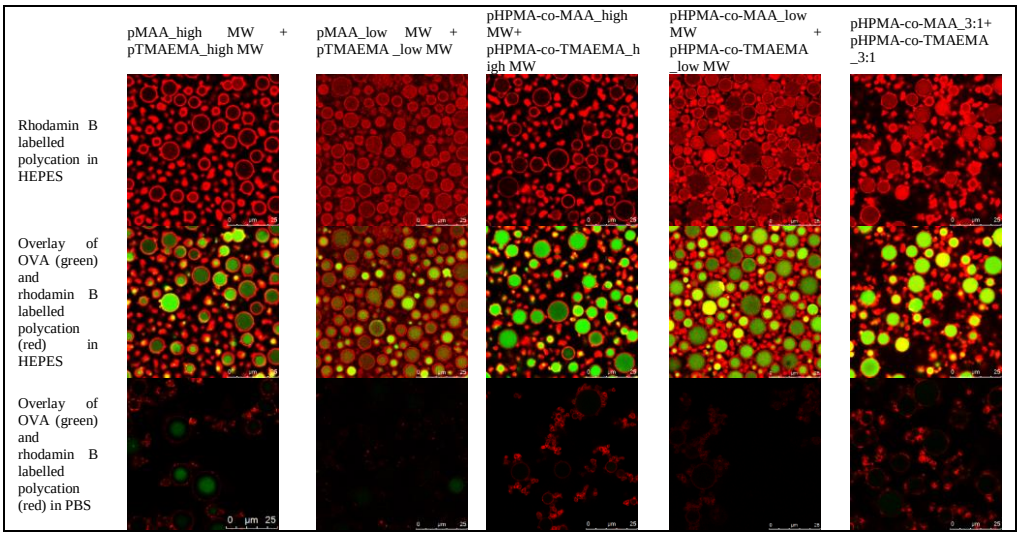

Figure S2. CLSM images of FITC-OVA loaded microgels coated with various polyanions /rhodamine B labelled polycations.

Synthesis of pHPMA-co-MAA-co-PDTEMA and pHPMA- co-TMAEMA-co-PDTEMA

To modify pHPMA-co-MAA with functional pyridyldisulfide groups, PDA (70 mg) and pHPMA-co-MAA (100 mg) were dissolved in 10 ml of water. DMTMM (50 mg) was added to the mixture and the amine groups of PDA were coupled to the carboxylic groups

of the pHPMA-co-MAA through DMTMM coupling. The reaction was performed at 50 ℃ for 15 hours and the modified polymer (pHPMA-co-MAA-co-PDTEMA) was dialyzed against water for one day and collected after lyophilization (yield 96%).

For the synthesis of pHPMA-co-TMAEMA-co-PDTEMA, HPMA (100 mg), TMAEMA (182 mg), PDTEMA (80 mg), and ABCPA (8 mg) were dissolved in 2 ml of 50% methanol in water, and O_2 was removed by application of three vacuum purge/nitrogen flush cycles. The polymerization was performed at 70 ℃ for 15 hours and subsequently the solution was transferred into a dialysis tube (molecular weight cutoff 14 kDa) and dialyzed against water for 2 days. pHPMA-co-TMAEMA-co-PDTEMA was obtained after lyophilization (yield 94%).

The content of pyridyldisulfide units in the synthesized polymers was determined by incubating the polymers (0.5 mg/mL) in DTT (10 mM in PBS) for 2 h at room temperature and then measuring the formed 2-mercaptopyridine by HPLC (Waters). The HPLC was equipped with a Sunfire C18 column 5 μm (4.6×150 mm, Waters) and tunable ultraviolet/visible light detector (Waters) was set at 280 nm. Elution was performed with a 10% ACN aqueous phase and ACN phase with the following gradient: 0-6 min, from 100% to 60% of 10% ACN aqueous phase. The flow rate was 1.0 mL/min and the injection volume was 20 μL for polymer samples and 2-mercaptopyridine standard solutions. The 2-mercaptopyridine calibration curve was linear between 5 and 100 μg/mL. The content of pyridyldisulfide units in the polymer was calculated by (the mol of PDTEMA incorporated in polymer)/the mol of polymer*100%.

Preparation and characterization of OVA loaded nanogels with disulfide crosslinked polymer shell

As described above, OVA (0.2 mL, 2 mg/mL) was loaded into the nanogels (0.5mL, 2mg/mL), and subsequently the nanogels were coated with alternating layers of pHPMA-co-MAA-co-PDTEMA (0.4 mL, 2 mg/mL) and pHPMA-co-TMAEMA-co-PDTEMA (0.4 mL, 2 mg/mL). To quantify the amount of each coating layer, DTT (10 mM, 1 mL) was added to cleave and release 2-mercaptopyridine from pyridyldisulfide units of the coating polymers after each absorption and centrifugation step. After 2 h incubation with DTT, the particles were spun down. The released 2-mercaptopyridine in the supernatant was measured by HPLC as described above and the mass of polymers coated on nanogels was determined. To crosslink the polymer layers, DTT of 0.5 molar equivalent

of pyridyldisulfide groups of the coating polymer was added after each adsorption and centrifugation step. The DTT cleaved the disulfide bonds of pyridyldisulfide groups and the exposed thiol groups reacted with the remaining 0.5 molar equivalent of pyridyldisulfide groups by thiol disulfide exchange reaction subsequently to yield the crosslinked network. The crosslinking efficiency was checked by measuring the released 2-mercaptopyridine, from which we calculated that 99% of pyridyldisulfide groups were reacted. After the coating and crosslinking of the last layer, the particles were spun down and washed once with water to remove reacted DTT and released 2-mercaptopyridine. OVA loaded nanogels coated with 1, 2 and 3 disulfide crosslinked polymer layers were prepared. The size and zeta-potential of these coated nanogels were measured by DLS and Zetasizer. The released OVA was measured in the supernatant after the coating and crosslinking process and loading efficiency (LE) and loading capacity (LC) were calculated as follows:

LE= (feed OVA- OVA loss in supernatant after coating and crosslinking) / feed OVA weight *100%

LC= loaded OVA / (loaded OVA + dry nanogels + coated polymer) weight *100%

In vitro OVA release from coated nanogels/microgels

Particles were dispersed in PBS (164 mM (containing 164 mM of Na^+, 140 mM of Cl^-. 8.7 mM of HPO_4^{2-}, and 1.8 mM of $H_2PO_4^-$), pH 7.4) to 1 mg/mL and incubated for 8 h. DTT was added at 8 h to a final concentration of 2.5 mM to reduce the crosslinked LbL coating and release the entrapped OVA. The release of OVA was monitored at 37 ℃ by taking samples at different time points, spinning down the particles (20,000 g, 30 min) and analyzing the supernatant for OVA concentration (see previous paragraph).

To visualize the coating and triggered release, FITC-OVA loaded microgels coated with crosslinked rhodamine B labeled polymer shell were prepared as described above. The CLSM images were taken after incubation of the microgels in HEPES (20 mM, pH 7.4), PBS (164 mM, pH 7.4), and DTT (2.5 mM in PBS) for 8h.

Intracellular release of OVA from nanogels with disulfide-crosslinked polymer shell

To visualize the internalization of particles and intracellular release of OVA, nanogels were labelled with Alexa Fluor 488 dye as described previously.[3, 13] Alexa Fluor 647 labelled

OVA (commercial available, Invitrogen) was loaded in labelled nanogels , and subsequently coated with various rhodamine B labelled polycations as described above. D1 cells (50,000 cells in fluorodish) were incubated with particles at a final concentration of 15 μg/mL for 2 and 24 h at 37 ℃. Subsequently, confocal images were taken by CLSM after washing cells with medium once.

Cytotoxicity of nanogels towards D1 cells

D1 cells (50,000 cells/well) in a 96-well plate were incubated with OVA loaded nanogels with various coating layers at titrated amounts for 24 h at 37 ℃. The relative cell viability was quantified by Cell Titer 96 AQueous One Solution Cell Proliferation Assay (MTS).[14] In short, after 24 h incubation, the medium was aspirated, and 20 μL of Cell Titer 96 AQueous One Solution Reagent in 100 μL of culture medium was added into each well of the 96-well plate. The plate was incubated for 1-2 h at 37 ℃. After centrifugation (4000 g, 10 min), 100 μL of the reaction solution of each well was transferred to a new well plate and the absorbance was measured at 490 nm.

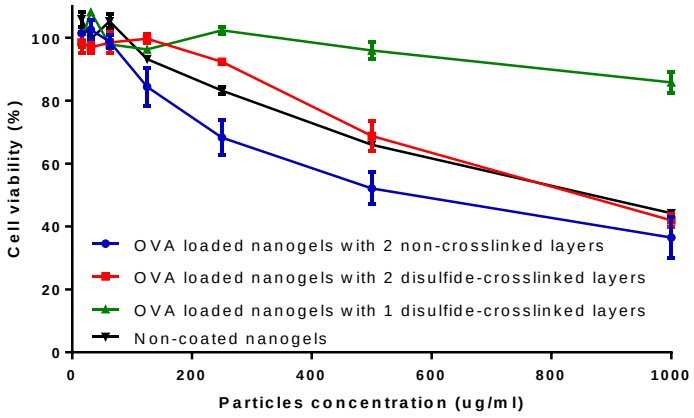

Figure S3. Viability of D1 cells, incubated for 24 h with particles. The colorimetric reading at 490 nm of non-treated cells was set at 100% and all data are shown as mean ± SD (n=3). Representative results from one out of three experiments are shown.

MHC class I antigen presentation assay

D1 cells (50,000 cells/well) in a 96-well plate were incubated with H-2Kb-restricted OVA class I epitope SIINFEKL, soluble OVA, and OVA loaded nanogels coated with various polymer layers at titrated amounts of OVA for 24 h at 37 ℃. SIINFEKL was used as a positive control.[15] Subsequently, B3Z cells (50,000 cells/well) were added to D1 cells and co-incubated with D1 cells for 24 h at 37 ℃. The hybridoma B3Z cells produce β-galactosidase after being activated by DCs that present SIINFEKL, thus allowing measurement of MHC class I antigen presentation by a colorimetric assay using CPRG.[16] β-Galactosidase activity of B3Z cells was measured by incubating the cells with 100 μL of CPRG buffer (9.6 mL of PBS (164 mM (containing 164 mM of Na^+, 140 mM of Cl^-. 8.7 mM of HPO_4^{2-}, and 1.8 mM of $H_2PO_4^-$), pH 7.4), 100 μL of CPRG (9 mg/ml freshly prepared in PBS), 90 μL of $MgCl_2$ (1 M), 125 μL of 10% IGEPAL CA-630 and 71 μL of β-mercaptoethanol). The β-galactosidase converted the yellow-orange substrate CPRG into the red chromophore chlorophenol absorbing at 590 nm, and the absorbance was measured by SPECTROstar (BMG Labtech, Germany).

5

References

1. van Dijk-Wolthuis, W. N. E.; Franssen, O.; Talsma, H.; van Steenbergen, M. J.; Kettenes-van den Bosch, J. J.; Hennink, W. E. Synthesis, characterization, and polymerization of glycidyl methacrylate derivatized dextran. *Macromolecules* 1995, 28, 6317-6322.
2. Ulbrich, K.; Šubr, V.; Strohalm, J.; Plocová, D.; Jelínková, M.; Říhová, B. Polymeric drugs based on conjugates of synthetic and natural macromolecules: I. Synthesis and physico-chemical characterisation. *J Control Release* 2000, 64, 63-79.
3. Li, D.; Kordalivand, N.; Fransen, M. F.; Ossendorp, F.; Raemdonck, K.; Vermonden, T.; Hennink, W. E.; van Nostrum, C. F. Reduction-sensitive dextran nanogels aimed for intracellular delivery of antigens. *Adv Func Mater* 2015, 25, 2993-3003.
4. Winzler, C.; Rovere, P.; Rescigno, M.; Granucci, F.; Penna, G.; Adorini, L.; Zimmermann, V. S.; Davoust, J.; Ricciardi-Castagnoli, P. Maturation stages of mouse dendritic cells in growth factor-dependent long-term cultures. *J Exp Med* 1997, 185, 317-28.
5. Sanderson, S.; Shastri, N. LacZ inducible, antigen/MHC-specific T cell hybrids. *Int Immunol* 1994, 6, 369-76.
6. Raemdonck, K.; Naeye, B.; Buyens, K.; Vandenbroucke, R. E.; Høgset, A.; Demeester, J.; De Smedt, S. C. Biodegradable dextran nanogels for rna interference: focusing on endosomal escape and intracellular siRNA delivery. *Adv Func Mater* 2009, 19, 1406-1415.
7. Franssen, O.; Hennink, W. E. A novel preparation method for polymeric microparticles without the use of organic solvents. *Int J Pharm* 1998, 168, 1-7.
8. Stenekes, R. J. H.; Franssen, O.; van Bommel, E. M. G.; Crommelin, D. J. A.; Hennink, W. E.

The preparation of dextran microspheres in an all-aqueous system: effect of the formulation parameters on particle characteristics. *Pharm Res* 1998, 15, 557-561.

9. van de Wetering, P.; Cherng, J.-Y.; Talsma, H.; Hennink, W. E. Relation between transfection efficiency and cytotoxicity of poly(2-(dimethylamino)ethyl methacrylate)/plasmid complexes. *J Control Release* 1997, 49, 59-69.
10. van de Wetering, P.; Cherng, J. Y.; Talsma, H.; Crommelin, D. J. A.; Hennink, W. E. 2-(dimethylamino)ethyl methacrylate based (co)polymers as gene transfer agents. *J Control Release* 1998, 53, 145-153.
11. Kaneko, Y.; Iwakiri, N.; Sato, S.; Kadokawa, J.-i. Stereospecific free-radical polymerization of methacrylic acid calcium salt for facile preparation of isotactic-rich polymers. *Macromolecules* 2008, 41, 489-492.
12. Reschel, T.; Koňák, Č. r.; Oupický, D.; Seymour, L. W.; Ulbrich, K. Physical properties and in vitro transfection efficiency of gene delivery vectors based on complexes of DNA with synthetic polycations. *J Control Release* 2002, 81, 201-217.
13. Naeye, B.; Raemdonck, K.; Remaut, K.; Sproat, B.; Demeester, J.; De Smedt, S. C. PEGylation of biodegradable dextran nanogels for siRNA delivery. *Eur J Pharm Sci* 2010, 40, 342-351.
14. Malich, G.; Markovic, B.; Winder, C. The sensitivity and specificity of the MTS tetrazolium assay for detecting the in vitro cytotoxicity of 20 chemicals using human cell lines. *Toxicology* 1997, 124, 179-192.
15. Falk, K.; Rötzschke, O.; Faath, S.; Goth, S.; Graef, I.; Shastri, N.; Rammensee, H.-G. Both human and mouse cells expressing h-2kb and ovalbumin process the same peptide, SIINFEKL. *Cell Immunol* 1993, 150, 447-452.
16. Karttunen, J.; Sanderson, S.; Shastri, N. Detection of rare antigen-presenting cells by the lacZ T-cell activation assay suggests an expression cloning strategy for T-cell antigens. *Proc Natl Acad Sci* 1992, 89, 6020-6024.

Chapter 6

Summary and perspectives

1. Summary

Cancer immunotherapy aims to activate the immune system to fight cancer.[1-3] Protein-based cancer vaccines have emerged as a promising approach of cancer immunotherapy, which evoke specific anticancer immunity against tumor cells.[4, 5] However, tumor associated protein antigens are poorly immunogenic due to the fact that they are not efficiently taken up by immune cells combined with a lack of so-called danger signals to stimulate the immune system. Furthermore, for effective anticancer therapy, cancer vaccines should be able to trigger $CD8^+$ T cells and activate anticancer cytotoxic T lymphocyte (CTL) responses, which require MHC class I pathway antigen presentation.[6] Dendritic cells (DCs) are professional antigen presenting cells (APCs) that initiate and regulate innate and adaptive immune responses, and therefore they are extremely relevant target cells for anticancer vaccines.[7, 8] The main function of DCs is to capture and process antigens into antigenic peptides, and present them to T cells. It should be noted that tumor associated protein antigens are usually processed in the endo/lysosomal compartments of DCs, which generally favors MCH class II rather than MHC class I antigen presentation.[9-11] Hence, enhancing MHC class I antigen presentation of tumor antigens (so called cross-presentation) is highly desirable to improve the anticancer efficacy of cancer vaccines.[12]

Nanogels have been reported as potent vaccine delivery systems.[13, 14] Due to their pathogen-like size, nanogels are readily taken up by APCs, especially DCs.[15] Tuning particle size and surface charge can further enhance uptake efficiency.[16-18] Nanogels can be loaded with tumor associated protein antigens, and therefore effectively enhance uptake of the loaded antigen by DCs. Certain nanogels can also facilitate DC maturation and activation resulting in enhanced antigen presenting capability and avoidance of immunological tolerance.[6, 16, 19] More interestingly, nanogels have been reported to promote antigen cross-presentation both *in vitro* and *in vivo*.[6, 20-22] Therefore, the main aim of this thesis was to develop vaccine delivery systems based on nanogels using ovalbumin (OVA) as a model antigen, and evaluate their efficacy *in vitro* as well as *in vivo*.

In **Chapter 1**, the principles of tumor vaccination are introduced including the poor immunogenicity of tumor associated antigens, and the need to deliver them to APCs for anticancer immunity. Nanogels as effective carriers for delivery of tumor associated antigens and the influence of their properties on modulation of the immune response are discussed. Furthermore, the intracellular antigen delivery strategy utilizing reducible disulfide linkages is discussed as promising method to boost both MHC class I and MHC class II antigen presentation.

Chapter 2 gives reviews the current literature of nanogel carrier systems for intracellular delivery of biotherapeutics (e.g. proteins, antigens, and genes), focusing on biologically responsive nanogels. The needs and challenges for intracellular delivery of biotherapeutics are discussed. Nanogels can be designed to rapidly release encapsulated biotherapeutics in a triggered manner by physiological differences between the intracellular environment and the extracellular space. Most of the biologically responsive nanogels discussed in this review showed a significantly enhanced therapeutic effect by delivery and release of higher doses of biotherapeutics intracellularly as compared to their non-responsive counterparts. Overall, this chapter highlights the current insights that biologically responsive nanogels are highly promising formulations for intracellular delivery of biomolecules including tumor vaccination applications.

The feasibility of using reduction-sensitive nanogel carrier systems for intracellular antigen delivery was evaluated in **Chapter 3** by conjugating a model antigen OVA to the network of cationic dextran nanogels. OVA is negatively charged at pH 7 because of its pI of 5.0. Therefore, cationic dextran nanogels also containing thiol-reactive groups were prepared from methacrylated dextran, trimethyl aminoethyl methacrylate and N-(4-(2-(pyridine-2-yldisulfanyl)ethyl)-amidobutyl) methacrylamide by inverse mini-emulsion photo-polymerization. OVA, derivatized with succinimidyl S-acetylthioacetate groups (SATA), was almost quantitatively absorbed in these nanogels exploiting electrostatic interactions in low ionic strength buffer (HEPES, 20 mM, pH 7.4). Subsequently, SATA-OVA was covalently conjugated to the gel network via disulfide bonds by a reaction of the thiolated OVA with pyridyldisulfide groups present in the nanogels. Control experiments showed that physically loaded OVA was released rapidly from the nanogels under physiological conditions (PBS, 164 mM, pH 7.4). In contrast, the nanogels in which OVA was chemically immobilized showed only a limited amount of released protein during 8 hours in PBS. More than 80% of the loaded amount of OVA was released within 1 hour under reducing conditions because of the cleavage of the disulfide bridges. To visualize the intracellular release of the conjugated OVA, this protein and the nanogels were labeled with Alexa Fluor 647 and Alexa Fluor 488, respectively. Confocal images showed that double labeled nanogels were efficiently taken up by DCs after 24 hours incubation at 37 ℃. The conjugated OVA was released from the nanogels upon their internalization by DCs, while non-conjugated OVA was already released before being taken up. Subsequently, the ability of the nanogels facilitating conjugated OVA to be cross-presented to $CD8^+$ T cells was evaluated *in vitro* using OVA-specific B3Z hybridoma T cells. The obtained results showed strong $CD8^+$ T cell activation induced by OVA conjugated nanogels, while free OVA and

non-conjugated OVA nanogels were not able to activate T cells. Taken together, the potential of reduction-sensitive nanogels as an antigen delivery system for inducing cellular immune responses *in vitro* is shown in this chapter.

Encouraged by the promising results obtained by the study discussed in chapter 3, we further investigated the influence of nanogel size and surface charge on the uptake by DCs, the capability of the nanogels to maturate DCs, and the intracellular delivery, transportation and processing of antigen by DCs *in vitro* in **Chapter 4**. Importantly, prophylactic and therapeutic vaccination with antigen conjugated nanogels *in vivo* was performed in this chapter. The binding and uptake studies showed that the nano sized gels with relatively high cationic surface charge were most efficiently taken up by DCs. Moreover, these highly cationic charged gel particles were also able to induce DCs maturation, which is independent of the size of the particles (200 to 2500 nm). Flow cytometry analysis showed that a higher amount of OVA was delivered and processed intracellularly in DCs by the nanogels with conjugated OVA as compared to nanogels that were physically loaded with OVA after 24 h incubation. Next, the fate of the nanogels and conjugated OVA in DCs was studied. Confocal images showed that the internalized nanogels were entrapped in the lysosomes of DCs during 24 h, while the processed fragments of the released antigen were transported to the cytosol, which is crucial for MHC class I antigen presentation. Next, we tested their efficacy *in vivo* in both a prophylactic and a therapeutic tumor model using B16OVA melanoma (expressing OVA antigen). C57BL/6 mice (10 animals per group) received various formulations subcutaneously (s.c.) before (prophylactic vaccination) or after (therapeutic vaccination) inoculation with s.c. administered tumor cells. Mice immunized with OVA conjugated nanogels effectively provoked an antigen specific T cell immune response as well as increased antigen specific antibody production, and thus induced a strong protective and curative effect against melanoma *in vivo*. In the prophylactic model, 90% of the mice vaccinated with OVA conjugated nanogels + poly(I:C) as adjuvant were protected against tumor formation for 55 days. In the therapeutic model, 40% of the mice eliminated their tumor cells, which was remarkable compared to other groups in which none of the mice showed tumor cell killing. In summary, the nanogels described in this study are promising formulations to induce antigen specific immunity against cancer in an animal model.

The potential of conjugating protein antigens to nanogels via reducible disulfide bonds for intracellular antigen delivery to boost anticancer immune response is addressed in Chapter 3 and 4. As described in these chapters, the antigen was covalently linked to the nanogel network which requires chemical modification of the OVA protein. In **Chapter 5**, we

therefore developed nanogels coated with a disulfide crosslinked polymer shell in which a native protein antigen was entrapped. For this technology, the chemical modification of the antigen is not necessary, making the delivery system more versatile. Native OVA was first loaded into cationic dextran nanogels via electrostatic interactions. Subsequently, oppositely charged polymers (anionic poly(N-(2-hydroxypropyl) methacrylamide-co-methacrylic acid) and cationic poly(N-(2-hydroxypropyl) methacrylamide-co-trimethyl aminoethyl methacrylate) carrying pyridyldisulfide groups were coated onto the nanogels in a layer-by-layer fashion exploiting electrostatic interactions. Next, dithiothreitol (DTT) corresponding to 0.5 molar equivalent of pyridyldisulfide groups of the coating polymers was added to cleave half of the pyridyldisulfide groups to yield thiol groups. Subsequently, these thiol groups reacted with the remaining 0.5 molar equivalent of pyridyldisulfide groups by thiol disulfide exchange, resulting in a disulfide-crosslinked polymer coating. Confocal images of the formulations coated with fluorescently labelled polymers showed a clear ring of the polymer shell surrounding the OVA loaded microgels. As expected, the disulfide-crosslinked shell was stable in non-reducing environment preventing leakage of OVA from the nanogels. Importantly, rapidly cleavage of these disulfide bonds under reducing conditions led to disintegration of the polymer shell and subsequent release of the loaded antigen. Furthermore, we demonstrated the ability of these core-shell nanogels for intracellular delivery of antigens to enhance the MHC class I antigen presentation as compared to their non-crosslinked counterparts.

2. Perspectives

This thesis describes nanogel carrier systems in which a protein antigen is either covalently conjugated to the nanogel networks via disulfide bonds, or physically entrapped in nanogels coated with a disulfide crosslinked polymer shell. Despite that the results obtained show that nanogels are promising carriers for tumor vaccination, further optimization and research is recommended to bring these formulations closer to clinical vaccination practice.

2.1 Biodegradable nanogels

The cationic nanogels used in this thesis were prepared by polymerization of glycidyl methacrylate derivatized dextran (dex-MA, Figure 1A), and the formed nanogels are non-degradable under physiological conditions.[23] These non-degradable nanogels were selected to avoid the influence of nanogel degradation on the release of their payloads, and make sure that the measured antigen release from the nanogels is only due to the cleavage

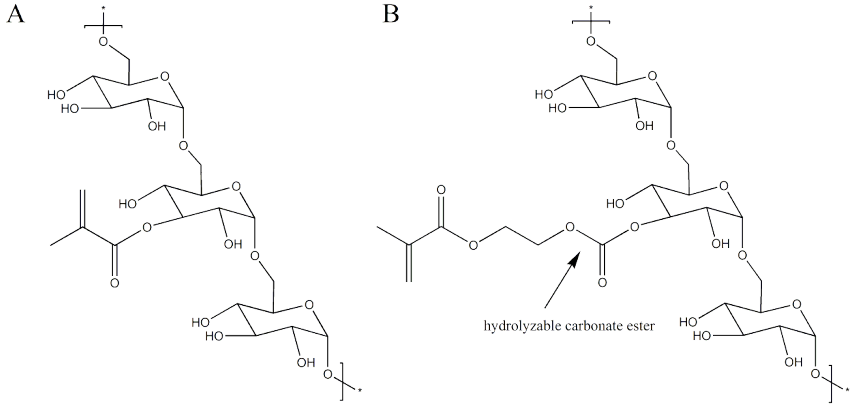

Figure 1. Chemical structures of dex-MA (A) and dex-HEMA (B).

of disulfide bonds. However, a major issue of non-degradable nanoparticles is their limited clearance from the body and consequently accumulation in different organs and tissues, which may interfere with biological processes and in turn cause toxicity.[24-26] Therefore, biodegradable nanogels are preferred for *in vivo* and ultimately clinical use. Degradable dextran based nanogels can be obtained by polymerization of hydroxyethyl methacrylated dextran (dex-HEMA, Figure 1B) in which hydrolysis-sensitive carbonate ester bonds are introduced between the dextran backbone and methacrylate side chains.[27-29] These gels are fully biodegradable under physiological conditions. Cationic dex-HEMA nanogels showed similar properties as dex-MA nanogels for disulfide-conjugated OVA, including size (~200 nm), surface charge (~23 mV), loading capacity of conjugated OVA (~12.5 wt%) and release profiles under non-reducing and reducing conditions as the Dex-MA nanogels (Figure 2). Therefore, by replacing dex-MA with dex-HEMA, biodegradability of reduction-sensitive dextran nanogels can be obtained for *in vivo* application.

2.2 The *in vivo* fate of cationic nanogels

The *in vivo* fate of the cationic nanogels as described in this thesis was not addressed, but it is essential to have knowledge about this behavior for future applications. After subcutaneous injection to mice, these nanogels are likely stuck at the injection site due to their cationic surface charge,[30] and they may serve as antigen reservoirs.[31, 32] The epidermis and dermis are highly populated by APCs, and DCs display important immunostimulatory and migratory activities.[33] DCs preferentially take up virus-sized particles (20-200 nm), whereas macrophages 'prefer' larger particles (0.5-5 μm).[34] The used cationic nanogels are likely taken up by both DCs and macrophages due to their electrostatic interaction with

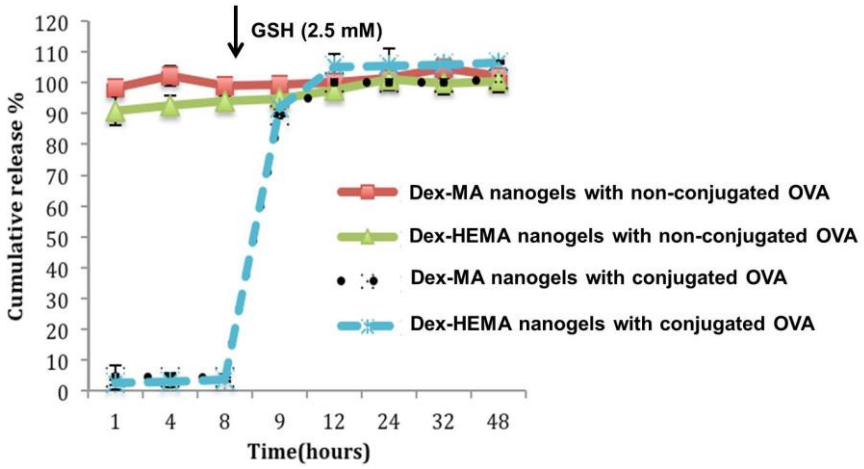

Figure 2. OVA release from dex-MA and dex-HEMA nanogels in PBS pH 7.4 at 37 ℃. GSH was added to concentration of 2.5 mM at 8 h. Anokhee Doshi, master thesis Utrecht University, 2014.

anionic cell membranes of both cells. After their uptake by APCs and subsequent antigen release, the APCs need to migrate from injection sites to draining lymph nodes where cells of the immune system reside, in particular T cells and B cells.[35, 36] Lymph nodes enable APCs, which reside in the lymph node or have migrated from peripheral tissues, to present the processed antigen to T cells and initiate a cellular and/or humoral immune response.[37-39] Future studies should address questions regarding the pathways of the antigen/nanogels and interaction of nanogels with immune and other cells after injection. Antigen and nanogels can be labeled with two distinct near-infrared (NIR) fluorescent dyes, and the presence of OVA and nanogels can be visualized and quantified simultaneously both at the injection site and in the draining lymph nodes.[40] This way, the uptake of fluorescently labeled antigen/nanogels by different populations of APCs and their migration to lymph nodes can be determined by flow cytometry analysis of the draining lymph nodes at different time points post injection.[20, 36] The interaction between nanogels and cells involved in the immune system and their *in vivo* fate affect their immune efficacy. Therefore, a thorough understanding of the fate of antigen/nanogels *in vivo* is required for further optimizing nanogel vaccines, which will be discussed in the next subsection.

2.3 Further optimization of OVA loaded nanogels for *in vivo* cancer vaccination

In Chapter 4, prophylactic and therapeutic vaccination were performed and nanogels with conjugated OVA + soluble poly(I:C) showed impressive antitumor effects, though there are

certainly possibilities for further improvement of the best performing formulation. In the therapeutic model, 8 out of 10 mice that received the nanogels with conjugated OVA + soluble poly(I:C) vaccine showed regression after boost. However, among these 8 mice that showed regression of the tumors, 4 of them were observed tumor regrowing rapidly ~10-15 days after the boost vaccination. A second boost might be given to avoid the observed re-growing of tumor after regression. In addition, administration of antigen conjugated nanogels and a soluble adjuvant can result in delivery of antigen to some DC populations and adjuvant to others. Those DCs that take up only the antigen in particulate form in the absence of adjuvant may induce immunologic tolerance, thereby inhibiting robust antitumor responses. To increase the potential of the vaccines, the antigen and adjuvant could be co-encapsulated and reversibly immobilized in the nanogels, which leads to both of antigen and adjuvant uptake by the same cell populations likely to result in a more potent immune stimulation.[41-43]

As discussed in section 2.2, antigen presentation of APCs to T cells and their priming mainly occur in lymph nodes after subcutaneous injection. Therefore, antigen specific immunity depends on the efficacy of the vaccine and/or antigen loaded APCs reaching these sites.[44, 45] Cationic nanogels likely have limited mobility after injection and their migration to lymph nodes relies on uptake and transportation by local DCs from the injection site.[46, 47] As a consequence, only a minor fraction of nanogel-loaded antigen reaches the lymph nodes and induces an antigen specific immune response. In contrast, particles with high mobility can either be taken up by local DCs, or be drained passively along the interstitial flow to the lymph nodes.[20, 48, 49] Once these particles arrive at the lymph nodes, they are exposed to a large number of APCs, which can process and present antigens and promote antigen specific immune responses.[50-52] Enhancing vaccine delivery into lymphatic systems might more efficiently establish long-term memory responses.[53-55] Therefore, a lymph node targeting vaccine can be a promising strategy to improve the efficiency of nano-vaccines. To optimize our nanogels for this purpose, the cationic charge of the nanogels can be shielded by PEGylation to increase their mobility for lymph node draining. Notably, PEGylation of cationic nano-vaccines was shown to affect their lymphatic draining, uptake by resident APCs, and consequent vaccine induced immune responses.[47, 54, 56] Zhuang et al. demonstrated that incorporation of PEG on cationic liposomes with different densities modulated their drainage from injection site into draining lymph nodes, their lymph node retention and biodistribution, and their contribution to enhanced vaccine specific immune responses.[47] When 1 mol% of PEG2000 was incorporated into the cationic liposomes, the surface charge of liposomes decreased but still

retained positive around +15 mV. These liposomes not only accelerated the drainage of liposomes into lymph nodes, but also prolonged their lymph node retention and enhanced their uptake by resident APCs. On the other hand, the surface charge was fully shielded after incorporating 5 mol% of PEG2000 into cationic liposomes, and remarkably, and the lymph node retention and uptake by APCs of these liposomes was lower than those of formulations with 1 mol% PEG2000. However, liposomes with 5 mol% PEG2000 showed prolonged blood circulation and increased splenic accumulation after s.c. injection, which in turn led to prolonged antigen presentation, thereby enhancing the secondary (memory) responses. For the nanogels described in this thesis, further studies are recommended to investigate the influence of PEGylation and its densities on lymph node accumulation and biodistribution of PEGylated nanogels, and the resulting immune responses. Furthermore, degradable linkages, such as ester bonds, can be introduced in between PEG and the nanogels, which can be cleaved after a certain time, ideally after nanogels migration to lymph nodes. The positive surface charge will then be exposed, thereby increasing the interaction of nanogels with resident APCs.

2.4 Development of the disulfide-crosslinked polymer shell coated nanogels and their application for other therapeutics

In Chapter 5, we developed nanogels coated with disulfide-crosslinked polymer shells in which a native protein antigen was stably entrapped. It should be noted that chemical modification of the encapsulated molecules is not necessary for this intracellular nanogel delivery system. Importantly, lower activity or loss of biological function caused by the modification and conjugation reaction can be avoided. Furthermore, the crosslinked shell may protect the loaded biomolecules from degradation. Hence, nanogels coated with reduction-sensitive polymer shells can be a promising system for intracellular delivery of biotherapeutics, such as therapeutic proteins, enzymes and nucleic acid based therapeutics. It should be noted that for biomolecules with different size, the crosslinked densities of the polymer shell need to be adjusted to ensure impermeability for the encapsulated molecules. Another issue to take into account is that the disulfide-crosslinked densities of the shell may affect its degradation rate and the subsequent release kinetics of the payloads in various cell types varying in redox state of their intracellular environments. In Chapter 5, we showed that the entrapped OVA was released from the layer-by-layer coated nanogels and subsequently processed by DCs, which enhance MHC class I antigen presentation as a consequence. However, direct evidence of cytosolic release of the antigen is still lacking.

Therefore, when applying this delivery system to other therapeutic molecules, especially those with their target site in the cytosol and nucleus, their fate in target cells and subsequent pharmacological and therapeutic effects need to be investigated.

2.5 OVA as a model antigen and other tumor relevant antigens

OVA is a major protein constituent of chicken egg whites, which is sufficiently large and complex to be mildly immunogenic.[57-60] OVA, containing both MHC class I and II epitopes, is widely used as a model antigen to study antigen uptake, processing and presentation *in vitro* and *in vivo* both in its free form and as nanoformulations.[40, 60-63] In addition, because of its immunogenicity, OVA transgene is often introduced into tumor cell lines to enforce expression of this model antigen to study cancer immunology *in vivo*, such as B16OVA cells used in this thesis.[64-66] Encouraged by the results obtained using OVA as the model antigen, other tumor relevant antigens, including tumor lysates, protein antigens and synthetic long peptides,[67-71] can be loaded in the reduction-sensitive nanogel delivery systems as described in this thesis to evaluate their immune efficacy on genetically unmodified tumor models. Human papillomavirus (HPV) is etiologically linked to the development of cervical cancer,[72] and HPV-encoded proteins are expressed in HPV-induced cervical cancer cells.[73-75] Therefore, HPV-encoded proteins and/or synthetic HPV long peptides would be interesting as antigens to investigate the efficacy of reduction-sensitive nanogels for inducing specific immune response against such cancer.[76-78]

2.6 Pharmaceutical production of nanogels

Endotoxin contamination of formulations can maturate DCs and activate the immune system.[79] Therefore, endotoxin free or low endotoxin containing vaccines are used for cell and *in vivo* studies to avoid non-specific immune activation by LPS contamination.[80] Since endotoxins are difficult to remove from a biomaterial,[81] it is important to prevent its contamination in the first place. First of all, clinical grade or low endotoxin raw materials, especially biological products, are preferred. Importantly, the use of pyrogen free water and buffers is a critical necessity during washing and dialysis procedures to avoid endotoxin contamination from laboratory distilled/deionized water. Further, using endotoxin-free containers is strongly recommended. Endotoxins can strongly adhere to glassware and equipment, which makes them potential sources of endotoxin. Heating at 250 °C for more than 30 min or 180 °C for more than 3 h will destroy endotoxins on glassware. On the

other hand, washing with a 1% alkaline solution will also remove endotoxins deposited on surfaces of equipment.[82] Finally, the production processes should be performed in inspected clean conditions with aseptic techniques, and reduce the time of materials exposure to air. The formulations used in this thesis were prepared according to the regulations described above. The yielded products were analyzed by limulus amebocyte lysate (LAL) test, and their endotoxin content was always below detection level (0.1 EU/mL). Therefore, it is possible to produce sterile/low LPS nanogel vaccines for clinical use.

During the production of antigen loaded nanogels in a lab setup, the yield of each step, such as nanogel preparation, antigen loading and purification, is above 90%. The size of a lab scale batch antigen loaded nanogels is mainly limited by the inverse mini-emulsion photo-polymerization step, which produces ~250 mg cationic dextran nanogels for each batch. Scaling up of nanogel preparation is still challenging because of ultrasonication and UV initiation.[83, 84] The droplet size of an emulsion-based dispersed phase can be brought down into the nanometer range when sufficiently strong shear forces are applied by using an ultrasonic homogenizer. To retain the same formulation size after scaling up, it needs to maintain the required intensity of the shear forces to process a lot more material per unit of time.[85] Moreover, high volumes of emulsion can prevent efficient light penetration, and radicals are only formed near the light sources, leading to low crosslinking efficiency of the droplets.[86] Nevertheless, scaling up of nanogel preparation is possible by using the right production-scale equipment.

3. Conclusion

The results described in this thesis present evidence that reduction-sensitive nanogels can be successfully used as systems for intracellular delivery of antigens and stimulate the immune system, which can significantly improve cancer vaccination efficacy.

References

1. Mehta, N. K.; Moynihan, K. D.; Irvine, D. J. Engineering new approaches to cancer vaccines. *Cancer Immunol Res* 2015, 3, 836-843.
2. Butterfield, L. H. Cancer vaccines. *The BMJ* 2015, 350, h988.
3. Melero, I.; Gaudernack, G.; Gerritsen, W.; Huber, C.; Parmiani, G.; Scholl, S.; Thatcher, N.; Wagstaff, J.; Zielinski, C.; Faulkner, I.; Mellstedt, H. Therapeutic vaccines for cancer: an overview of clinical trials. *Nat Rev Clin Oncol* 2014, 11, 509-524.

4. Jain, N. K.; Sahni, N.; Kumru, O. S.; Joshi, S. B.; Volkin, D. B.; Russell Middaugh, C. Formulation and stabilization of recombinant protein based virus-like particle vaccines. *Adv Drug Deliv Rev* 2015, 93, 42-55.
5. Braun, M.; Perret, R.; Scholz, G.; Romero, P. Peptide and protein-based cancer vaccines. *Cancer Immunotherapy: Paradigms, Practice and Promise* 2012, 111-146.
6. Wang, C.; Li, P.; Liu, L.; Pan, H.; Li, H.; Cai, L.; Ma, Y. Self-adjuvanted nanovaccine for cancer immunotherapy: Role of lysosomal rupture-induced ROS in MHC class I antigen presentation. *Biomaterials* 2016, 79, 88-100.
7. Steinman, R. M. Dendritic cells: versatile controllers of the immune system. *Nat Med* 2007, 13, 1155-1159.
8. Liu, Y.-J. Dendritic cell subsets and lineages, and their functions in innate and adaptive immunity. *Cell* 2001, 106, 259-262.
9. Roche, P. A.; Furuta, K. The ins and outs of MHC class II-mediated antigen processing and presentation. *Nat Rev Immunol* 2015, 15, 203-216.
10. Pouniotis, D. S.; Esparon, S.; Apostolopoulos, V.; Pietersz, G. A. Whole protein and defined $CD8^+$ and $CD4^+$ peptides linked to penetratin targets both MHC class I and II antigen presentation pathways. *Immunol Cell Biol* 2011, 89, 904-913.
11. Rodriguez, A.; Regnault, A.; Kleijmeer, M.; Ricciardi-Castagnoli, P.; Amigorena, S. Selective transport of internalized antigens to the cytosol for MHC class I presentation in dendritic cells. *Nat Cell Biol* 1999, 1, 362-368.
12. Joffre, O. P.; Segura, E.; Savina, A.; Amigorena, S. Cross-presentation by dendritic cells. *Nat Rev Immunol* 2012, 12, 557-569.
13. Tahara, Y.; Akiyoshi, K. Current advances in self-assembled nanogel delivery systems for immunotherapy. *Adv Drug Deliv Rev* 2015, 95, 65-76.
14. Ferreira, S. A.; Gama, F. M.; Vilanova, M. Polymeric nanogels as vaccine delivery systems. *Nanomedicine* 2013, 9, 159-173.
15. Fang, R. H.; Kroll, A. V.; Zhang, L. Nanoparticle-based manipulation of antigen-presenting cells for cancer immunotherapy. *Small* 2015, 11, 5483-5496.
16. Thomann-Harwood, L. J.; Kaeuper, P.; Rossi, N.; Milona, P.; Herrmann, B.; McCullough, K. C. Nanogel vaccines targeting dendritic cells: Contributions of the surface decoration and vaccine cargo on cell targeting and activation. *J Control Release* 2013, 166, 95-105.
17. De Temmerman, M.-L.; Rejman, J.; Demeester, J.; Irvine, D. J.; Gander, B.; De Smedt, S. C. Particulate vaccines: on the quest for optimal delivery and immune response. *Drug Discov Today* 2011, 16, 569-582.
18. Benne, N.; van Duijn, J.; Kuiper, J.; Jiskoot, W.; Slütter, B. Orchestrating immune responses: How size, shape and rigidity affect the immunogenicity of particulate vaccines. *J Controlled Release* 2016, 234, 124-134.

19. Démoulins, T.; Bassi, I.; Thomann-Harwood, L.; Jandus, C.; Kaeuper, P.; Simon, H.-U.; von Gunten, S.; McCullough, K. C. Alginate-coated chitosan nanogel capacity to modulate the effect of TLR ligands on blood dendritic cells. *Nanomedicine* 9, 806-817.
20. Nuhn, L.; Vanparijs, N.; De Beuckelaer, A.; Lybaert, L.; Verstraete, G.; Deswarte, K.; Lienenklaus, S.; Shukla, N. M.; Salyer, A. C. D.; Lambrecht, B. N.; Grooten, J.; David, S. A.; De Koker, S.; De Geest, B. G. pH-degradable imidazoquinoline-ligated nanogels for lymph node-focused immune activation. *Proc Natl Acad Sci* 2016, 113, 8098-8103.
21. Li, D.; Kordalivand, N.; Fransen, M. F.; Ossendorp, F.; Raemdonck, K.; Vermonden, T.; Hennink, W. E.; van Nostrum, C. F. Reduction-sensitive dextran nanogels aimed for intracellular delivery of antigens. *Adv Func Mater* 2015, 25, 2993-3003.
22. Li, P.; Luo, Z.; Liu, P.; Gao, N.; Zhang, Y.; Pan, H.; Liu, L.; Wang, C.; Cai, L.; Ma, Y. Bioreducible alginate-poly(ethylenimine) nanogels as an antigen-delivery system robustly enhance vaccine-elicited humoral and cellular immune responses. *J Control Release* 2013, 168, 271-279.
23. van Dijk-Wolthuis, W. N. E.; Franssen, O.; Talsma, H.; van Steenbergen, M. J.; Kettenes-van den Bosch, J. J.; Hennink, W. E. Synthesis, characterization, and polymerization of glycidyl methacrylate derivatized dextran. *Macromolecules* 1995, 28, 6317-6322.
24. Stern, S. T.; McNeil, S. E. Nanotechnology Safety Concerns Revisited. *Toxicol Sci* 2008, 101, 4-21.
25. Garnett, M. C.; Kallinteri, P. Nanomedicines and nanotoxicology: some physiological principles. *Occup Med* 2006, 56, 307-311.
26. Zhao, L.; Seth, A.; Wibowo, N.; Zhao, C.-X.; Mitter, N.; Yu, C.; Middelberg, A. P. J. Nanoparticle vaccines. *Vaccine* 2014, 32, 327-337.
27. Franssen, O.; Vandervennet, L.; Roders, P.; Hennink, W. E. Degradable dextran hydrogels: controlled release of a model protein from cylinders and microspheres. *J Controlled Release* 1999, 60, 211-221.
28. Van Tomme, S. R.; Hennink, W. E. Biodegradable dextran hydrogels for protein delivery applications. *Expert Rev Med Devices* 2007, 4, 147-64.
29. Raemdonck, K.; Van Thienen, T. G.; Vandenbroucke, R. E.; Sanders, N. N.; Demeester, J.; De Smedt, S. C. Dextran microgels for time-controlled delivery of siRNA. *Adv Func Mat* 2008, 18, 993-1001.
30. Xiang, J.; Xu, L.; Gong, H.; Zhu, W.; Wang, C.; Xu, J.; Feng, L.; Cheng, L.; Peng, R.; Liu, Z. Antigen-loaded upconversion nanoparticles for dendritic cell stimulation, tracking, and vaccination in dendritic cell-based immunotherapy. *ACS Nano* 2015, 9, 6401-6411.
31. Henriksen-Lacey, M.; Bramwell, V. W.; Christensen, D.; Agger, E.-M.; Andersen, P.; Perrie, Y. Liposomes based on dimethyldioctadecylammonium promote a depot effect and enhance immunogenicity of soluble antigen. *J Controlled Release* 2010, 142, 180-186.

32. Henriksen-Lacey, M.; Christensen, D.; Bramwell, V. W.; Lindenstrøm, T.; Agger, E. M.; Andersen, P.; Perrie, Y. Comparison of the depot effect and immunogenicity of liposomes based on dimethyldioctadecylammonium (DDA), 3β-[N-(N′,N′-dimethylaminoethane)carbomyl] cholesterol (DC-Chol), and 1,2-dioleoyl-3-trimethylammonium propane (DOTAP): prolonged liposome retention mediates stronger Th1 responses. *Mol Pharm* 2011, 8, 153-161.
33. Mathers, A. R.; Larregina, A. T. Professional antigen-presenting cells of the skin. *Immunol Res* 2006, 36, 127-136.
34. Xiang, S. D.; Scholzen, A.; Minigo, G.; David, C.; Apostolopoulos, V.; Mottram, P. L.; Plebanski, M. Pathogen recognition and development of particulate vaccines: Does size matter? *Methods* 2006, 40, 1-9.
35. Randolph, G. J.; Angeli, V.; Swartz, M. A. Dendritic-cell trafficking to lymph nodes through lymphatic vessels. *Nat Rev Immunol* 2005, 5, 617-628.
36. De Koker, S.; Cui, J.; Vanparijs, N.; Albertazzi, L.; Grooten, J.; Caruso, F.; De Geest, B. G. Engineering polymer hydrogel nanoparticles for lymph node-targeted delivery. *Angewandte* 2016, 55, 1334-1339.
37. Shi, H.-Z.; Humbles, A.; Gerard, C.; Jin, Z.; Weller, P. F. Lymph node trafficking and antigen presentation by endobronchial eosinophils. *J Clin Invest* 105, 945-953.
38. Mempel, T. R.; Henrickson, S. E.; von Andrian, U. H. T-cell priming by dendriticcells in lymph nodes occurs in three distinct phases. *Nature* 2004, 427, 154-159.
39. Itano, A. A.; Jenkins, M. K. Antigen presentation to naive CD4 T cells in the lymph node. *Nature immunol* 2003, 4, 733-739.
40. Rahimian, S.; Kleinovink, J. W.; Fransen, M. F.; Mezzanotte, L.; Gold, H.; Wisse, P.; Overkleeft, H.; Amidi, M.; Jiskoot, W.; Löwik, C. W.; Ossendorp, F.; Hennink, W. E. Near-infrared labeled, ovalbumin loaded polymeric nanoparticles based on a hydrophilic polyester as model vaccine: In vivo tracking and evaluation of antigen-specific $CD8^+$ T cell immune response. *Biomaterials* 2015, 37, 469-477.
41. Scott, E. A.; Stano, A.; Gillard, M.; Maio-Liu, A. C.; Swartz, M. A.; Hubbell, J. A. Dendritic cell activation and T cell priming with adjuvant- and antigen-loaded oxidation-sensitive polymersomes. *Biomaterials* 2012, 33, 6211-6219.
42. Moon, J. J.; Suh, H.; Bershteyn, A.; Stephan, M. T.; Liu, H.; Huang, B.; Sohail, M.; Luo, S.; Ho Um, S.; Khant, H.; Goodwin, J. T.; Ramos, J.; Chiu, W.; Irvine, D. J. Interbilayer-crosslinked multilamellar vesicles as synthetic vaccines for potent humoral and cellular immune responses. *Nat Mater* 2011, 10, 243-251.
43. Dölen, Y.; Kreutz, M.; Gileadi, U.; Tel, J.; Vasaturo, A.; van Dinther, E. A.; van Hout-Kuijer, M. A.; Cerundolo, V.; Figdor, C. G. Co-delivery of PLGA encapsulated invariant NKT cell agonist with antigenic protein induce strong T cell-mediated anti-tumor immune responses. *OncoImmunology* 2015, 00-00.

44. Jewell, C. M.; Bustamante López, S. C.; Irvine, D. J. In situ engineering of the lymph node microenvironment via intranodal injection of adjuvant-releasing polymer particles. *Proc Natl Acad Sci* 2011, 108, 15745-15750.
45. Liu, H.; Moynihan, K. D.; Zheng, Y.; Szeto, G. L.; Li, A. V.; Huang, B.; Van Egeren, D. S.; Park, C.; Irvine, D. J. Structure-based programming of lymph-node targeting in molecular vaccines. *Nature* 2014, 507, 519-522.
46. Fromen, C. A.; Rahhal, T. B.; Robbins, G. R.; Kai, M. P.; Shen, T. W.; Luft, J. C.; DeSimone, J. M. Nanoparticle surface charge impacts distribution, uptake and lymph node trafficking by pulmonary antigen-presenting cells. *Nanomedicine* 2016, 12, 677-687.
47. Zhuang, Y.; Ma, Y.; Wang, C.; Hai, L.; Yan, C.; Zhang, Y.; Liu, F.; Cai, L. PEGylated cationic liposomes robustly augment vaccine-induced immune responses: Role of lymphatic trafficking and biodistribution. *J Control Release* 2012, 159, 135-142.
48. Thomas, S. N.; Vokali, E.; Lund, A. W.; Hubbell, J. A.; Swartz, M. A. Targeting the tumor-draining lymph node with adjuvanted nanoparticles reshapes the anti-tumor immune response. *Biomaterials* 2014, 35, 814-824.
49. Reddy, S. T.; van der Vlies, A. J.; Simeoni, E.; Angeli, V.; Randolph, G. J.; O'Neil, C. P.; Lee, L. K.; Swartz, M. A.; Hubbell, J. A. Exploiting lymphatic transport and complement activation in nanoparticle vaccines. *Nat Biotech* 2007, 25, 1159-1164.
50. Wilson, N. S.; El-Sukkari, D.; Belz, G. T.; Smith, C. M.; Steptoe, R. J.; Heath, W. R.; Shortman, K.; Villadangos, J. A. Most lymphoid organ dendritic cell types are phenotypically and functionally immature. *Blood* 2003, 102, 2187-2194.
51. Manolova, V.; Flace, A.; Bauer, M.; Schwarz, K.; Saudan, P.; Bachmann, M. F. Nanoparticles target distinct dendritic cell populations according to their size. *Eur J Immunol* 2008, 38, 1404-1413.
52. Mohanan, D.; Slütter, B.; Henriksen-Lacey, M.; Jiskoot, W.; Bouwstra, J. A.; Perrie, Y.; Kündig, T. M.; Gander, B.; Johansen, P. Administration routes affect the quality of immune responses: A cross-sectional evaluation of particulate antigen-delivery systems. *J Control Release* 2010, 147, 342-349.
53. Waeckerle-Men, Y.; Bruffaerts, N.; Liang, Y.; Jurion, F.; Sander, P.; Kündig, T. M.; Huygen, K.; Johansen, P. Lymph node targeting of BCG vaccines amplifies CD4 and CD8 T-cell responses and protection against mycobacterium tuberculosis. *Vaccine* 2013, 31, 1057-1064.
54. Wang, C.; Liu, P.; Zhuang, Y.; Li, P.; Jiang, B.; Pan, H.; Liu, L.; Cai, L.; Ma, Y. Lymphatic-targeted cationic liposomes: A robust vaccine adjuvant for promoting long-term immunological memory. *Vaccine* 2014, 32, 5475-5483.
55. Ahlers, J. D.; Belyakov, I. M. Memories that last forever: strategies for optimizing vaccine T-cell memory. *Blood* 2010, 115, 1678-1689.
56. Kaur, R.; Bramwell, V. W.; Kirby, D. J.; Perrie, Y. Manipulation of the surface pegylation in

combination with reduced vesicle size of cationic liposomal adjuvants modifies their clearance kinetics from the injection site, and the rate and type of T cell response. *J Control Release* 2012, 164, 331-337.

57. Huntington, J. A.; Stein, P. E. Structure and properties of ovalbumin. *J Chromatogr B Biomed Sci Appl* 2001, 756, 189-198.
58. Elsayed, S.; Apold, J.; Holen, E.; Vik, H.; Florvaag, E.; Dybendal, T. The structural requirements of epitopes with ige binding capacity demonstrated by three major allergens from fish, egg and tree pollen. *Scand J Clin Lab Invest* 1991, 51, 17-31.
59. Mine, Y.; Yang, M. Recent advances in the understanding of egg allergens: basic, industrial, and clinical perspectives. *J Agric Food Chem* 2008, 56, 4874-4900.
60. Nisbet, A. D.; Saundry, R. H.; Moir, A. J. G.; Fothergill, L. A.; Fothergill, J. E. The complete amino-acid sequence of hen ovalbumin. *Eur J Biochem* 1981, 115, 335-345.
61. Moore, M. W.; Carbone, F. R.; Bevan, M. J. Introduction of soluble protein into the class I pathway of antigen processing and presentation. *Cell* 1988, 54, 777-785.
62. Hwang, H. S.; Kim, J. Y.; Park, H.; Jeong, J.; Hyun, H.; Yoon, T. J.; Park, H.-Y.; Choi, H.-D.; Kim, H. H. Cleavage of the terminal N-acetylglucosamine of egg-white ovalbumin N-glycans significantly reduces IgE production and Th2 cytokine secretion. *Biochem Biophys Res Commun* 2014, 450, 1247-1254.
63. Simerska, P.; Suksamran, T.; Ziora, Z. M.; Rivera, F. d. L.; Engwerda, C.; Toth, I. Ovalbumin lipid core peptide vaccines and their $CD4^+$ and $CD8^+$ T cell responses. *Vaccine* 2014, 32, 4743-4750.
64. Koncz, C.; Kreuzaler, F.; Kalman, Z.; Schell, J. A simple method to transfer, integrate and study expression of foreign genes, such as chicken ovalbumin and alpha-actin in plant tumors. *EMBO J* 1984, 3, 1029-37.
65. Hariharan, K.; Braslawsky, G.; Black, A.; Raychaudhuri, S.; Hanna, N. The induction of cytotoxic T cells and tumor regression by soluble antigen formulation. *Cancer Res* 1995, 55, 3486-3489.
66. Mandl, S.; Sigal, L. J.; Rock, K. L.; Andino, R. Poliovirus vaccine vectors elicit antigen-specific cytotoxic T cells and protect mice against lethal challenge with malignant melanoma cells expressing a model antigen. *Proc Natl Acad Sci* 1998, 95, 8216-8221.
67. Prasad, S.; Cody, V.; Saucier-Sawyer, J. K.; Saltzman, W. M.; Sasaki, C. T.; Edelson, R. L.; Birchall, M. A.; Hanlon, D. J. Polymer nanoparticles containing tumor lysates as antigen delivery vehicles for dendritic cell–based antitumor immunotherapy. *Nanomedicine* 2011, 7, 1-10.
68. Rosenberg, S. A.; Yang, J. C.; Restifo, N. P. Cancer immunotherapy: moving beyond current vaccines. *Nat Med* 2004, 10, 909-915.
69. Rammensee, H.-G.; Singh-Jasuja, H. HLA ligandome tumor antigen discovery for personalized

vaccine approach. *Expert Rev Vaccines* 2013, 12, 1211-1217.

70. Solbrig, C. M.; Saucier-Sawyer, J. K.; Cody, V.; Saltzman, W. M.; Hanlon, D. J. Polymer nanoparticles for immunotherapy from encapsulated tumor-associated antigens and whole tumor cells. *Mol Pharm* 2007, 4, 47-57.
71. Yamada, A.; Sasada, T.; Noguchi, M.; Itoh, K. Next-generation peptide vaccines for advanced cancer. *Cancer Sci* 2013, 104, 15-21.
72. Haedicke, J.; Iftner, T. Human papillomaviruses and cancer. *Radiother Oncol* 2013, 108, 397-402.
73. Heck, D. V.; Yee, C. L.; Howley, P. M.; Münger, K. Efficiency of binding the retinoblastoma protein correlates with the transforming capacity of the E7 oncoproteins of the human papillomaviruses. *Proc Natl Acad Sci* 1992, 89, 4442-4446.
74. Frazer, I. H. Prevention of cervical cancer through papillomavirus vaccination. *Nat Rev Immunol* 2004, 4, 46-55.
75. Yang, A.; Jeang, J.; Cheng, K.; Cheng, T.; Yang, B.; Wu, T. C.; Hung, C.-F. Current state in the development of candidate therapeutic HPV vaccines. *Expert Rev Vaccines* 2016, 15, 989-1007.
76. Rahimian, S.; Fransen, M. F.; Kleinovink, J. W.; Christensen, J. R.; Amidi, M.; Hennink, W. E.; Ossendorp, F. Polymeric nanoparticles for co-delivery of synthetic long peptide antigen and poly IC as therapeutic cancer vaccine formulation. *J Control Release* 2015, 203, 16-22.
77. Tran, N. P.; Hung, C.-F.; Roden, R.; Wu, T.-C. Control of HPV infection and related cancer through vaccination. *Recent Results Cancer Res*, 2014, 193, 149-171.
78. Bolhassani, A.; Mohit, E.; Rafati, S. R. Different spectra of therapeutic vaccine development against HPV infections. *Human Vaccines* 2009, 5, 671-689.
79. Yang, J. S.; Kim, H. J.; Ryu, Y. H.; Yun, C.-H.; Chung, D. K.; Han, S. H. Endotoxin Contamination in Commercially Available Pokeweed Mitogen Contributes to the Activation of Murine Macrophages and Human Dendritic Cell Maturation. *Clin Vaccine Immunol* 2006, 13, 309-313.
80. Brito, L. A.; Singh, M. Acceptable levels of endotoxin in vaccine formulations during preclinical research. *J Pharm Sci* 2011, 100, 34-37.
81. Magalhaes, P. O.; Lopes, A. M.; Mazzola, P. G.; Rangel-Yagui, C.; Penna, T. C.; Pessoa, A., Jr. Methods of endotoxin removal from biological preparations: a review. *J Pharm Pharm Sci* 2007, 10, 388-404.
82. Gorbet, M. B.; Sefton, M. V. Endotoxin: The uninvited guest. *Biomaterials* 2005, 26, 6811-6817.
83. Marek, S. R.; Conn, C. A.; Peppas, N. A. Cationic nanogels based on diethylaminoethyl methacrylate. *Polymer* 2010, 51, 1237-1243.
84. Asua, J. M. Challenges for industrialization of miniemulsion polymerization. *Prog Polym Sci* 2014, 39, 1797-1826.

85. Gaikwad, S. G.; Pandit, A. B. Ultrasound emulsification: Effect of ultrasonic and physicochemical properties on dispersed phase volume and droplet size. *Ultrason Sonochem* 2008, 15, 554-563.

86. Lu, H.; Schmidt, M. A.; Jensen, K. F. Photochemical reactions and on-line UV detection in microfabricated reactors. *Lab Chip* 2001, 1, 22-28.

Appendices

Nederlandse samenvatting

Curriculum vitae and list of publications

Acknowledgments

Nederlandse samenvatting

Immunotherapie van kanker, met behulp van kankervaccins op basis van eiwitten, is een veelbelovende methode om het immuunsysteem te activeren in het bestrijden van de tumor. Tumoreiwit-antigenen zijn echter beperkt immunogeen, omdat ze niet erg efficiënt opgenomen worden door de cellen van het immuunsysteem, in combinatie met een gebrek aan zogenaamde *danger signals* om het immuunsysteem te stimuleren. Daarnaast dienen de antigenen aan het immuunsysteem gepresenteerd te worden via de MHC klasse I route, om $CD8^+$ T-cellen en het cytotoxische T-lymfocietrespons (CTL) te activeren. Omdat dendritische cellen (DCs) de antigenen presenteren en daarmee het immuunrespons initiëren en reguleren, zullen deze cellen het belangrijkste aangrijpingspunt zijn van een kankervaccin. De belangrijkste functie van DCs is het opnemen en verwerken van lichaamsvreemde eiwitten tot antigen-peptiden, en deze te presenteren aan T-cellen. Daarbij moet opgemerkt worden dat eiwitten gewoonlijk verwerkt worden in het endo-/lysosomale compartiment van DCs, wat in het algemeen leidt tot presentatie via de MHC klasse II in plaats van de gewenste klasse I route. Daarom is het bevorderen van MHC klasse I antigenpresentatie (zogenaamde kruispresentatie) zeer gewenst om de antitumorwerking van kankervaccins te verbeteren.

Nanogelen worden sinds kort onderzocht als afgiftesysteem voor vaccins. Omdat nanogelen dezelfde grootte hebben als pathogenen, worden ze gemakkelijk opgenomen door APCs, in het bijzonder DCs. Het juist instellen van de deeltjesgrootte en oppervlaktelading is belangrijk voor de opname-efficiëntie. Nanogelen kunnen worden beladen met tumoreiwit-antigenen, en daarmee de opname van het antigen door DCs bevorderen. Sommige nanogelen kunnen ook zorgen voor maturatie en activatie van de DCs, resulterend in verbeterde antigenpresentatie en het voorkómen van immuuntolerantie. Het is ook interessant dat er gerapporteerd is dat nanogelen kruispresentatie van antigenen kunnen bevorderen, zowel *in vitro* als *in vivo*. Het doel van dit proefschrift is om afgiftesystemen voor vaccins te ontwikkelen op basis van nanogelen, met behulp van het ovalbumine (OVA) antigen als voorbeeld, en hun *in vitro* en *in vivo* effectiviteit te evalueren.

In **Hoofdstuk 1** wordt uitgelegd wat de principes zijn van tumorvaccinatie, en wordt de zwakke immunogeniteit van tumorantigenen en de noodzaak om deze aan te leveren aan APCs om kankerimmuniteit te verkrijgen nader belicht. Nanogelen worden besproken als effectieve dragers voor de afgifte van tumorantigenen, waarbij de invloed van de nanogeleigenschappen op modulatie van het immuunrespons wordt uiteengezet. Daarnaast

wordt de strategie geïntroduceerd waarbij reduceerbare disulfidebindingen ingezet worden om antigenen intracellulair af te geven en daarmee zowel MHC klasse I als II antigenpresentatie te bevorderen.

Hoofdstuk 2 geeft een overzicht van de huidige literatuur op het gebied van nanogelen ten behoeve van de intracellulaire afgifte van biotherapeutica (bijv. eiwitten, antigenen, en genetisch materiaal), met vooral aandacht voor bioresponsieve nanogelen. De noodzaak en uitdagingen op het gebied van intracellulaire afgifte van biotherapeutica worden uiteengezet. Nanogelen kunnen zodanig worden ontworpen dat ze ingesloten biotherapeutica snel kunnen vrijstellen als gevolg van fysiologische verschillen tussen de intracellulaire en de extracellulaire omgeving. De meeste van de beschreven bioresponsieve nanogelen vertoonden een significante verbetering van het therapeutisch effect ten opzichte van vergelijkbare niet-responsieve nanogelen, als gevolg van de afgifte en het vrijstellen van hoge doses biotherapeutica in de cel. Dit hoofdstuk brengt aan het voetlicht dat bioresponsieve nanogelen veelbelovende materialen zijn ten behoeve van de intracellulaire afgifte van biomoleculen, inclusief de toepassing in tumorvaccinatie.

De toepasbaarheid van reductiegevoelige nanogel dragersystemen voor de intracellulaire antigen-afgifte is geëvalueerd in **Hoofdstuk 3**, door het voorbeeldantigen OVA te binden aan het netwerk van kationische dextraan nanogelen. OVA is negatief geladen bij pH 7 vanwege zijn pI van 5,0. Daarom werden kationische dextraan nanogelen, die tevens thiolreactieve groepen bevatten, bereid uit gemethacryleerd dextraan, trimethyl aminoethyl methacrylaat en N-(4-(2-(pyridine-2-yldisulfanyl)ethyl)-amidobutyl) methacrylamide, door middel van inverse mini-emulsie fotopolymerisatie. OVA, gederivatiseerd met succinimidyl S-acetylthioacetaat (SATA) groepen, werd vrijwel kwantitatief geabsorbeerd in deze nanogelen als gevolg van elektrostatische interacties in een buffer met lage ionsterkte (HEPES, 20 mM, pH 7,4). Vervolgens werd SATA-OVA covalent geconjugeerd in het gelnetwerk via disulfidebindingen, door reactie van het gethioleerde OVA met de in de nanogel aanwezige pyridyldisulfide groepen. Controle-experimenten lieten zien dat fysisch beladen OVA snel werd vrijgesteld uit de nanogelen onder fysiologische omstandigheden (PBS, 164 mM, pH 7,4). Daarentegen gaven nanogelen waarin OVA chemisch vastgezet was, slechts een beperkte hoeveelheid eiwit vrij gedurende 8 uur in PBS. Meer dan 80% van het beladen eiwit werd vervolgens onder reducerende omstandigheden binnen een uur vrijgesteld, ten gevolge van splitsing van de disulfide bruggen. Om intracellulaire vrijstelling van het geconjugeerde OVA te visualiseren, werden het eiwit en de nanogelen voorzien van respectievelijk Alexa Fluor 647 en Alexa Fluor 488. Confocale afbeeldingen lieten zien dat de dubbel gelabelde nanogelen efficiënt werden opgenomen door DCs na 24

uur incubatie bij 37 °C. Het geconjugeerde OVA werd vrijgegeven uit de nanogelen na internalisatie door DCs, terwijl het niet-geconjugeerde OVA al werd vrijgegeven voordat het werd opgenomen. Vervolgens werd geëvalueerd of de nanogelen *in vitro* in staat waren tot kruispresentatie van geconjugeerd OVA aan $CD8^+$ T-cellen, met behulp van OVA-specifieke B3Z hybridoma T-cellen. De verkregen resultaten lieten sterke $CD8^+$ T-celactivatie zien door OVA-geconjugeerde nanogelen, terwijl vrij OVA en niet-geconjugeerde OVA-nanogelen niet in staat waren tot T-celactivatie. Samengevat, dit hoofdstuk heeft *in vitro* de toepasbaarheid aangetoond van reductie-gevoelige nanogelen als afgiftesysteem voor antigenen, ten behoeve van inductie van een cellulair immuunrespons.

Bemoedigd door de veelbelovende resultaten uit hoofdstuk 3 hebben we in **Hoofdstuk 4** de invloed van de grootte en oppervlaktelading van de nanogel op de opname door DCs verder *in vitro* onderzocht, evenals de capaciteit van de nanogel om DCs te matureren, en de intracellulaire afgifte, transport en verwerking van het antigen door DCs. Daarnaast is in dit hoofdstuk een profylactische en therapeutische vaccinatie uitgevoerd met antigen-geconjugeerde nanogelen *in vivo*. De bindings- en opnamestudies lieten zien dat gelen van nano-grootte met relatief hoge kationische oppervlaktelading het meest efficiënt opgenomen werden door DCs. Bovendien waren deze sterk kationisch geladen deeltjes in staat tot maturatie van de DCs, wat onafhankelijk was van de deeltjesgrootte (200 tot 2500 nm). Analyse met flowcytometrie liet zien dat na 24 uur incubatie met de nanogelen met geconjugeerd OVA, een grotere hoeveelheid OVA intracellulair werd afgegeven en verwerkt in DCs ten opzichte van nanogelen die fysisch beladen waren met OVA. Vervolgens is bestudeerd wat er met de nanogelen en het geconjugeerde OVA gebeurt in de DCs. Confocale afbeeldingen toonden aan dat de opgenomen nanogelen in lysosomen van DCs werden ingevangen, terwijl fragmenten van het vrijgegeven antigen werden getransporteerd naar het cytosol, wat belangrijk is voor MHC klasse I antigenpresentatie. Vervolgens hebben we de *in vivo* effectiviteit getest in zowel een profylactisch als therapeutisch tumormodel gebaseerd op B16OVA melanoma (welke het OVA antigen tot expressie brengt). C57BL/6 muizen (10 dieren per groep) kregen diverse formuleringen subcutaan (s.c.) toegediend, voor of na inoculatie met s.c. aangebrachte tumorcellen. Muizen die geïmmuniseerd werden met OVA-geconjugeerde nanogelen lieten een antigenspecifiek T-cel immuunrespons zien en tevens een toename in antigenspecifieke antilichaamproductie. Daarmee werd een sterke bescherming en genezing van melanoma verkregen. In het profylactische model werd 90% van de muizen, die gevaccineerd waren met OVA-geconjugeerde nanogelen en poly(I:C) als adjuvans, gedurende 55 dagen beschermd tegen tumorvorming. In het therapeutisch model verdween bij 40% van de

muizen de tumor volledig, wat een opmerkelijk verschil was vergeleken met de andere groepen, waarbij geen enkele muis dat het geval was. Samengevat zijn de nanogelen, die beschreven zijn in deze studie, veelbelovende formuleringen om in een diermodel een antigenspecifieke immuniteit tegen kanker te ontwikkelen.

In Hoofdstuk 3 en 4 is de intracellulaire afgifte van eiwitantigenen bewerkstelligd door conjugatie van het eiwit in de nanogelen via reduceerbare disulfide bindingen. De covalente binding vereist echter chemische modificatie van het eiwit. In **Hoofdstuk 5** hebben we daarom nanogelen ontwikkeld die gecoat zijn met een disulfide-verknoopte polymeerschil, en waarin het oorspronkelijke eiwitantigen ingesloten is. Voor deze benadering is chemische modificatie van het antigen niet noodzakelijk, wat het afgiftesysteem veelzijdiger maakt. Ongemodificeerd OVA werd eerst beladen in kationische dextraan nanogelen via elektrostatische interacties. Vervolgens werden, middels een laag-voor-laag methode via elektrostatische interacties, polymeren aangebracht met een tegenovergestelde lading (het anionische poly(N-(2-hydroxypropyl)methacrylamide-co-methacrylzuur) en het kationische poly(N-(2-hydroxypropyl)methacrylamide-co-trimethyl aminoethylmethacrylaat) welke pyrydyldisulfide-groepen bevatte. Daarna werd dithiothreitol (DTT) toegevoegd, corresponderend met 0,5 molequivalent pyridyldisulfide-groepen in de coatingpolymeren, om de helft van de pyridyldisulfide-groepen te splitsen tot thiolgroepen. Vervolgens reageerden deze thiolgroepen met de overgebleven 0,5 molequivalent pyridyldisulfide-groepen via een thiol/disulfide-uitwisseling, resulterend in een disulfide-verknoopte polymeercoating. Confocale afbeeldingen van OVA-beladen microgelen die gecoat waren met fluorescent gelabelde polymeren lieten een duidelijk ring van de polymeerschil zien rondom de microgelen. Zoals verwacht was de disulfide-verknoopte schil stabiel in een niet-reducerende omgeving, waarmee lekkage van OVA uit de nanogelen werd voorkomen. Belangrijk is dat splitsing van deze disulfidebindingen onder reducerende condities leidde tot het snel uiteenvallen van de polymeerschil en vervolgens afgifte van het ingesloten antigen. Daarnaast toonden we aan dat intracellulaire afgifte van antigen door middel van deze verknoopte kern-schil nanogelen, MHC klasse I antigenpresentatie bevorderden ten opzichte van de nanogelen waarvan de coating niet verknoopt werd.

Curriculum vitae

Dandan Li was born in 1986 in Guangxi, China. In 2005 she obtained her high school diploma and started studying pharmaceutics in College of Pharmacy, China Pharmaceutical University. During her bachelor's program, she performed a 6 months internship at the Department of Pharmaceutics, China Pharmaceutical University, investigating ophthalmic Azithromycin gel. From 2009 till 2012 she was studying pharmaceutics and earned a master's degree at National Institute of Pharmaceutical Industry of China, developing oral drug delivery systems (including β-cyclodextrin inclusion complex tablet, self-micro emulsion and solid self-micro emulsion) for SIPI-4887 (an insoluble and unstable first type of new drug, statin). Afterwards she started her PhD research project at the Department of Pharmaceutics at Utrecht University, the Netherlands. Her PhD research was supervised Prof. dr. Ir. W.E. Hennink, Dr. C.F. van Nostrum and Dr. T. Vermonden, focused on design and synthesis of reduction-sensitive nanogels for intracellular delivery of proteins/antigens. The results of her work are described in this PhD thesis entitled "Reduction-sensitive nanogels for tumor vaccination", which was defended on December 21st, 2016.

List of publications

D. Li, N. Kordalivand, M. F. Fransen, F. Ossendorp , K. Raemdonck, T. Vermonden, W. E. Hennink, C. F. van Nostrum. Reduction-sensitive dextran nanogels aimed for intracellular delivery of antigens. Advanced Functional Materials 2015, 25, 2993-3003.

D. Li, F. Sun, M.Bourajjaj, Y. Chen, E. H. Pieters, J. Chen, J. B. van den Dikkenberg, B. Lou, M. G. M. Camps, F. Ossendorp, W. E. Hennink, T. Vermonden, C. F. van Nostrum. Strong in vivo antitumor responses induced by an antigen immobilized in nanogels via reducible bonds. Nanoscale 2016, DOI: 10.1039/C6NR05583D.

D. Li, Y. Chen, E. Mastrobattista, C. F. van Nostrum, W. E. Hennink, T. Vermonden. Reduction-sensitive polymer shell coated nanogels for intracellular delivery of proteins. Submitted for publication.

D. Li, C. F. van Nostrum, E. Mastrobattista, T. Vermonden W. E. Hennink. Nonaogels for intracellular delivery of biotherapeutics. Submitted for publication.

Y. Chen, M. J. van Steenbergen, D. Li, J. B. van de Dikkenberg, T. Lammers, C. F. van Nostrum, J. M. Metselaar, W. E. Hennink. polymeric nanogels with tailorable degradation behavior. Macromolecular Bioscience 2016, 16, 1122-1137.

Acknowledgments

Ever since I have memory, my mom kind of made my birthday wish for me every year. The wishes kept changing from going to college, to going to a famous university, to becoming a scientist, and to becoming the president of China at the end! Although my mom is crazy about the last idea, I always feel like that I should become a scientist. Besides becoming a scientist, I have another dream that I will travel over the world and live abroad for a while. The dream of living abroad has been coming true for four years now in the Netherlands, and about traveling around the world, I have finished ~13% so far. Most excitingly, this thesis is a sign that I am becoming a scientist, I guess?

Looking back of my four-year PhD, I had the most challenging period during the first half year. Besides that I needed to adapt to a new lifestyle and Dutch culture, the main challenge came from my dear promotor Prof. Dr. Wim Hennink. Dear Wim, you must not know that I couldn't eat, couldn't sleep before the meeting with you, and I needed one whole week to recover after. But later, I found that you are such a caring person deeply in your heart, and I truly admire and inspire by your pure scientific soul and your passion for polymers and drug delivery systems. I would like to express my sincere gratitude to you for your guidance, instructive input and continuous support. Now it is a good time to say that it is an honor to accomplish my PhD under your supervision.

I would like to extend my deepest gratitude to my copromotors, Dr. Rene van Nostrum and Dr. Tina Vermonden for your patience and guidance during the whole period of my PhD. I am so lucky to have you both as my daily supervisors. Thank you for your trust, constant supporting and warm encouraging during the difficult times.

My sincere thanks also goes to my collaborators, Dr. Koen Raemdonck, Prof. Dr. Ferry Ossendorp, Dr. Marieke F. Fransen and Marcel G. M. Camps, who provided me the opportunity to learn their research techniques. Without they precious support it would not be possible to conduct this research. I would like to thank Prof. Dr. Bruno De Geest, Dr. Enrico Mastrobattista, Dr. Maryam Amidi, Mazda Rad Malekshahi, Dr. Jian Chen, George Dakwar and Bo Lou for their wise suggestions for my research project.

I am very grateful to our lovely technicians for their support in the daily lab work. Mies, thank you for showing me how to synthesize dex-MA during my first week in the lab. You eliminated my nervousness about the new lab. Joep, thank you for teaching me the cell culture technique, and I will benefit from it for the rest of my scientific life. Ebel, thank you

for helping me to deal with DEC application. Roel and Louis, thank you for always keeping an eye on us.

I would like to give a special thanks to Dr. Meriem Bourajjij. Dear Meriem, I could never start my in vivo experiments without you. Thank you so much for giving useful suggestions, making the in vivo study plan and writing the DEC for me. I wish all the best for you. Besides, the in vivo chapter could not be finished without the help of my “in vivo crew”, Anja, Paul, Feilong, Yinan and Bo.

I would like to acknowledge my students that spent time with me in my project. Dear Anokhee, Juliet, Lennart, Yuan and Mark, I enjoyed explaining my work to you and your challenging to me which pushed me to learn more. I am sorry that both Juliet and Lennart got ill during your internships. I once doubted that the dextran nanogels might be lethal chemical/biological weapons. You both have the intension to continue your academic careers, so my advice would be: stay away from nanogels!

I would like to thank our secretary Barbara, for assisting me in many different ways and handling the paperwork.

It is a pleasure to thank many of my old and new colleagues at the Department of Pharmaceutics, Sima, Filis, Isil, Roy, Grzegorz, Erik (long hair), Markus, Kimberley, Negar B, Sytze, Niels, Edu, Sohail, Kristel, Mazda, Farshad, Merel, Burcin, Mehrnoosh, Neda S, Mohadeseh, Afrouz, Jos, Luis, Andhyk, Orn, Shima, Yvonne, Nataliia, Mathew, Leena, Daiki, Erik OB, Mohammed, Maarten, Maria C, Jan Jaap, Ellen, Amr, Anna, Karina, Lies, Gui, Jeffery, Sjaak, Gina, Aida, Carl and Kung for providing such a nice environment. I really enjoyed spending time with you during various activities, like labout day, Christmas dinner, poker tournament and football poule.

I would like to thank our M3 lady-only lunch group members, Neda, Lucia, Negar S, Marzieh, Yinan, Haili, Maria G, Mahsa and Genoveva. I enjoyed lunch and nice chats with you every work day! You were my motivation to come to work every day during my last several months stay in DDW.

I would like to thank our Olympos gym team and also my close friends, Neda, Lucia, Negar, Marzieh and Yinan. I know that I was a bit pushing on you to go to gym often, especially on Negar. At least Yinan, Neda and Lucia can maintain your workout routine after, I hope! At the meantime, I am so grateful for your company and sharing those shocking cultures with each other. I remember all those foods tasting from different countries, parties and activities we had together with Dani, Mehdi, Aveed, Vida, Kamal, Oana, Maripaz,

Massimiliano, Maria, Haili, Feilong, Jerry, Mahsa and Genoveva. Neda and Lucia, special thanks to you for taking the responsibility being my paranymphs.

I would like to thank our Biopharm Chinese community, Yang, Qizhi, Weiluan, Yinan, Feilong, Bo, Haili, Yanna, Jerry, Linglei, Qinxue, Jian, Yuan, Lemeng, Mengshan and Jibin. 多谢大家四年来的照顾，以后也要经常聚聚，分享信息，相互帮助。还有各位到了乌得勒支认识的朋友们，Chuck，刘博洋，韦江绿，刘萍，付欧，张金强，刘芳，肖玲，杨欣，余光允，李靖，余颖欣，施杰，赵玉珑，付东龙，郎一飞，鲁文静，张浩，很高兴能认识你们。

I most want to thank Yinan. We know each other for more than 11 years now and we have spent quite some quality time together. Four years ago, we took the same flight to this stranger country and start our adventure. During these four years in the Netherlands, we made a perfect team. You cook, and I clean. You make travelling plan, and I just follow your lead. We also fought about foods, watching TV, apartments, furniture, drug delivery and every tiny thing. But mostly I remember that we comforted each other after the meeting with our dear promotor Prof. Hennink, we walked for hours to search for nice food, we trembled in Vilnius at -20℃, we got sun burn in southern Italy at 45℃, we spent whole night sitting on a crowded train in Romania but only traveled 450 km, and we said that we should quit doing stupid things but we are still doing it. Thank you for your company and support for all these years.

Last but not the least, I would like to thank my family: my parents, my brothers and my sister-in-law for supporting me spiritually throughout my four-year stay in the Netherlands. My mom keep telling me that I can fly as high, as far as I wish, and they will always save a place for me no matter what and when. I don’t often have the chance to spend time with my brother after we grew up, but as he said: “I always got you back”. 感谢老爸老妈阿哥阿嫂四年来对我的支持，你们总说你们就是我最坚强的后盾，我也会成为你们坚强的后盾!

Thank you all for everything!

Dandan